This is to certify that the

dissertation entitled

MODELING, DYNAMICS AND CONTROL OF
LARGE AMPLITUDE MOTIONS OF VESSELS
IN BEAM SEAS

presented by

Shyh-Leh Chen

has been accepted towards fulfillment
of the requirements for

Ph.D. degree in Mechanical Engineering

Major professor

Date May 20, 1996

MODELING, DYNAMICS AND CONTROL OF LARGE AMPLITUDE MOTIONS OF VESSELS IN BEAM SEAS

By

Shyh-Leh Chen

A DISSERTATION

Submitted to
Michigan State University
in partial fulfillment of the requirements
for the degree of

DOCTOR OF PHILOSOPHY

Department of Mechanical Engineering

1996

ABSTRACT

MODELING, DYNAMICS AND CONTROL OF LARGE AMPLITUDE MOTIONS OF VESSELS IN BEAM SEAS

By

Shyh-Leh Chen

The modeling, dynamics and control of large amplitude motions of vessels traveling in regular beam seas are considered. We first derive a 3-DOF model that considers roll, sway and heave motions of arbitrary amplitude occurring in a (vertical) plane for a vessel subjected to excitation from regular beam seas. By exploiting natural time and force scales of the system, the equations of motion are transformed into a singularly perturbed form through a nondimensionalization and rescaling process. Analysis of this dynamical system using chaotic transport theory and a Melnikov analysis provides a ship capsizing criterion in terms of vessel parameters and the sea state. The coupling effects from sway and heave are examined in order to assess the validity of commonly used models which include only roll dynamics.

Next, active anti-roll tanks are added to the system as a means of preventing large amplitude roll motions. A robust state feedback controller is designed that can handle model uncertainties, which arise primarily from unknown hydrodynamic contributions. The approach for the controller design is a combination of sliding mode control and composite control for singularly perturbed systems, with the help of the backstepping technique. It is shown that a pump/tank system containing water representing less than 5% of the vessel displacement can effectively control roll

motions.

Numerical simulation results for an existing fishing vessel, the twice-capsized *Patti-B*, are used to verify the analysis for the capsize criteria and the controller design.

To my parents and my brother

ACKNOWLEDGMENTS

Completing a thesis in an unfamiliar country has never been an easy task. It is my great pleasure to acknowledge those who made this possible. Professor Steven Shaw, my advisor, has allowed me to do virtually whatever I want, but also has given me critical guidance whenever I needed it. I have learned a lot from his insights throughout this research. I am proud of being his student. I would like to thank Professor Armin Troesch of The University of Michigan for his invaluable help on modeling issues. I would also like to express my sincere gratitude to Professor Hassan Khalil for his enthusiastic help on the control part of this thesis, and for introducing me to nonlinear systems analysis and control through his excellent teaching on those subjects.

I am grateful to Professors Alan Haddow and Brian Feeny for their constant encouragement and helpful comments. I also thank Professor Sheldon Newhouse for stimulating discussions on chaotic transport theory.

In addition, I thank them all for serving on my dissertation committee. Working with these scholars has been more than enjoyable.

I am indebted to my former advisor, the late Professor Edge Chu Yeh of National Tsing Hua University, Taiwan, for motivating me to the wonderful research world that I will never leave.

A special thank goes to my mentor, Professor Jing-Sin Liu of Academia Sinica, Taiwan, for valuable discussions and financial support during my summer stays in Taiwan.

My brother, Shyh-Fang, has taken care of my parents and family matters for the past four years so that I could obtain my degree smoothly. Without him, I would have not been able to study overseas. It is to him and my parents that this thesis is dedicated.

There are many friends who constantly supported, encouraged, and helped me during my stay here at MSU. The members of Dynamics and Vibration Group, including Dr. Ching-Ming Yuan, Dr. Jin-Wei Liang, Dr. Cheng-Tang Lee, Mr. Chang-Po Chao, Mr. Ramana Kappagantu, Mr. Wei Li and Mr. Chris Hause, have provided me with constructive criticism and wonderful discussions in many ways of life. They also create an excellent atmosphere for research. I also thank Yeou-Guang and Hui-Fen, Feng-Jong and Mei-Hui, Jyh-Shen and Chien-Yi, my roommates Hui-Min and Wen-Hua, my host family Anne and David, and many others for giving me the warm feeling of home in this otherwise cold Michigan.

TABLE OF CONTENTS

LIST OF FIGURES

Figure

LIST OF TABLES

<u>**Table**</u>

LIST OF APPENDICES

Appendix

n

n

w

st

th

not

reg

fish

is ul

DOF

this.

Most

CHAPTER 1

INTRODUCTION

This dissertation is concerned with three important issues of small fishing vessels traveling in regular beam seas: modeling, large amplitude dynamics, and control. The eventual goal of this study is to answer the following two questions. First, for a given vessel under a given sea state, what is the probability that it will capsize within a prescribed time interval? Second, what can one do to prevent it from capsizing? The importance of vessel capsize is clear since it can cause the loss of life and property. The reason for focusing on small fishing vessels is that the sea state does not respect ship size and hence small fishing vessels usually experience more nonlinear sea-keeping processes than do large ships.

It is obvious that ship capsizing involves highly nonlinear, large amplitude dynamics of the ship under the excitation of a typically random seaway. However, calm water static stability, characterized by the so-called righting arm, is still the cornerstone of current vessel safety regulations. Important factors, such as the nature of the seaway or the dynamic response of the vessel are not explicitly (and many times not even implicitly) included. This is why vessels may still capsize even when these regulations are met (e.g., [42]). Moreover, it is one of the reasons why commercial fishing is the most dangerous occupation in the United States [29]. The present work is ultimately motivated by this fact.

As one will see in Chapter 2, most previous studies considered the simple single DOF (Degree-Of-Freedom) models for vessel rolling. There are two main reasons for this. First, few reasonable multi-DOF mathematical models exist for ship dynamics. Most ship models are either too complicated to be tractable for analysis or too simplified to be realistic. Second, the tools available for analyzing nonlinear multi-DOF models are not as well developed as those for single DOF models. While all vessels capsize primarily in roll, the influence of other DOF may also be important due to dynamic coupling effects.

There are three objectives for this study. First, we aim to derive a ship dynamics model that takes into account as many degrees of freedom as possible, yet remains tractable for analysis. This model is then used to propose a ship capsizing criterion. Finally, a stabilizing controller is designed based on this model. The model considered in the present work is a 3-DOF beam sea model, one that considers roll, sway and heave motions occurring in a (vertical) plane. The vessel is assumed to be at anchor or under low speed for work and hence has negligible forward speed. We will pay close attention to the coupling effects of heave and sway on roll motions and their effects on capsize. The design of the controller will focus on the robustness to the uncertainties arising in the modeling. It will be pointed out in the conclusions a strategy for how this model can be generalized to the full six degrees of freedom.

It should be noted that the analysis of this problem, as is typical in nonlinear systems, is facilitated by judicious choices of coordinates throughout the process. This should be kept in mind as one reads this thesis.

The large amplitude dynamics problem will be investigated from the viewpoint of dynamical systems. Ship capsizing is characterized in phase space by the escape of a solution trajectory from a potential well (the safe region) under the action of external excitation (induced by waves), as described in [23]. In this way, it is related to the study of phase space transport of Wiggins [67]. The main tools for the analysis of phase space transport are the Melnikov function and lobe dynamics [67]. It will be shown in Section 3.4 that the present system can be transformed into the form of a slowly varying oscillator which is amenable to a Melnikov analysis. Although lobes are well defined in two dimensional diffeomorphisms, they are not well defined t

t

th

th

in

an

for

mo

ord

a M

in three or more dimensions (except for special cases), which, unfortunately, are encountered here. However, an invariant manifold approach provided in Appendix A will allow us an avenue around this difficulty.

Ship roll stabilization problem is considered after the dynamics analysis. There are several methodologies for ship stabilization, such as gyroscopes, moving weight stabilizers, anti-roll tanks, fin stabilizers, and rudder-roll stabilization systems. The method of anti-roll tanks will be used here since others are either impractical, such as the gyroscopic method and moving weight scheme, or not effective at low vessel speeds, such as the fin stabilizer and rudder-roll systems. The main goal of the anti-roll tank is to dynamically change the horizontal position of a ship's center of gravity in such a way that the roll motions are reduced. However, the position of CG cannot be shifted instantaneously, and therefore the control scheme will involve a dynamic state feedback controller. Our approach for the robust controller design is based on a smooth version of sliding mode control, which handles the uncertainties, together with the backstepping method and the idea of composite control for singularly perturbed systems [31].

The upcoming chapters are briefly summarized below. In Chapter 2, we survey the previous work on ship dynamics and ship roll stabilization. Chapter 3 deals with the ship modeling problem. We begin in Section 3.1 by deriving a ship model under the conditions of calm water, no damping, and no wind. Since the wave excitation, the hydrodynamic damping, and the wind forces are generally small in relation to inertial effects, this ship model will constitute the prototype of the *unperturbed* model and is referred to as the calm water model. Next, the wave motion, the hydrodynamic forces, and the wind forces are discussed in Section 3.2 in preparation for the general modeling of a vessel in regular beam seas, which is presented in Section 3.3. In order to bring the general model into a "nearly integrable" form which allows for a Melnikov analysis, several steps are carried out in Section 3.4. First, a singular

C

d

L

by

va

by

con

wor

T

and

First,

perturbation formulation is sought through a nondimensionalization and rescaling process. It will be seen that the roll/sway motion is typically slow compared to heave and hence their dynamics lie on a slow invariant manifold. It can be shown that this slow manifold exists globally (up to the angles of vanishing stability) and is locally attractive. The slow dynamics turns out to be in the form of a slowly varying oscillator, which is readily handled by Melnikov analysis and has been studied in a number of papers (e.g., [55], [68], [69], [70]).

In Chapter 4, the large amplitude dynamics which may lead to capsize are analyzed using chaotic transport theory. As an introduction to the phase space transport theory, its application to 1-DOF roll models is reviewed in Section 4.1. Phase space transport in slowly varying oscillators using a fast manifold approach is discussed in Section 4.2. In Section 4.3, capsizing criteria for both biased and unbiased ships are proposed based on the results in Section 4.2. The present criteria will be compared to those obtained by 1-DOF roll models in Section 4.4 to examine the coupling effects.

The design of a robust stabilizing controller against capsizing is presented in Chapter 5. In Section 5.1, the uncertainties existing in the current ship model are discussed. Next, the robust stabilizing controller is designed in Section 5.2 using a Lyapunov-based approach. By assuming the slow sway velocity is constant, we begin by designing the slow control on the slow manifold. Then, the effects of the slowly varying sway motions and the fast heave dynamics are investigated.

The analytical analyses established in previous chapters are verified in Chapter 6 by numerical simulations for a specific fishing vessel, the clam dredge *Patti-B*. Some conclusions are drawn in Chapter 7, where we also provide some directions for future work on this topic.

This work has extended in several ways the study of ship dynamics and control and has generated some more fundamental results in dynamical systems theory. First, we have developed a systematic method for modeling multi-DOF ship motions in waves, even for the full six DOF dynamics. The resulting model retains realistic features of the vessel system and is tractable for analysis. Second, based on results from chaotic transport theory, we have quantitatively estimated the amount of phase space transport for 2-D maps using a Melnikov analysis. Also, we have provided a new approach to obtaining the Melnikov function for homoclinic orbits in slowly varying oscillators, which gives some useful insight into the structure of the dynamical system. These results together with our estimate of the phase space transport have allowed us to propose a capsizing criterion for multi-DOF ship models. Finally, we have applied some newly developed nonlinear control strategies to the ship stabilization problem. The results are very satisfactory and they demonstrate the promising future that nonlinear dynamics and control methods hold for advancing our understanding the motion and control of seagoing vessels.

CHAPTER 2

LITERATURE REVIEW

2.1 Ship Modeling and Dynamics

The general form for the six DOF ship model can be derived from Newton's law or Lagrange's method, and is given in a variety of references (e.g. [1], [16]). However, due to the difficulties with obtaining the hydrodynamic forces and with nonlinear multi-DOF problems, the general model is usually linearized or reduced to a 1-DOF roll model for analysis [24]. The reduction of the full ship model to the 1-DOF ones is commonly done by the introduction of the so-called *roll center* ([25], [26], [34], [40]).

The study of ship dynamics began as early as the eighteenth century, when the laws of dynamics were discovered by Newton and the basic laws of fluid dynamics were discovered by Bernoulli and others. More detailed historic accounts on the development of ship dynamics can be found in an excellent survey paper by Hutchison [24]. Here we will concentrate on the recent efforts on the analysis of nonlinear rolling motions.

The analysis of nonlinear rolling motions has been focused on the decoupled 1-DOF roll equation. The steady state periodic solutions for such a system can be obtained by perturbation techniques such as the harmonic balance method [54], the method of multiple scales ([5], [6], [43], [44]), and the averaging method [71]. Floquet theory is commonly used to study the stability of these steady state solutions ([43], [44]).

Most perturbation techniques are intended for weakly nonlinear systems. They usually fail for large amplitude dynamics, which is the main interest of this thesis. Several approaches have been attempted for investigating the dynamics and stability of large amplitude ship motions, especially the capsizing problem. Odabassi used Lyapunov's direct method to propose a conservative capsizing criterion [49]. An approximate deterministic capsizing criterion from an energy point of view is given in [64]. Thompson and co-workers observed that the initially safe basin will be *eroded* as the wave amplitude increases, resulting in the fractal-like transient basin boundaries ([57], [60]). They also argued that it is the transient behavior, not the steady state, that is dominant in ship capsizing process. Intensive numerical simulations were then carried out by them to introduce a capsizing criterion called *integrity measure* ([37], [57], [60], [61]).

Parallel to the above deterministic approaches, stochastic methods were also developed in order to take into account the random nature of the seaway. A numerical scheme for a 1-DOF roll model with a zero-mean Gaussian distributed excitation was proposed by Dalzell [11]. While Francescutto used an approximate perturbation method to study ship dynamics in irregular seas ([18], [19]), Roberts related ship capsizing to the first passage problem and employed the stochastic averaging method to analyze the problem ([50], [51]). Roberts' idea was shared by Moshchuk *et al.* who applied the method of asymptotic expansion to solve the first passage problem of ship nonlinear roll oscillations in random sea waves [41]. By characterizing the capsize as the escape from a potential well under random external excitation, Frey and Simiu ([20], [56]) and Hsieh *el al.* [23] studied the problem by combining modern geometric method (see below) with stochastic analyses.

Besides the various methods presented above, there is yet another promising approach to understanding the large amplitude dynamics, especially the capsizing, of vessel systems. It is a geometric method for nonlinear dynamical systems which deals mainly with the qualitative behaviors of the system. An excellent introductory book for this method is Wiggins [66]. Inspired by this rapidly growing field and by Thompson's emphasis on transients for ship capsizing, Shaw and co-workers successfully proposed good capsizing criteria for regular and irregular beam sea models using this approach ([13], [23], [27]). The main tools in their analyses are the Melnikov method and the theory of phase space transport which deals exclusively with the transient behavior [67]. This approach is followed here and will be generalized to multi-DOF models.

Despite the fact that the 1-DOF roll model has dominated the development of the analysis, there are several studies considering multi-DOF models. Weakly nonlinear coupled pitch-roll motions were investigated by Nayfeh *et al.* ([40], [45]) and coupled heave-roll motions were studied by Liaw *et al.* ([35], [36]). However, perturbation techniques and numerical simulations have dominated these analyses. This thesis represents a study using multi-DOF models which considers large amplitude ship motions, including capsize.

2.2 Ship Roll Stabilization

Attempts at controlling or reducing ship rolling motions have a long history dating back to late nineteenth century. For a historic account of this subject,see [4]. There are several methodologies proposed. Passive methods appeared first, such as bilge keels ([34], [53]), anti-roll tanks ([17], [34], [53]), moving weights ([17], [34]), and gyroscopic methods [52]. Following the development of control theory, active methods began to emerge, many of which were inspired by or modified from the passive ones, such as fin stabilizers ([2], [8]), activated tanks ([8], [38], [39]), controlled moving weights [48], and active gyroscopic methods [58].

As control theory was progressed further and ship dynamics are better understood, new control strategies have been brought to bear on this problem. For example, in view of the chaotic motion observed in ship roll dynamics, a newly developed controlling chaos technique was proposed in [12] to stabilize the ship rolling motions from capsizing in regular or irregular sea states. Another example is a controlled-wing method (similar to fin stabilizers) with an adaptive controller based on gain scheduling and neural network reported recently in [15].

Also, new stabilizing actuators other than classical ones are proposed. One such example is the rudder-roll stabilization system. The rudder-roll stabilization system has been incorporated with optimal control [16], adaptive control and gain scheduling [63]. A good collection of recent developments on the rudder-roll stabilization system is provided in the book by Fossen [16], where the control system designs for other aspects of ocean vehicles, such as auto-pilot and ship positioning, are also discussed in detail.

CHAPTER 3

MODELING OF SHIP DYNAMICS IN REGULAR BEAM SEAS

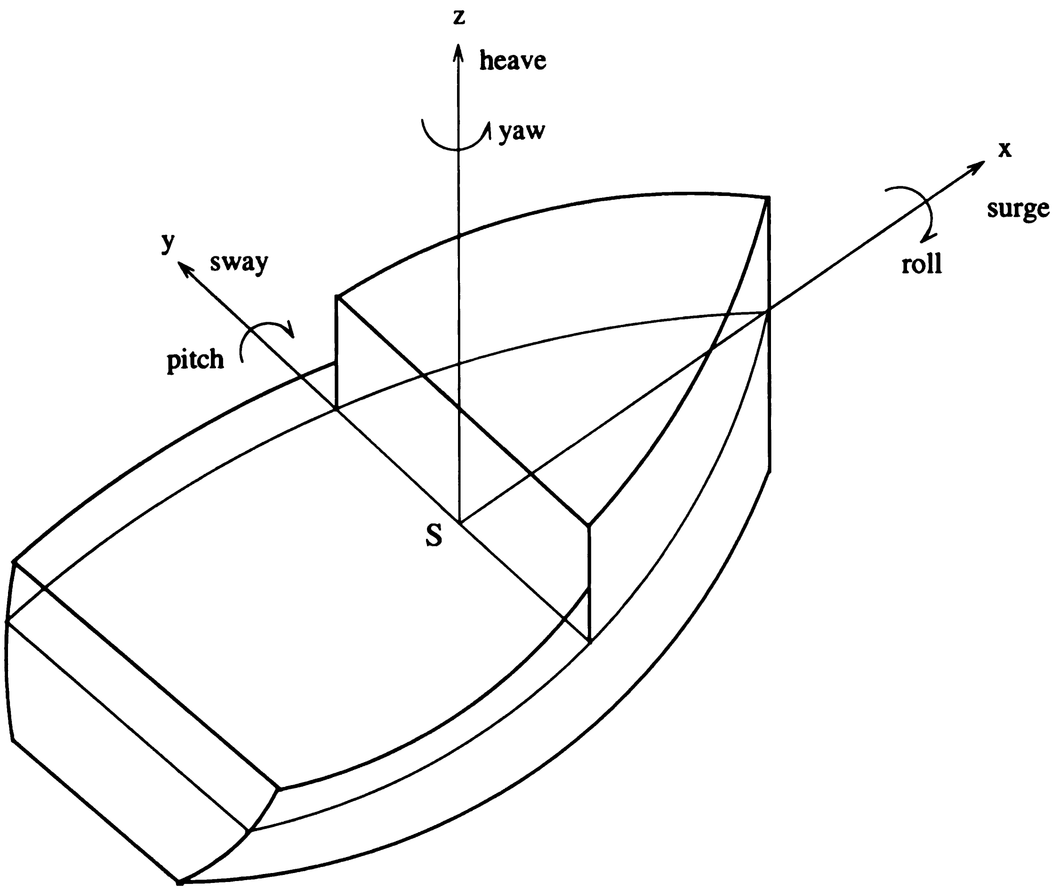

Figure 3.1: The six degrees of freedom for a ship.

In general, a rigid body floating on the free surface of a liquid interface has six DOF, i.e., surge, sway, heave, roll, pitch, and yaw; see Figure 3.1. Under beam sea conditions, in which waves hit the vessel directly broadside, one can assume that the three DOF – roll, sway, and heave – will dominate. Essentially these DOF live in a submanifold of the full phase space that should be dynamically stable unless a parametric or internal resonance occurs ([35], [46])[1]. Our approach here will be to account for the nonlinear effects of hydrostatics and inertia and to model the hydrodynamics in an essentially linear way. The reason for this is simply that it is the best that can be done currently short of brute force, large-scale computations.

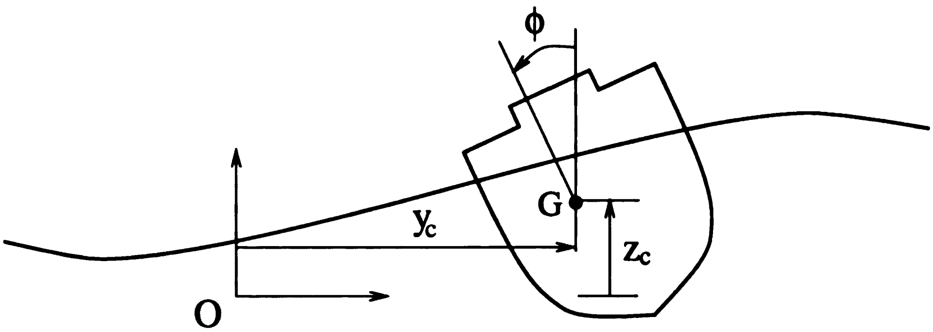

Figure 3.2: An inertial coordinate system for the vessel system.

With the inertial coordinate system shown in Figure 3.2, the equations of motion for these 3 DOF can be expressed as follows by applying Newton's law to the center of gravity (CG) denoted by G:

$$I_{44}\phi'' = K, \tag{3.1}$$

$$my_c'' = \hat{Y}, \tag{3.2}$$

$$mz_c'' = \hat{Z}, \tag{3.3}$$

where $(\cdot)' = \frac{d}{dt}(\cdot)$, ϕ is the roll angle, (y_c, z_c) is the coordinate of G, I_{44} is mass moment of inertia of the body about G, m is mass of the body, K is the roll moment, $\hat{Y}$ is the horizontal force, and $\hat{Z}$ is the vertical force[2]. We will follow the convention used in naval architecture, wherein subscripts 2, 3, and 4 represent sway, heave, and roll, respectively. Also note that conventionally, sway and heave are referred to the body-fixed coordinate system. In contrast, in this work, we refer to them in a

---

[1] Motions to other DOF can be excited by non-beam components of the sea state, or by large fore/aft nonsymmetries in the ship hull.

[2] The symbols Y and Z are saved to denote, respectively, forces parallel and perpendicular to water surfaces.

slightly different sense, i.e. in the wave-fixed coordinate system. The sway mode will represent the motion parallel to the local water surface and the heave mode will represent the motion perpendicular to the local water surface. This turns out to give a dynamical model that is more amenable to the analysis of interest here.

It is well known that modeling the fully nonlinear dynamics of a ship traveling on the water is a nontrivial task [64]. The difficulty comes mostly from the modeling of the force components[3] $K, \hat{Y}$, and $\hat{Z}$. In particular, an accurate measure of the contributions of hydrodynamics to these forces, especially in the presence of wave excitation, is virtually impossible to obtain. These issues will be discussed in more detail in Section 3.2. Generally speaking, each force component can be decomposed into four major parts, due to gravitation, hydrostatics, hydrodynamics, and wind, which are written as $(\cdot)_g$, $(\cdot)_{hs}$, $(\cdot)_{hd}$, $(\cdot)_w$, respectively. This decomposition is not unique but has wide acceptance. The sum of gravitational and hydrostatic forces will be called static forces and written as $(\cdot)_s$. That is,

$$(\cdot)_g + (\cdot)_{hs} = (\cdot)_s.$$

Before obtaining a general beam sea model, we shall first derive a ship model under the conditions of calm water, no damping, and no wind. Under these conditions, the hydrodynamic forces are assumed to contain only added mass contributions. In addition to this simple hydrodynamic force, the force components $K, \hat{Y}$ and $\hat{Z}$ will consist of only static forces. The effects of wave motions and hydrodynamic damping are considered later. (The motivation for this approach is that we desire a calm water model that is conservative and autonomous.)

[3] Unless otherwise stated, forces refer to generalized forces, including moments.

3.1 The Calm Water Model

3.1.1 The Static Forces

In the calm water condition, there is no horizontal static force. The vertical static force is simply the buoyancy force minus the ship weight, and the static roll moment is the buoyancy force multiplied by the righting arm GZ.

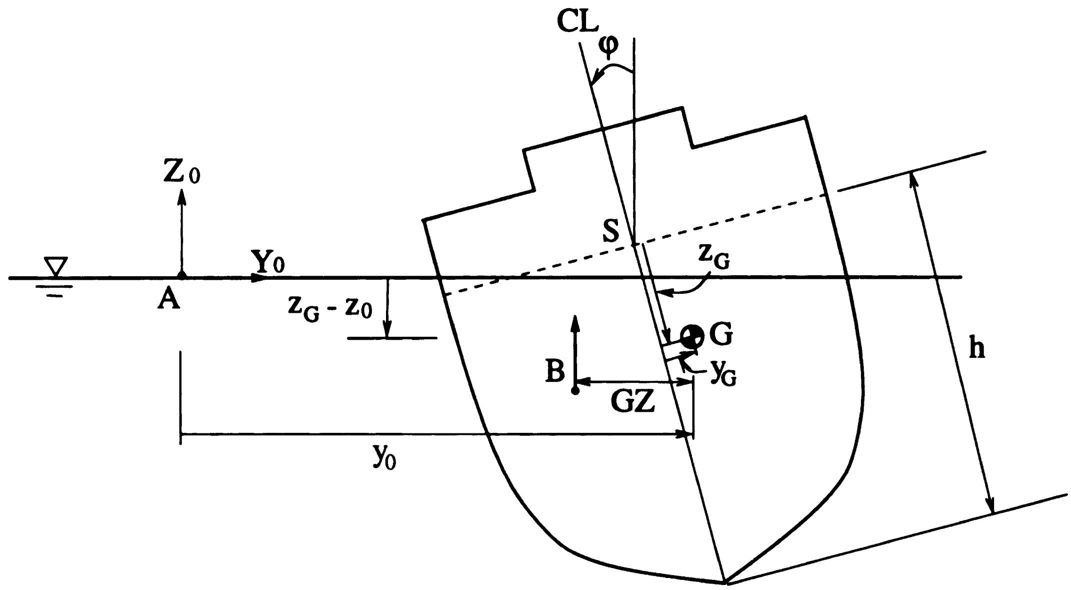

Figure 3.3: Geometry of a vessel with symmetric hull shape.

We now introduce some notations. Consider the front view of a cross section of a symmetric ship hull moving in calm water, as shown in Figure 3.3. Let A be a fixed point on the water surface and B denote the vessel's buoyancy center. S is the point fixed on the ship such that when the ship is in the upright position and S is on the water surface, the buoyancy force will be equal to the ship weight. φ is the roll angle of the vessel relative to water surface. h is the distance from S to the bottom of the vessel. y_G is the distance between G and the symmetric center line CL (y_G is positive if G is on the port side). z_G is the distance from G to the water surface when $\varphi = 0$ and S is on the water surface (z_G is positive if G is below the water line). Also, GZ

is positive if B is on the left-hand-side of G; see Figure 3.3. We attach to point A an axis system Y_0Z_0 and denote the coordinate of G in this system by $(y_0, z_0 - z_G)$.

Now consider the case where there is an unbiased CG, i.e. $y_G = 0$. Let V_0 be the volume of water displaced by the ship whose weight gives the buoyancy force, and let $R_0 = \rho V_0 - m$. Then it is clear that V_0, and hence R_0, are functions of z_0 and φ. Moreover, $R_0(z_0, \varphi)$ is even in φ and the righting arm $GZ_0(z_0, \varphi)$ is odd in φ by the symmetry of the vessel hull. Also note that $R_0(0,0) = 0$.

For the general case where y_G is not necessarily 0, it is shown in Appendix B that

$$\begin{aligned} R(z_0, \varphi) &= R_0(z_0 + y_G \sin\varphi, \varphi), \\ GZ(z_0, \varphi) &= y_G \cos\varphi + GZ_0(z_0 + y_G \sin\varphi, \varphi), \end{aligned}$$

where R and GZ represent counterparts of R_0 and GZ_0 for the general case.

Therefore, we have an expression for the static forces:

$$\begin{aligned} K_{sc}(z_0, \varphi) &= -g[m + R(z_0, \varphi)]GZ(z_0, \varphi) \\ &= -g[m + R_0(z_0 + y_G \sin\varphi, \varphi)][y_G \cos\varphi \\ &\quad + GZ_0(z_0 + y_G \sin\varphi, \varphi)], \qquad (3.4) \\ Y_{sc}(z_0, \varphi) &= 0, \qquad (3.5) \\ Z_{sc}(z_0, \varphi) &= gR(z_0, \varphi) \\ &= gR_0(z_0 + y_G \sin\varphi, \varphi), \qquad (3.6) \end{aligned}$$

where the subscript "sc" stands for the static forces in the calm water case.

3.1.2 The Equations of Motion for the Calm Water Model

Recalling that the hydrodynamic forces in this case will include only added mass contributions, we write

$$K_{hdc} = -(a_{44}\varphi'' + a_{42}y_0'' + a_{43}z_0''), \qquad (3.7)$$

$$Y_{hdc} = -(a_{24}\varphi'' + a_{22}y_0'' + a_{23}z_0''), \tag{3.8}$$

$$Z_{hdc} = -(a_{34}\varphi'' + a_{32}y_0'' + a_{33}z_0''). \tag{3.9}$$

Thus, the equations of motion can be obtained by substitution of equations (3.4)-(3.9) into equations (3.1)-(3.3) and recognizing that $\phi = \varphi$, $y_c = y_0$, and $z_c = z_0 - z_G$ under the calm water situation. This yields

$$\begin{aligned} I_{44}\varphi'' &= K_{sc}(z_0, \varphi) + K_{hdc} \\ &= K_{sc}(z_0, \varphi) - (a_{44}\varphi'' + a_{42}y_0'' + a_{43}z_0''), \end{aligned} \tag{3.10}$$

$$\begin{aligned} my_0'' &= Y_{hdc} \\ &= -(a_{24}\varphi'' + a_{22}y_0'' + a_{23}z_0''), \end{aligned} \tag{3.11}$$

$$\begin{aligned} mz_0'' &= Z_{sc}(z_0, \varphi) + Z_{hdc} \\ &= Z_{sc}(z_0, \varphi) - (a_{34}\varphi'' + a_{32}y_0'' + a_{33}z_0''). \end{aligned} \tag{3.12}$$

By introducing the transformation

$$v_0 = y_0' + \frac{a_{24}}{m_2}\varphi' + \frac{a_{23}}{m_2}z_0', \tag{3.13}$$

the equations of motion (3.10)-(3.12) can be put into the following concise form in which the new "sway" coordinate v_0 is uncoupled from roll and heave:

$$m_4\varphi'' + m_{43}z_0'' = K_{sc}(z_0, \varphi), \tag{3.14}$$

$$m_{34}\varphi'' + m_3 z_0'' = Z_{sc}(z_0, \varphi), \tag{3.15}$$

$$m_2 v_0' = 0, \tag{3.16}$$

where the system constants m_i's and m_{ij}'s are given in Table 3.1. From equations (3.14) and (3.15), one can uncouple the inertial terms in roll and heave, resulting in

$$m_0\varphi'' = m_3 K_{sc}(z_0, \varphi) - m_{43} Z_{sc}(z_0, \varphi) \stackrel{\text{def}}{=} F_4(z_0, \varphi), \tag{3.17}$$

$$m_0 z_0'' = -m_{34} K_{sc}(z_0, \varphi) + m_4 Z_{sc}(z_0, \varphi) \stackrel{\text{def}}{=} F_3(z_0, \varphi), \tag{3.18}$$

where m_0 can be found in Table 3.1.

η
η
η
η_4
η_{45}
μ_{31}
μ_{33}
μ_{42}

Table 3.1: System constants.

symbol	definition	symbol	definition
m_2	$m + a_{22}$	m_3	$m + a_{33} - \frac{a_{32}a_{23}}{m_2}$
m_4	$I_{44} + a_{44} - \frac{a_{42}a_{24}}{m_2}$	m_{43}	$a_{43} - \frac{a_{42}a_{23}}{m_2}$
m_{34}	$a_{34} - \frac{a_{32}a_{24}}{m_2}$	m_0	$m_3m_4 - m_{43}m_{34}$
c_{23}	$b_{23} - \frac{a_{23}}{m_2}b_{22}$	c_{24}	$b_{24} - \frac{a_{24}}{m_2}b_{22}$
c_{32}	$b_{32} - \frac{a_{32}}{m_2}b_{22}$	c_{33}	$b_{33} - \frac{a_{23}}{m_2}b_{32} - \frac{a_{32}}{m_2}c_{23}$
c_{34}	$b_{34} - \frac{a_{24}}{m_2}b_{32} - \frac{a_{32}}{m_2}c_{24}$	c_{42}	$b_{42} - \frac{a_{42}}{m_2}b_{22}$
c_{43}	$b_{43} - \frac{a_{23}}{m_2}b_{42} - \frac{a_{42}}{m_2}c_{23}$	c_{44}	$b_{44} - \frac{a_{24}}{m_2}b_{42} - \frac{a_{42}}{m_2}c_{24}$
β_{32}	$-m_{34}c_{42} + m_4c_{32}$	β_{33}	$-m_{34}c_{43} + m_4c_{33}$
β_{34}	$-m_{34}c_{44} + m_4c_{34}$	β_{34q}	$-m_{34}b_{44q}$
β_{42}	$m_3c_{42} - m_{43}c_{32}$	β_{43}	$m_3c_{43} - m_{43}c_{33}$
β_{44}	$m_3c_{44} - m_{43}c_{34}$	β_{44q}	m_3b_{44q}
η_{21}	$\frac{mz_G\omega_w^4a}{g}$	η_{22}	$\frac{-m\omega_w^4a}{g}$
η_{23}	$\frac{2m\omega_w^3a}{g}$	η_{24}	$\frac{m\omega_w^6a^2}{g^2}$
η_{31}	$(-m_{34}I_{44} - \frac{m_4ma_{32}-m_{34}ma_{42}}{m_2}z_G)\frac{\omega_w^4a}{g}$	η_{32}	$m_4m\frac{\omega_w^4a}{g}$
η_{33}	$\frac{(m_4ma_{32}-m_{34}ma_{42})\omega_w^4a}{m_2g}$	η_{34}	$\frac{2m_4ma_{24}\omega_w^3a}{m_2g}$
η_{35}	$\frac{-2m_4m\omega_w^3a}{m_2g}$	η_{36}	$\frac{-2m(m_4a_{32}-m_{34}a_{42})\omega_w^3a}{m_2g}$
η_{37}	$m_4mz_G\frac{\omega_w^6a^2}{g^2}$	η_{38}	$\frac{-m_4ma_{32}\omega_w^6a^2}{m_2g^2}$
η_{39}	$m_4m\frac{\omega_w^6a^2}{g^2}$	η_{41}	$(m_3I_{44} + \frac{m_{43}ma_{32}-m_3ma_{42}}{m_2}z_G)\frac{\omega_w^4a}{g}$
η_{42}	$-m_{43}m\frac{\omega_w^4a}{g}$	η_{43}	$\frac{-(m_{43}ma_{32}-m_3ma_{42})\omega_w^4a}{m_2g}$
η_{44}	$\frac{-2m_{43}ma_{24}\omega_w^3a}{m_2g}$	η_{45}	$\frac{2m_{43}m\omega_w^3a}{m_2g}$
η_{46}	$\frac{2m(m_{43}a_{32}-m_3a_{42})\omega_w^3a}{m_2g}$	η_{47}	$-m_{43}mz_G\frac{\omega_w^6a^2}{g^2}$
η_{48}	$\frac{m_{43}ma_{32}\omega_w^6a^2}{m_2g^2}$	η_{49}	$-m_{43}m\frac{\omega_w^6a^2}{g^2}$
μ_{31}	$\frac{p_2}{m_2}(-m_4a_{32} + m_{34}a_{42})$	μ_{32}	$-m_{34}p_1$
μ_{33}	m_4p_2	μ_{41}	$\frac{p_2}{m_2}(m_{43}a_{32} - m_3a_{42})$
μ_{42}	m_3p_1	μ_{43}	$-m_{43}p_2$

bi

whe

Note

in gen

have

Supp

vertical a

angle can

righting a

positive ch

the righting

we conclude

latter much

in Section 3.

Linearizing equations (3.17) and (3.18) about the stable equilibrium for the unbiased ship, $(0,0)$, yields

$$\begin{aligned} m_0\varphi'' &= -\alpha_1\varphi + \alpha_2 z_0, \\ m_0 z_0'' &= \alpha_3\varphi - \alpha_4 z_0, \end{aligned}$$

where

$$\begin{aligned} \alpha_1 = -\frac{\partial F_4(0,0)}{\partial\varphi} \quad &, \quad \alpha_2 = \frac{\partial F_4(0,0)}{\partial z_0}, \\ \alpha_3 = \frac{\partial F_3(0,0)}{\partial\varphi} \quad &, \quad \alpha_4 = -\frac{\partial F_3(0,0)}{\partial z_0}. \end{aligned}$$

Note that these constants α_i's are dependent on y_G and z_G, the position of G. Since in general m_{34} and m_{43}, the coupling inertia between heave and roll, are small, we have

$$\begin{aligned} \alpha_1 \propto -\frac{\partial K_{sc}(0,0)}{\partial\varphi} \quad &, \quad \alpha_2 \propto \frac{\partial K_{sc}(0,0)}{\partial z_0}, \\ \alpha_3 \propto \frac{\partial Z_{sc}(0,0)}{\partial\varphi} \quad &, \quad \alpha_4 \propto -\frac{\partial Z_{sc}(0,0)}{\partial z_0}. \end{aligned}$$

Suppose that the slope of the ship hull at the water line when $\phi = 0$ is near vertical as shown in Figure 3.4. Then one can see that a positive change in the roll angle can hardly affect the magnitude of buoyancy force. However, it does alter the righting arm by a negative amount. Also from Figure 3.4, it is easy to see that a positive change in z_0 will give rise to a large amount of negative buoyancy force, but the righting arm, and thus the roll moment K_{sc}, will remain unchanged. Therefore, we conclude that α_2 and α_3 are very small, and both α_1 and α_4 are positive with the latter much greater than the former. This will be important to the rescaling process in Section 3.4 below.

a

Th

unl

follo

This

eg. bu

loaded

large cr

point an

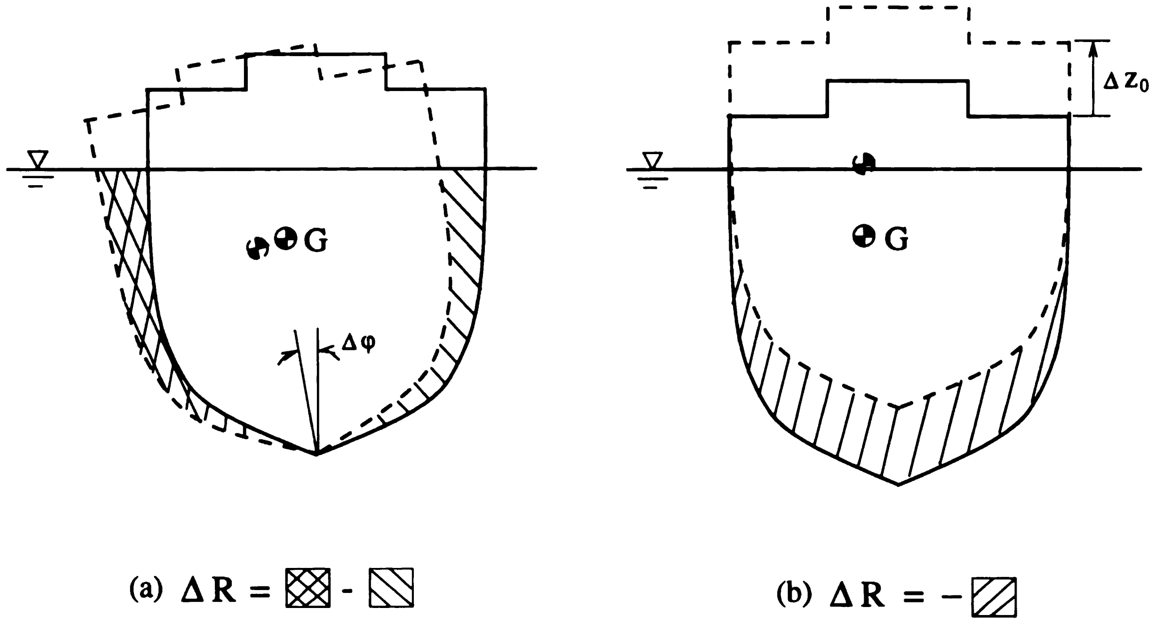

Figure 3.4: Change of buoyancy force due to (a) roll, and (b) heave displacements.

Define

$$\omega_r = \sqrt{\frac{\alpha_1}{m_0}}$$

and

$$\omega_h = \sqrt{\frac{\alpha_4}{m_0}}.$$

Then ω_r and ω_h are approximately the roll and heave natural frequencies for the unbiased vessel under the calm water conditions. The above discussions lead to the following conclusion

$$\frac{\omega_r}{\omega_h} < 1. \tag{3.19}$$

This ratio is often small, typically on the order of $1/2 \sim 1/7$. Note that ω_r depends on z_G, but ω_h does not. Therefore, the ratio will be much smaller when the vessel is fully loaded. The inequality (3.19) says that the vessel is "soft" in roll which represents a large class of ships. When the ship is biased, the origin is no longer an equilibrium point and the natural frequencies will be changed accordingly. However, the order of magnitude for each quantity will remain the same. Hence, the relationship in (3.19) is still valid for the general case.

3.2 Wave Motions, Hydrodynamic Forces and Wind Forces

In preparation for modeling the ship in beam sea conditions, the linear wave motion, hydrodynamic forces and wind forces are discussed in this section.

3.2.1 The Linear Wave Motion

As mentioned previously, the modeling of the force components in the presence of wave excitation is too complicated to be analyzed in general terms. Therefore, several assumptions must be made in order to proceed. They are:

(A1) conservation of mass,

(A2) constant fluid density,

(A3) irrotational flow,

(A4) inviscid flow,

(A5) linear free surface conditions,

(A6) the ship does not affect the wave,

(A7) water surface is a flat plane in the vicinity of the ship.

The first four assumptions are standard in potential fluid dynamics. Assumptions (A5)-(A7) usually hold for small fishing vessels in long waves. That is, the boat's w

Si

eq

Fur

Φ a

Toge

(BC1

V

(BC2)

er

equation

importan

be obtain

Unfort

in general

to nonlinea

kinematic b

width is small compared to the wavelength.

Let Φ be the velocity potential of the flow, i.e.,

$$v_f = \frac{\partial \Phi}{\partial y} \text{ and } w_f = \frac{\partial \Phi}{\partial z},$$

where v_f and w_f represents the horizontal and vertical flow velocities, respectively. Since it is a beam sea, $u_f = 0$. Then assumptions (A1)-(A3) will yield the Laplace equation for Φ:

$$\frac{\partial^2 \Phi}{\partial y^2} + \frac{\partial^2 \Phi}{\partial z^2} = 0. \tag{3.20}$$

Furthermore, with an additional assumption (A4), we have Bernoulli's equation for Φ and the pressure P:

$$\frac{P}{\rho} + \frac{\partial \Phi}{\partial t} + \frac{1}{2}\nabla\Phi \cdot \nabla\Phi + gz = 0. \tag{3.21}$$

Together with the free surface boundary conditions, namely:

(BC1) The kinematic boundary condition (a geometric constraint): the *normal* velocity of the fluid on the water surface equals that of the water surface;

(BC2) The dynamic boundary condition (a physical constraint): the pressure everywhere on the water surface is constant,

equations (3.20) and (3.21), if solved, can yield the velocity potential Φ and more importantly, the pressure P. Then, from assumption (A6), the force components can be obtained by integrating the pressure along the ship hull.

Unfortunately, equations (3.20) and (3.21) can not be solved analytically because in general the free surface conditions, which depend on the incident waves, will lead to nonlinear boundary conditions. However, if the wave slope is small, then the kinematic boundary condition (BC1) can be modified to:

(I

wh

T

and

movi

gravi

the

(BC1′) The *vertical* velocity of the fluid on the water surface equals that of the water surface,

which is the statement of assumption (A5); see Figure 3.5.

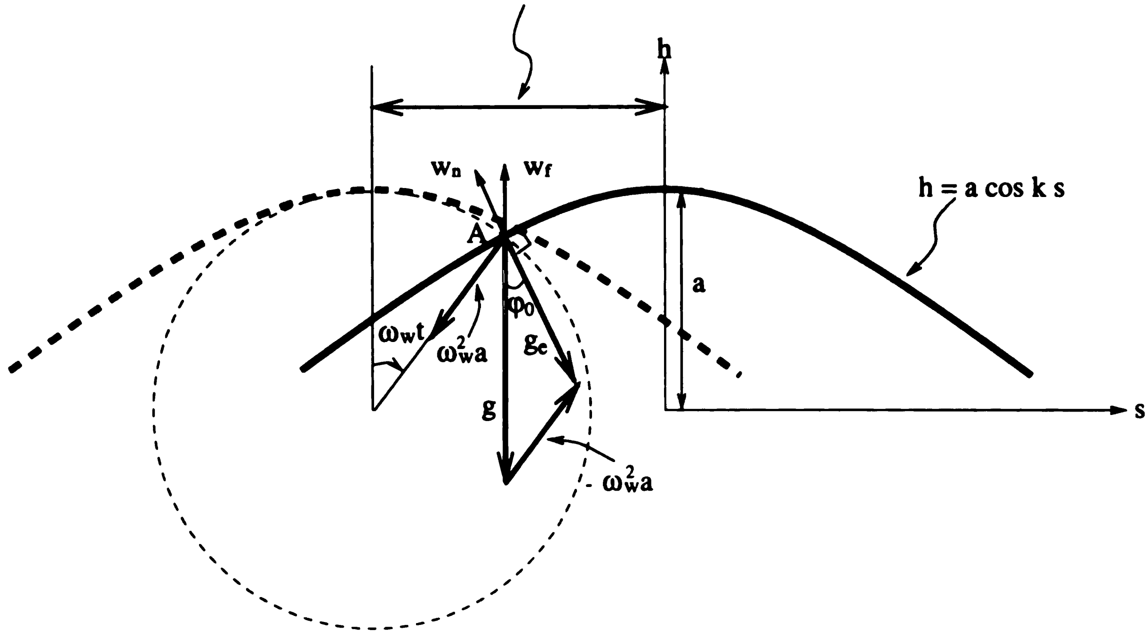

wn : normal velocity of the water particle A.
wf : vertical velocity of the water particle A.
g : usual gravitational acceleration.
ge : effective gravitational acceleration.
ω²wa : centrifugal acceleration.

Figure 3.5: Linear wave motion and effective gravitational acceleration.

Then, in the situation of periodic beam seas, one can show from equations (3.20) and (3.21) with boundary conditions (BC1′) and (BC2) that the water particle is moving in a circular path [62]. Therefore, the water particle experiences not only gravitational but also a centrifugal acceleration. The resulting acceleration is called the "effective gravitational acceleration" and is denoted by $g_e(t)$. It can be approximately expressed as

$$g_e(t) = g - \omega_w^2 a \cos \omega_w t, \tag{3.22}$$

where ω_w is the wave frequency and a is the wave amplitude. This relationship is depicted in Figure 3.5. Here we have assumed that the particle is at the peak of the wave at $t = 0$.

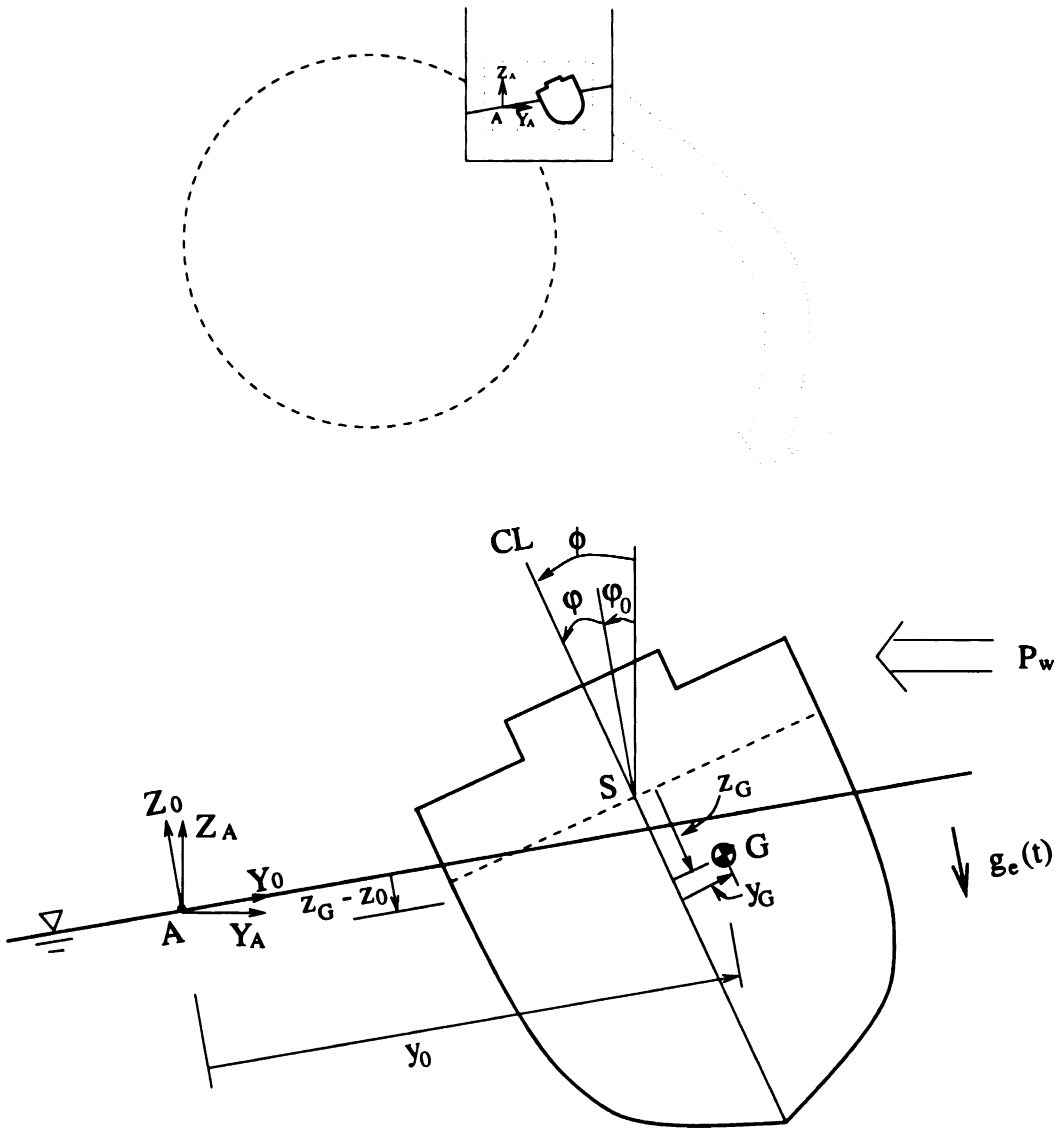

Figure 3.6: The wave-fixed coordinate frame for the vessel system.

Throughout this study, we shall observe the ship motion as if on a surface water particle. Precisely, the ship model will be derived in a coordinate system tied with a water particle; see Figure 3.6. In this coordinate system, the ship motion can be viewed as under the influence of the effective gravitational field $g_e(t)$, instead of g. By doing so, the constant hydrostatic pressure surfaces will be parallel to the water surface since $g_e(t)$ is always perpendicular to the local water surface. By assumption (A7), this surface is a flat plane, as shown in Figure 3.6. Therefore, the static forces are the same as in the calm water case, except for a small modification (i.e., replacing g by $g_e(t)$):

$$K_s = \frac{g_e(t)}{g} K_{sc}(z_0, \varphi), \tag{3.23}$$

$$Y_s = 0, \tag{3.24}$$

$$Z_s = \frac{g_e(t)}{g} Z_{sc}(z_0, \varphi). \tag{3.25}$$

One should note that under the effective gravitational field, the forces Y_i's are parallel to, and Z_i's are perpendicular to, the water plane.

3.2.2 The Hydrodynamic Forces

From equation (3.21), it is easy to see that gz represents the contribution of hydrostatic effects and $\frac{\partial \Phi}{\partial t} + \frac{1}{2}\nabla\Phi \cdot \nabla\Phi$ represents hydrodynamic contributions. Now, by introducing the effective gravitational field and replacing gz by $g_e(t)z$, the hydrostatic forces will have accounted for part of the hydrodynamic forces. Hence we will include in "hd" terms only those hydrodynamic forces proportional to acceleration and velocity (i.e., added masses and damping), except for in the roll moment K_{hd}, where, as is standard in this field, an additional quadratic damping term is included.

Thus,

$$K_{hd} = -(a_{44}\varphi'' + b_{44}\varphi' + b_{44q}\varphi'|\varphi'| + a_{42}y_0'' + b_{42}y_0' + a_{43}z_0'' + b_{43}z_0'), \quad (3.26)$$

$$Y_{hd} = -(a_{24}\varphi'' + b_{24}\varphi' + a_{22}y_0'' + b_{22}y_0' + a_{23}z_0'' + b_{23}z_0'), \quad (3.27)$$

$$Z_{hd} = -(a_{34}\varphi'' + b_{34}\varphi' + a_{32}y_0'' + b_{32}y_0' + a_{33}z_0'' + b_{33}z_0'), \quad (3.28)$$

where the hydrodynamic coefficients a_{ij}'s and b_{ij}'s can be determined either by experiment or by an approximate analytical approach, such as the strip theory commonly used in naval architecture. Note that most ships have a symmetric hull shape with respect to the $xz-$plane, resulting in $a_{ij} = a_{ji}$ and $b_{ij} = b_{ji}$. Usually, for a given vessel, these coefficients are obtained with respect to the point S in Figure 3.3, i.e., the vessel's geometric center on the calm water plane. However, in this study, they are taken with respect to the CG. The relationship between these two sets of hydrodynamic coefficients is given in Table 3.2, where those with respect to S are denoted by $\hat{a}_{ij}$'s and $\hat{b}_{ij}$'s.

Table 3.2: The relationship between two sets of hydrodynamic coefficients.

a_{22}	$\hat{a}_{22}$	$a_{23}(= a_{32})$	0
$a_{24}(= a_{42})$	$\hat{a}_{24} - \hat{a}_{22}z_G$	a_{33}	$\hat{a}_{33}$
$a_{34}(= a_{43})$	$-\hat{a}_{33}y_G$	a_{44}	$\hat{a}_{44} - 2\hat{a}_{24}z_G + \hat{a}_{22}z_G^2 + \hat{a}_{33}y_G^2$
b_{22}	$\hat{b}_{22}$	$b_{23}(= b_{32})$	0
$b_{24}(= b_{42})$	$\hat{b}_{24} - \hat{b}_{22}z_G$	b_{33}	$\hat{b}_{33}$
$b_{34}(= b_{43})$	$-\hat{b}_{33}y_G$	b_{44}	$\hat{b}_{44} - 2\hat{b}_{24}z_G + \hat{b}_{22}z_G^2 + \hat{b}_{33}y_G^2$
b_{44q}	$\hat{b}_{44q}$		

The assumptions on the hydrodynamics are the most suspect of all modeling issues used in the present study. The linearization of these loads leaves much to be desired. It would be possible to include nonlinear hydrodynamic coefficients to account for higher order effects, and the analysis would follow as presented, although a substantially larger number of coefficients would be involved. However, even the linear coefficients are not well known for most hull shapes, and virtually nothing is known about nonlinear terms. Furthermore, more accurate modeling would need to account for the memory effects associated with the hydrodynamic loads [27].

3.2.3 The Wind Forces

Assume that the wind is steady in the horizontal direction with a constant wind pressure P_w; see Figure 3.6. Assume also that since the heave displacement is small, the area exposed to the wind is constant. The wind force can then be expressed as

$$K_w = p_1 \cos^2 \phi, \tag{3.29}$$

$$Y_w = p_2 \cos \phi \cos \varphi_0 \approx p_2 \cos \phi, \tag{3.30}$$

$$Z_w = p_2 \cos \phi \sin \varphi_0 \approx p_2 \varphi_0 \cos \phi, \tag{3.31}$$

where p_1 and p_2 are constants, and $\varphi_0 = \frac{\omega_w^2 a}{g} \sin \omega_w t$ is the angle of water surface relative to the horizontal plane, which is assumed to be small; see Figure 3.6.

3.2.4 Remarks

The idea of using an effective gravitational field and the ship motion modeling that follows from it are not new. Basically, we follow the work of Thompson *et al.* [61]. However, the derivation in their work was heuristic, whereas we have put it on a solid footing. Moreover, they did not include any hydrodynamic coupling effects, allowing them to arrive at a simple one DOF roll model.

3.3 The General Ship Model in Regular Beam Seas

With the preliminary results established in previous sections, we are now in a position to derive a general model for ship motions in regular beam sea conditions.

Figure 3.6 shows the coordinate systems used in the analysis. Both the $Y_A Z_A$ and $Y_0 Z_0$ coordinate systems are tied with a water particle A on the water plane, which is moving along a circle. $Y_A Z_A$ is a nonrotational frame. Hence, it can be regarded as an inertial, lab-fixed coordinate system if one recognizes the effective gravitational field in this system. $Y_0 Z_0$ is a wave-fixed frame rotating with the water plane.

It should be clear that the calm water model is valid only in the $Y_0 Z_0$ frame. (As one can see, the water is "at rest" with respect to $Y_0 Z_0$.) Also, the force components given in equations (3.23)-(3.31) are all parallel to the axes of the $Y_0 Z_0$ system.

The time derivative of a quantity in the $Y_0 Z_0$ system is related to that in the inertial $Y_A Z_A$ system by

$$(\cdot)'_A = (\cdot)'_0 + \varphi'_0 \times (\cdot), \tag{3.32}$$

where the subscripts indicate the respective frames and φ'_0 is the angular velocity of $Y_0 Z_0$. The position vector of the center of gravity G in $Y_0 Z_0$ is

$$\vec{r}_G = y_0 \vec{j}_0 + (z_0 - z_G)\vec{k}_0,$$

where $\vec{j}_0$ and $\vec{k}_0$ are the unit bases for $Y_0 Z_0$. Then by equation (3.32), we obtain the acceleration

$$(\vec{r}_G)''_A = [y_0'' - \varphi_0''(z_0 - z_G) - \varphi_0'(2z_0' + \varphi_0' y_0)]\vec{j}_0 + [z_0'' + \varphi_0'' y_0 + \varphi_0'(2y_0' + \varphi_0'(z_0 - z_G))]\vec{k}_0.$$

Therefore, the dynamics of the 3 DOF beam sea model can be written as

$$\begin{aligned} I_{44}\phi'' &= K = K_s + K_{hd} + K_w, \\ m[y_0'' - \varphi_0''(z_0 - z_G) - \varphi_0'(2z_0' + \varphi_0' y_0)] &= Y = Y_s + Y_{hd} + Y_w, \\ m[z_0'' + \varphi_0'' y_0 + \varphi_0'(2y_0' + \varphi_0'(z_0 - z_G))] &= Z = Z_s + Z_{hd} + Z_w, \end{aligned}$$

where the K_i's, Y_i's, and Z_i's are given by equations (3.23)-(3.31). Again, by the transformation (3.13), the above equations can be rewritten in a form similar to (3.14)-(3.16):

$$\begin{aligned} m_4\varphi'' + m_{43}z_0'' &= K_s - I_{44}\varphi_0'' - \frac{a_{42}}{m_2}Y_e + K_w - \frac{a_{42}}{m_2}Y_w \\ &\quad - (c_{44}\varphi' + b_{44q}\varphi'|\varphi'| + c_{42}v_0 + c_{43}z_0'), \end{aligned} \tag{3.33}$$

$$m_2 v_0' = Y_e + Y_w - (c_{24}\varphi' + b_{22}v_0 + c_{23}z_0'), \tag{3.34}$$

$$\begin{aligned} m_{34}\varphi'' + m_3 z_0'' &= Z_s + Z_e - \frac{a_{32}}{m_2}Y_e + Z_w - \frac{a_{32}}{m_2}Y_w \\ &\quad - (c_{34}\varphi' + c_{32}v_0 + c_{33}z_0'), \end{aligned} \tag{3.35}$$

where the c_{ij} coefficients can be found in Table 3.1 and

$$\begin{aligned} Y_e &= m[\varphi_0''(z_0 - z_G) + 2\varphi_0' z_0' + \varphi_0'^2 y_0)], \\ Z_e &= m[-\varphi_0'' y_0 - 2\varphi_0'(v_0 - \frac{a_{24}}{m_2}\varphi' - \frac{a_{23}}{m_2}z_0') + \varphi_0'^2(z_0 - z_G))]. \end{aligned}$$

Finally, the equations of motion can be obtained from equations (3.33)-(3.35) and are given below:

$$m_0\varphi'' = \frac{g_e(t)}{g}F_4(z_0, \varphi) + D_4(\varphi', v_0, z_0')$$

$$+ E_4(\varphi', v_0, z_0', y_0, z_0, t) + W_4(\varphi, t), \tag{3.36}$$

$$m_2 v_0' = D_2(\varphi', v_0, z_0') + E_2(z_0', y_0, z_0, t) + W_2(\varphi, t), \tag{3.37}$$

$$\begin{aligned} m_0 z_0'' &= \frac{g_e(t)}{g} F_3(z_0, \varphi) + D_3(\varphi', v_0, z_0') \\ &\quad + E_3(\varphi', v_0, z_0', y_0, z_0, t) + W_3(\varphi, t), \end{aligned} \tag{3.38}$$

where F_4 and F_3 are given in equations (3.17) and (3.18), and

$$\begin{aligned}
D_4 &= -\beta_{44}\varphi' - \beta_{44q}\varphi'|\varphi'| - \beta_{42}v_0 - \beta_{43}z_0', \\
D_2 &= -c_{24}\varphi' - b_{22}v_0 - c_{23}z_0', \\
D_3 &= -\beta_{34}\varphi' - \beta_{34q}\varphi'|\varphi'| - \beta_{32}v_0 - \beta_{33}z_0', \\
E_4 &= (\eta_{41} + \eta_{42}y_0 + \eta_{43}z_0)\sin\omega_w t + (\eta_{44}\varphi' + \eta_{45}v_0 \\
&\quad + \eta_{46}z_0')\cos\omega_w t + (\eta_{47} + \eta_{48}y_0 + \eta_{49}z_0)\cos^2\omega_w t, \\
E_2 &= (\eta_{21} + \eta_{22}z_0)\sin\omega_w t + \eta_{23}z_0'\cos\omega_w t + \eta_{24}y_0\cos^2\omega_w t, \\
E_3 &= (\eta_{31} + \eta_{32}y_0 + \eta_{33}z_0)\sin\omega_w t + (\eta_{34}\varphi' + \eta_{35}v_0 \\
&\quad + \eta_{36}z_0')\cos\omega_w t + (\eta_{37} + \eta_{38}y_0 + \eta_{39}z_0)\cos^2\omega_w t, \\
W_4 &= \mu_{41}\cos\phi + \mu_{42}\cos^2\phi + \mu_{43}\varphi_0\cos\phi, \\
W_2 &= p_2\cos\phi, \\
W_3 &= \mu_{31}\cos\phi + \mu_{32}\cos^2\phi + \mu_{33}\varphi_0\cos\phi,
\end{aligned}$$

and where the coefficients β_{ij}'s, η_{ij}'s, and μ_{ij}'s are also collected in Table 3.1. In the equations of motion, the F_i's are the restoring forces due to hydrostatics and ship weight, the D_i's are the hydrodynamic damping, the E_i's contain excitation terms due to wave motion, and the W_i's include the wind forces.

3.4 Singular Perturbation Formulation

The present system, described by equations (3.36)-(3.38), is too complicated for a direct attack by analysis. This section is devoted to the purpose of a systematic simplification by exploiting some special features of this dynamical system.

First of all, the heave natural frequency is in general significantly higher than the roll natural frequency, as stated in (3.19). The ratio of heave frequency to roll frequency is about 2.5 for the unloaded clam dredge *Patti-B* and is significantly larger when fully loaded. It can also be much larger for other fishing vessels.

Secondly, heave displacements (modulus wave amplitude) z_0 are usually small compared to vessel geometry. Thus we have

$$|z_0| \ll h. \tag{3.39}$$

Furthermore, by the smallness of z_0, we can simplify the restoring forces F_i's by expanding them in a series of z_0 as follows:

$$F_4(z_0, \varphi) = \alpha_1[f_1(\varphi) + f_2(\varphi)\frac{z_0}{h} + O((\frac{z_0}{h})^2)], \tag{3.40}$$

$$F_3(z_0, \varphi) = \alpha_1 h[f_3(\varphi) + f_4(\varphi)\frac{z_0}{h} + O((\frac{z_0}{h})^2)], \tag{3.41}$$

where

$$\begin{aligned} f_1(\varphi) &= \frac{F_4(0,\varphi)}{\alpha_1}, \\ f_2(\varphi) &= \frac{h}{\alpha_1}\frac{\partial F_4(0,\varphi)}{\partial z_0}, \\ f_3(\varphi) &= \frac{F_3(0,\varphi)}{\alpha_1 h}, \\ f_4(\varphi) &= \frac{1}{\alpha_1}\frac{\partial F_3(0,\varphi)}{\partial z_0}, \end{aligned}$$

are dimensionless functions. This step amounts to extracting the leading order contributions from the restoring forces and decomposing them into two classes: those independent of the vertical position (the first terms in (3.40) and (3.41)) and those due to incremental changes in the vertical position (the second terms in (3.40) and (3.41)). Considering equations (3.17) and (3.18) and recalling that m_{34} and m_{43} are small, one can interpret F_4 as the static roll moment and F_3 as the static vertical force. By the argument given at the end of Section 3.1.2, we know that the vertical force is much more sensitive to z_0 than is the roll moment. Therefore, $f_4(\varphi)$ is a relatively large negative quantity for any fixed roll angle φ, and

$$|f_3(\varphi)| \ll |f_4(\varphi)|. \tag{3.42}$$

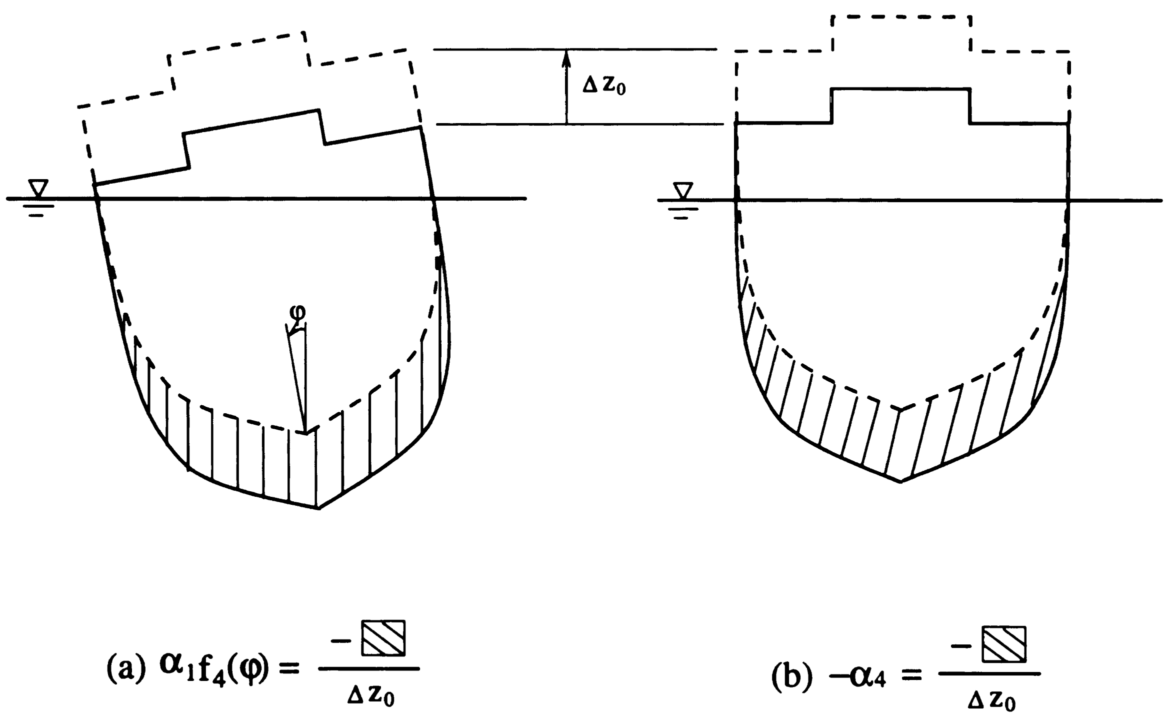

Figure 3.7: Physical interpretation of equation (3.43).

Moreover, $f_4(\varphi)$ can be further expanded as follows

$$f_4(\varphi) = -\frac{\alpha_4}{\alpha_1} + f_5(\varphi), \tag{3.43}$$

where $f_5(\varphi) = \frac{1}{\alpha_1}[\frac{\partial F_3}{\partial z_0}(0,\varphi) - \frac{\partial F_3}{\partial z_0}(0,0)]$ satisfies $f_5(0) = 0$. Recall that $\alpha_4 = -\frac{\partial F_3}{\partial z_0}(0,0)$, which is much larger than $\alpha_1 = -\frac{\partial F_4}{\partial \varphi}(0,0)$. Physically, the relation in (3.43) is demonstrated in Figure 3.7, as now described. Note that

$$f_4(\varphi) = \frac{1}{\alpha_1}\frac{\partial F_3(0,\varphi)}{\partial z_0} \propto \frac{\partial Z_{sc}(0,\varphi)}{\partial z_0} \propto \frac{\partial R(0,\varphi)}{\partial z_0},$$

which is the sensitivity of the buoyancy force to z_0 at a roll angle of φ. Note also that α_4 is simply this quantity at zero roll angle:

$$-\alpha_4 \propto \frac{\partial R(0,0)}{\partial z_0}.$$

Hence the shaded area in Figure 3.7(a) corresponds to $\alpha_1 f_4(\varphi)$ and that in Figure 3.7(b) to $-\alpha_4$. The difference between them is that corresponding to $\alpha_1 f_5(\varphi)$. It should be clear now that $f_5(\varphi)$ makes only a minor contribution to $f_4(\varphi)$. Thus, it is assumed that

$$|f_5(\varphi)| \ll \frac{\alpha_4}{\alpha_1}. \tag{3.44}$$

Also, in terms of α_1 and α_4, (3.42) can be expressed as

$$|f_3(\varphi)| \ll \frac{\alpha_4}{\alpha_1}. \tag{3.45}$$

Finally, in practice the wave excitation, hydrodynamic dampiñg (except for the heave damping), and wind forces are small compared to the inertial terms. Specifically, we have the following relationships

$$\omega_w^2 a \ll g, \tag{3.46}$$

$$|D_2| \ll mg \quad \text{and} \quad |D_3|, |D_4| \ll m^2 gh \text{ (except for } \beta_{33} z_0' \text{ in } D_3) \tag{3.47}$$

$$|p_1| \ll mgh \quad \text{and} \quad |p_2| \ll mg. \tag{3.48}$$

Hence, the equations of motion derived in the calm water case, namely equations (3.16)-(3.18), are taken to be the dominant terms in equations (3.36)-(3.38).

It is interesting to note that the sway displacement y_0 does not appear in the calm water model, as it is immaterial to the nature of the system dynamics. In terms of dynamics, the sway variable is said to be an *ignorable coordinate* under calm water conditions. However, this is not the case when the waves are introduced. As one can see, y_0 does show up in equations (3.36)-(3.38). Nevertheless, it will be shown in the sequel that all terms containing y_0 can be pushed out to higher orders in the analysis through rescaling, since they are induced by wave excitation.

Therefore, a singularly perturbed form is expected for the equations of motion if they are properly nondimensionalized and rescaled. In this form, the heave motion will be significantly stiffer, and thus faster, than the roll motion. Indeed, by the following change of variables and scaling of parameters, based on equations (3.19) and (3.39):

$$\frac{\omega_h}{\omega_r} = \epsilon^{-1}\bar{\omega}, \quad \frac{\omega_w}{\omega_r} = \Omega, \quad \tau = \omega_r t,$$
$$\frac{v_0}{\omega_r h} = \bar{v}, \quad \frac{z_0}{h} = \epsilon\bar{z}, \quad (\dot{\cdot}) = \frac{d}{d\tau}(\cdot),$$

and using the relationships (3.40)-(3.48), equations (3.36)-(3.38) can be transformed into the following form:

$$\dot{x}_1 = x_2, \tag{3.49}$$

$$\dot{x}_2 = f_1(x_1) + \epsilon g_1(x_1, x_2, y, z_1, z_2, \tau, \epsilon), \tag{3.50}$$

$$\dot{y} = \epsilon g_2(x_1, x_2, y, z_2, \tau, \epsilon), \tag{3.51}$$

$$\epsilon\dot{z}_1 = z_2, \tag{3.52}$$

$$\epsilon \dot{z}_2 = -\bar{\omega}^2 z_1 - \delta_{33} z_2 + \epsilon g_3(x_1, x_2, y, z_1, z_2, \tau, \epsilon), \tag{3.53}$$

where $x_1 = \varphi,\ x_2 = \dot{\varphi},\ y = \bar{v},\ z_1 = \bar{z},\ z_2 = \epsilon \dot{\bar{z}}$, and

$$\begin{aligned} g_1(x_1, x_2, y, z_1, z_2, \tau, \epsilon) &= \sigma_{41} \cos x_1 + \sigma_{42} \cos^2 x_1 + f_2(x_1) z_1 - \delta_{44} x_2 - \delta_{44q} x_2 |x_2| \\ &\quad - \delta_{42} y - \delta_{43} z_2 - \lambda f_1(x_1) \cos \Omega\tau + \gamma_{41} \sin \Omega\tau + O(\epsilon), \\ g_2(x_1, x_2, y, z_2, \tau, \epsilon) &= \sigma_{21} \cos x_1 - \delta_{24} x_2 - \delta_{22} y - \delta_{23} z_2 \\ &\quad + \gamma_{23} z_2 \cos \Omega\tau + \gamma_{21} \sin \Omega\tau + O(\epsilon), \\ g_3(x_1, x_2, y, z_1, z_2, \tau, \epsilon) &= f_3(x_1) + \sigma_{31} \cos x_1 - \delta_{34} x_2 - \delta_{32} y \\ &\quad + \lambda \bar{\omega}^2 z_1 \cos \Omega\tau + O(\epsilon), \end{aligned}$$

and where the nondimensional coefficients λ, σ_{ij}'s, δ_{ij}'s, and γ_{ij}'s are given in Table 3.3. Here we have used the unperturbed natural frequencies ω_r and ω_h as the rescaling basis. This is valid since the relative magnitudes of the heave and roll frequencies will remain the same even when the perturbations are introduced. It is important to note that if the small perturbations g_i's are omitted, the system will reduce to the calm water model, equations (3.16)-(3.18), as pointed out previously.

It follows from equations (3.49)-(3.53) that the coupled roll/sway motion lies on a slow manifold which is determined to be given by

$$z_1 = \epsilon \bar{\omega}^{-2} [f_3(x_1) + \sigma_{31} \cos x_1 - \delta_{34} x_2 - \delta_{32} y] + O(\epsilon^2), \tag{3.54}$$

$$z_2 = O(\epsilon^2). \tag{3.55}$$

This is a surface in the phase space which accounts for the quasi-static heave displacements induced by roll and sway motion, but it does not include any heave dynamics. Perturbations away from this manifold represent the small amplitude,

Table 3.3: Nondimensional coefficients.

symbol	definition	symbol	definition
$\epsilon\lambda$	$\frac{\omega_w^2 a}{g}$	$\epsilon\gamma_{21}$	$\frac{\eta_{21}}{m_2\omega_r^2 h}$
$\epsilon\gamma_{23}$	$\frac{\eta_{23}}{m_2\omega_r}$	$\epsilon\gamma_{41}$	$\frac{\eta_{41}}{\alpha_1}$
$\epsilon\sigma_{21}$	$\frac{p_2}{m_2\omega_r^2}$	$\epsilon\sigma_{31}$	$\frac{\mu_{31}}{\alpha_1 h}$
$\epsilon\sigma_{41}$	$\frac{\mu_{41}}{\alpha_1}$	$\epsilon\sigma_{42}$	$\frac{\mu_{42}}{\alpha_1}$
$\epsilon\delta_{22}$	$\frac{b_{22}}{m_2\omega_r}$	$\epsilon\delta_{23}$	$\frac{c_{23}}{m_2\omega_r}$
$\epsilon\delta_{24}$	$\frac{c_{24}}{m_2\omega_r h}$	δ_{32}	$\frac{\beta_{32}}{m_0\omega_r}$
$\epsilon^{-1}\delta_{33}$	$\frac{\beta_{33}}{m_0\omega_r}$	δ_{34}	$\frac{\beta_{34}}{m_0\omega_r h}$
$\epsilon\delta_{42}$	$\frac{\beta_{42}h}{m_0\omega_r}$	$\epsilon\delta_{43}$	$\frac{\beta_{43}h}{m_0\omega_r}$
$\epsilon\delta_{44}$	$\frac{\beta_{44}}{m_0\omega_r}$	$\epsilon\delta_{44q}$	$\frac{\beta_{44q}}{m_0}$

fast, and heavily damped heave motions. Such responses will quickly come onto the roll/sway manifold, where the dynamics are significantly slower. (For a more thorough treatment of such problems, see the work of Georgiou and co-workers [21].)

Using the global center manifold theorem ([7], [21]), it can be shown that this slow manifold exists globally up to the angles of vanishing stability for sufficiently small ϵ. Furthermore, it can also be shown that the slow manifold is locally attractive ([21], [31]). In other words, within the angles of vanishing stability, trajectories in the state space will eventually approach the slow invariant manifold which describes the roll/sway motion; see Figure 3.8.

The dynamics on the slow manifold can be obtained by inserting equations (3.54) and (3.55) into equations (3.49)-(3.51), which yields

$$\dot{x}_1 = x_2, \tag{3.56}$$

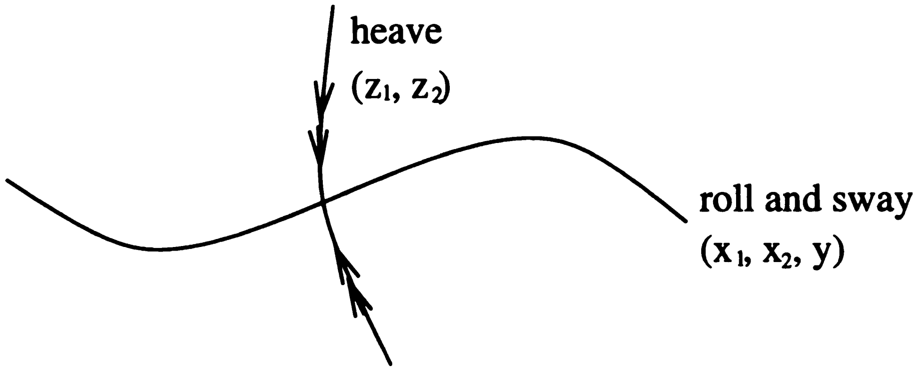

Figure 3.8: Schematic diagram of the slow and fast manifold.

$$\dot{x}_2 = f_1(x_1) + \epsilon\hat{g}_1(x_1, x_2, y, \tau, \epsilon), \tag{3.57}$$

$$\dot{y} = \epsilon\hat{g}_2(x_1, x_2, y, \tau, \epsilon), \tag{3.58}$$

where

$$\begin{aligned} \hat{g}_1(x_1, x_2, y, \tau, \epsilon) &= \sigma_{41}\cos x_1 + \sigma_{42}\cos^2 x_1 - \delta_{44}x_2 - \delta_{44q}x_2|x_2| - \delta_{42}y \\ &\quad - \lambda f_1(x_1)\cos\Omega\tau + \gamma_{41}\sin\Omega\tau + O(\epsilon), \\ \hat{g}_2(x_1, x_2, y, \tau, \epsilon) &= \sigma_{21}\cos x_1 - \delta_{24}x_2 - \delta_{22}y + \gamma_{21}\sin\Omega\tau + O(\epsilon). \end{aligned}$$

One can see from equations (3.49)-(3.58) that up to $O(\epsilon)$, the sway displacement y_0 does not appear, indicating that all terms with y_0 are of order ϵ^2 or higher, as claimed earlier. This implies that sway still behaves like an ignorable coordinate to first order, even in the presence of wave excitation.

CHAPTER 4

CAPSIZING CRITERION BY CHAOTIC TRANSPORT THEORY

We now turn to the vessel capsizing problem for the 3-DOF model. The main tool we are using is the theory of phase space transport [67]. It has been successfully used for proposing capsizing criteria for single DOF ship models ([13], [23], [27]). In those studies, ship capsizing is characterized in phase space by the escape of a solution trajectory from the safe region into the unsafe one under the action of wave excitation. In order to study our 3-DOF ship capsizing problem using the same concept, some general background and its application to capsize are provided in Section 4.1 for 1-DOF roll models, in which sway and heave are simply ignored. In Section 4.2, the difficulty in applying chaotic transport theory to slowly varying oscillators is discussed, and an approach using the fast invariant manifold concept is introduced. We then apply the results of Sections 4.1 and 4.2 to the ship dynamic model to propose a capsizing criterion in Section 4.3. In Section 4.4, the proposed capsizing criterion is compared with those obtained from 1-DOF roll models to examine the coupling effects from sway and heave motions.

4.1 Phase Space Transport for 1-DOF Roll Models

From equation (3.33), the 1-DOF roll model is obtained simply by setting v_0 and z_0 to zero, yielding

$$(I_{44} + a_{44})\varphi'' + b_{44}\varphi' + b_{44q}\varphi'|\varphi'| + \frac{g_e(t)}{g}k(\varphi) = f(t), \tag{4.1}$$

where $k(\varphi) = K_{sc}(0, \varphi)$ is the static restoring moment and $f(t) = -I_{44}\varphi_0''(t)$ is the wave excitation. Here, without loss of generality, the wind force is also neglected for the sake of brevity. The unperturbed system is that for which the roll damping, b_{44} and b_{44q}, and wave excitation, $f(t)$, are zero and $g_e(t) \equiv g$ in equation (4.1).

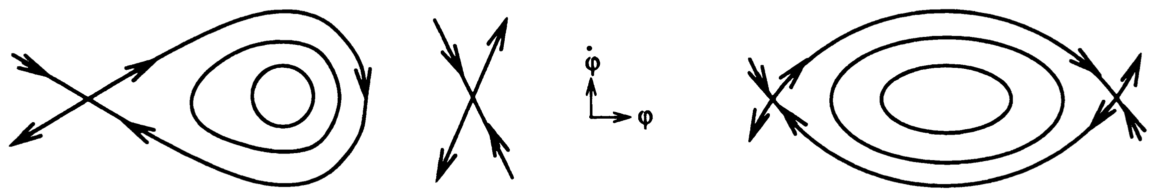

(a) biased model

(b) unbiased model

Figure 4.1: The unperturbed structure for 1-DOF ship models.

Figure 4.1 shows the structures of the unperturbed 1-DOF roll model with and without bias in phase space (for the Poincaré map). Both cases possess two fixed points of saddle type which are referred to as "the angles of vanishing stability" and one fixed point of center type between the saddles, representing the upright equilibrium position. The biased system has a homoclinic orbit connecting to one saddle point and encircling the center, whereas the unbiased system has a heteroclinic cycle connecting the two saddle points and also encircling the center. The safe region is defined to be the one bounded by the homoclinic orbit for the biased system or by the heteroclinic cycle for the case of the unbiased model. This is because every initial condition located in those regions will lead to a bounded oscillatory motion. Outside those regions, the motion will be unbounded, corresponding to capsize.

As the damping is brought in, the homoclinic and heteroclinic orbits will break and the center type fixed point will become stable, as shown in Figure 4.2. Note that Figures 4.1 and 4.2 can be regarded either as trajectories for the flow, or as those for the Poincaré map since they represent autonomous systems. In order to be consistent and comparable with the following figures, we shall consider them to be

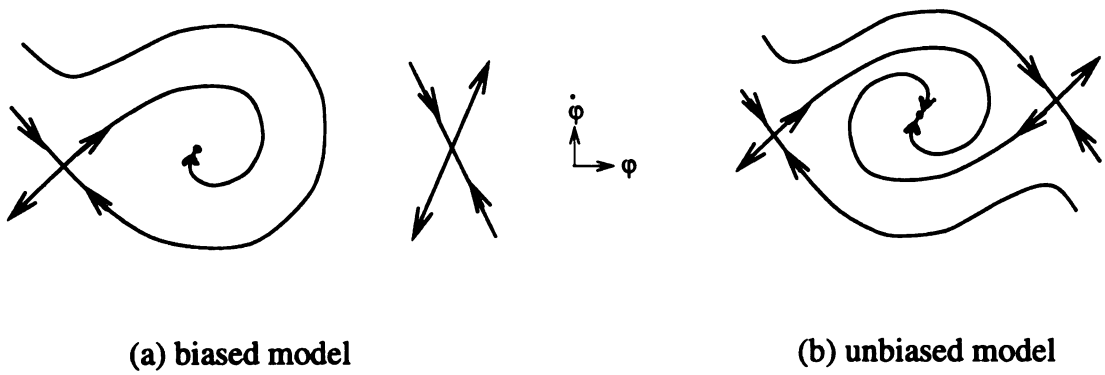

Figure 4.2: The structure for 1-DOF, damped ship models.

for mappings in which the states are sampled once per period of the forcing.

Figure 4.3 depicts the situation when the wave excitation is turned on with increasing amplitudes. One can see that the stable and unstable manifolds of the saddle points are distorted. For small enough wave amplitudes, the system's behavior is qualitatively the same as in Figure 4.2; see Figures 4.3(a) and 4.3(b). When the wave amplitude passes a critical value, which depends on the damping coefficients and wave frequency, the stable and unstable manifolds of the saddles will will intersect, resulting in homoclinic or heteroclinic tangles; see Figures 4.3(c) and 4.3(d).

Unlike the case without tangles, where the evolution of any initial condition is clear, the long-term behavior of systems with tangles is unpredictable due to the horseshoe structure and fractal basin boundaries resulting from the homoclinic and heteroclinic tangles. The mechanism and dynamics leading to these phenomena are relatively complicated. Let us take the homoclinic case as an example. The situation for heteroclinic case is virtually the same.

It is obvious that there exist homoclinic tangencies at a parameter value somewhere between those in Figures 4.3(a) and 4.3(c). As a consequence, an infinite sequence of saddle node and period doubling bifurcations will occur just before the homoclinic tangency occurs ([22], [66]). Moreover, due to the results of Newhouse ([47], [66]), the homoclinic tangency persists in a neighborhood of the major homo-

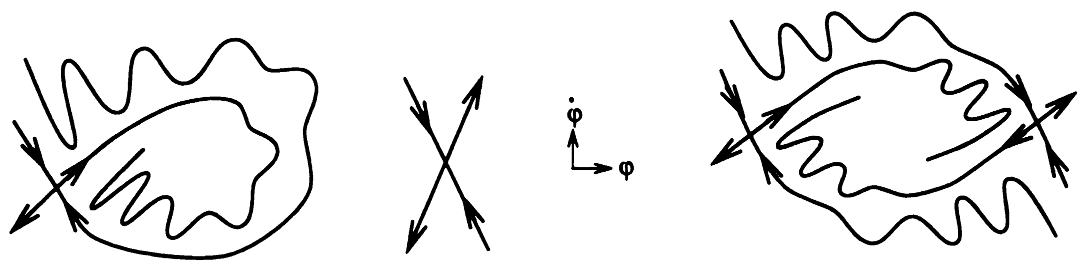

(a) biased, small amplitude

(b) unbiased, small amplitude

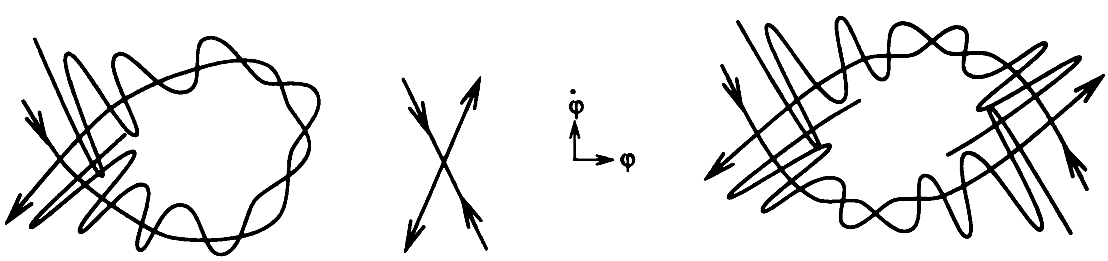

(c) biased, larger amplitude

(d) unbiased, larger amplitude

Figure 4.3: The structures for 1-DOF ship models with increasing wave amplitudes.

clinic bifurcation point. In other words, if a homoclinic tangency is destroyed by slightly shifting the parameter, another will be created elsewhere in the homoclinic tangle [66]. This implies that there are infinitely many periodic attractors coexisting with the horseshoe structure around the homoclinic bifurcation point ([47], [66]). Therefore, the safe region, i.e. the transient basin of attraction of the stable fixed point (in unperturbed system), will be eroded by these periodic attractors, making its boundary fractal-like [57].

Thompson *et al.* [61] have proposed a capsizing criterion called *index of capsizability* by numerically quantifying the erosion of fractal safe basins. While such a numerical approach can yield accurate results, it has some serious drawbacks. It is time consuming and problem dependent. Their method provides no analytical estimates for the index. It must be computed on a case-by-case basis. Also, when the system's DOF increases, the time spent on the calculations can grow unreasonably large. Therefore, it is not suitable for multi-DOF systems like the present model. On the other hand, based on chaotic transport theory, Shaw and co-workers were able to propose analytical capsizing criteria for periodic and random seas ([13], [23], [27]). Their basic ideas with some new results are summarized below and will be followed in this study.

Although the long-term prediction of the behavior for systems with tangles is seemingly impossible, the system's short-term evolution can be predicted using the techniques of lobe dynamics. In Figure 4.4, an enlarged version of Figure 4.3(c), the homoclinic point r is called a *primary intersection point* [67]. The segment $\widehat{sr} \cup \widehat{rs}$ is referred to as the *pseudoseparatrix.* The *safe region* for the perturbed system is defined to be the interior of the pseudoseparatrix. The bounded regions L_i's in this phase space of the Poincare map are called *lobes.* The arrows relating the lobes in the figure designate the mapping direction. For instance, L_{-2} is mapped to L_0, which is mapped to L_2, which is mapped to L_4, and so on.

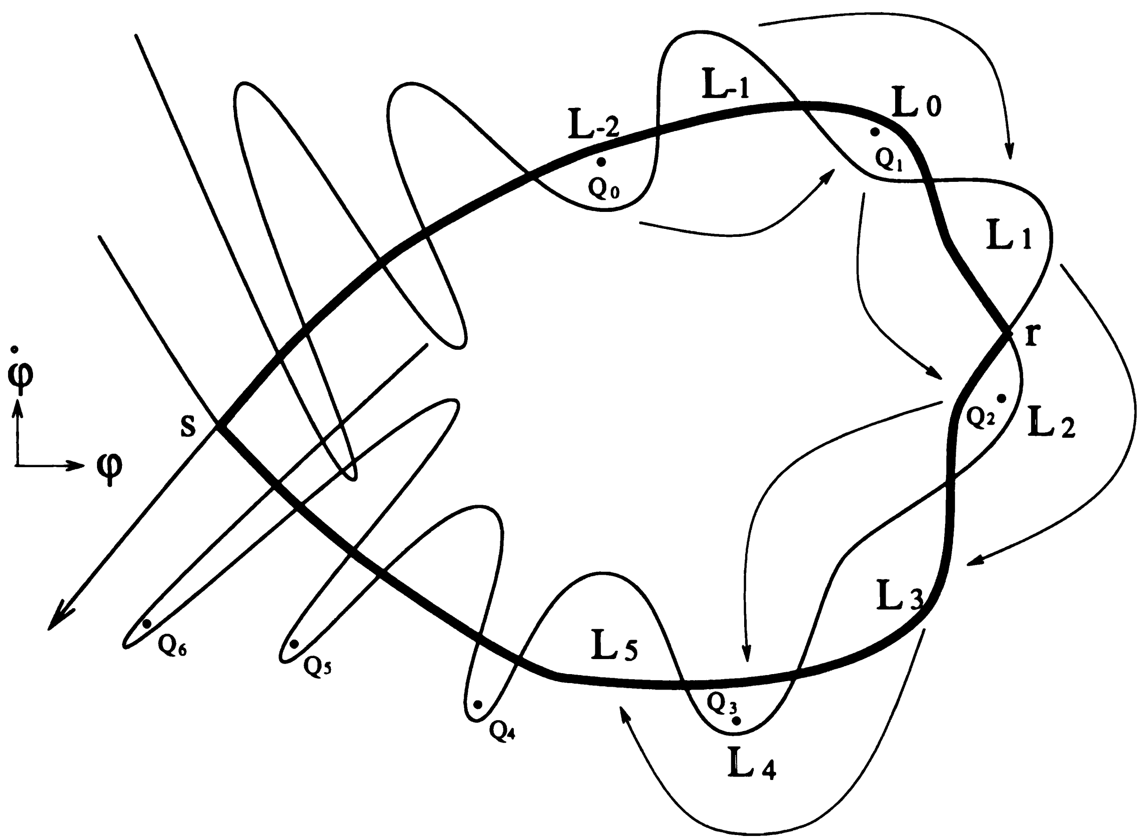

Figure 4.4: The pseudoseparatrix (the bold lines) and the lobes.

It is clear that when the homoclinic tangle exists, some points initially located in the safe region can be mapped to the unsafe region, leading to capsize. Point Q_0 in Figure 4.4 is such an example. The physical situation is that the vessel slowly rolls over to one side with small oscillations modulated on this main motion. The small oscillations have approximately the same frequency as the excitation. Figure 4.5 illustrates this scenario.

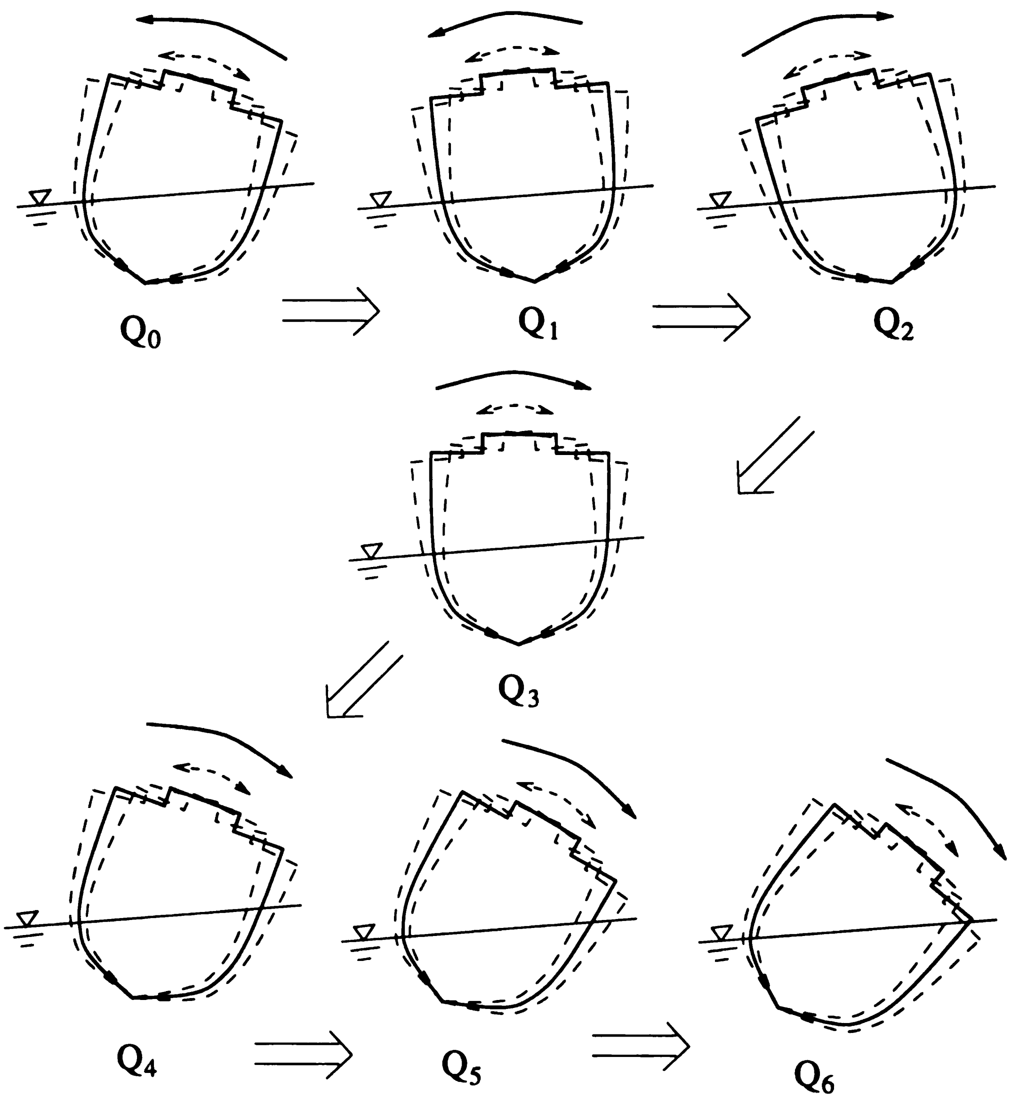

Figure 4.5: The scenario for chaotic transport leading to capsize.

One can show that the only points which are transported from the safe region to the unsafe one under one period of excitation are those in L_0 [67]. This particular lobe is called a *turnstile* lobe, and for $\epsilon \ll 1$ its area is related to the associated Melnikov function [67]. Referring to Figure 4.6, this relationship is given by

$$\mu(L_0) = \epsilon \int_0^T M^+(\theta, \phi_0) d\theta + O(\epsilon^2) = \epsilon \int_{\theta_1}^{\theta_2} M(\theta, \phi_0) d\theta + O(\epsilon^2), \tag{4.2}$$

where $\mu(L_0)$ represents the area of the set L_0, M^+ denotes the positive part of the Melnikov function, θ is the time parameter on the unperturbed homoclinic/heteroclinic orbit $q_0(t)$, ϕ_0 is the phase difference with respect to the excitation, ϵ is the order of the perturbations and T is the period of the excitation. This area, $\mu(L_0)$, is that of the lobe containing point Q_1 in Figure 4.4. By equation (4.2), every other lobe has the same area as L_0 up to $O(\epsilon)$ since the Melnikov function is periodic in θ. (Note that these lobe areas are affected by the system dissipation, but it is of order ϵ.) Also, let A_s be the area of the safe region of the unperturbed model; here we will use A_s to approximate that for its perturbed counterpart, since the size of the safe region remains essentially unchanged after perturbation.

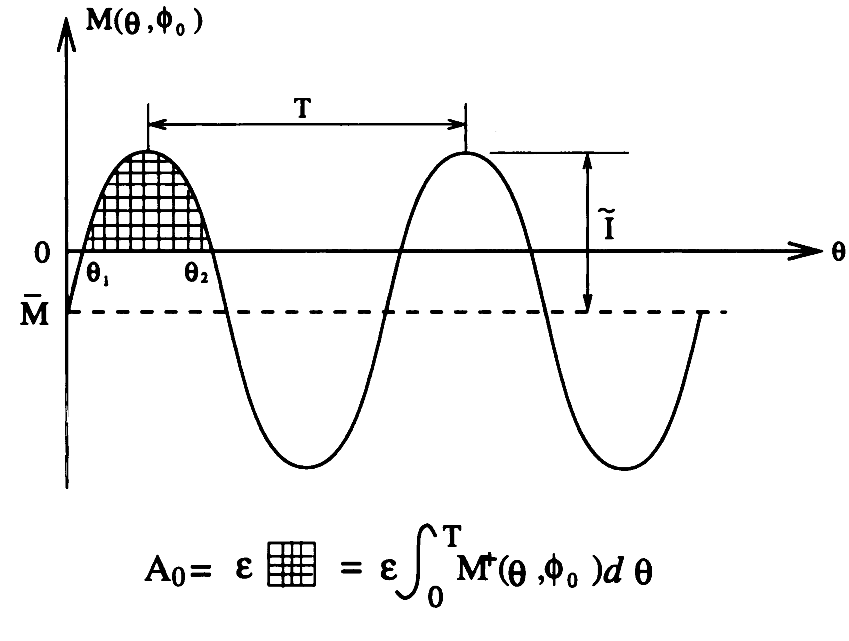

Figure 4.6: The correspondence between lobes and the Melnikov function.

We are now interested in the initial conditions in the safe region which are transported to the unsafe one after N periods of wave excitation. Let the set of these initial points be denoted by E_N. A candidate for E_N is L_0 plus its $N-1$ pre-images. However, part of the turnstile lobe's pre-images is not in the safe region. Indeed, for area-preserving maps (non-dissipative systems), we have ([67])

$$\mu(L_0) = \sum_{k=1}^{\infty} \mu(L_0 \cap f^k(L_1)), \tag{4.3}$$

where $f^k(L_1)$ denotes the k-th image of L_1. Equation (4.3) says that L_0 is completely filled with images of L_1, a lobe in the unsafe region, as shown in Figure 4.7.

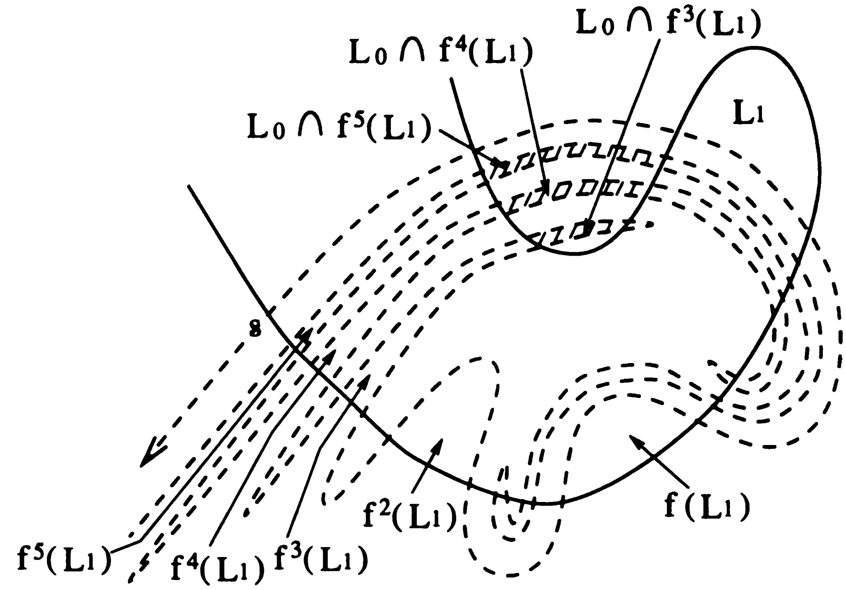

Figure 4.7: The relationship between L_0 and the images of L_1.

Since every lobe has the same area as L_0, the area of E_N can be expressed in terms of L_0 and L_1 as follows ([67])

$$\mu(E_N) = N\mu(L_0) - \sum_{k=1}^{N-1} (N-k)\mu(L_0 \cap f^k(L_1)), \tag{4.4}$$

for $N \geq 2$. The last term in equation (4.4) accounts for the portions in L_0 whose pre-images are located in the unsafe region.

While the quantity $\mu(L_0)$ is related to the Melnikov function by equation (4.2), there are no analytical results on the estimate for $\mu(L_0 \cap f^k(L_1))$. In view of equation (4.3) and the fact that typically $L_0 \cap f(L_1) = \emptyset$, we shall assume

$$\mu(L_0 \cap f(L_1)) = 0 \tag{4.5}$$

and

$$\mu(L_0 \cap f^k(L_1)) = 2^{-k+1}\mu(L_0), \ \forall k = 2, 3, \ldots \tag{4.6}$$

The reason for choosing 1/2 as the decay rate is that equations (4.5) and (4.6) will add up to equation (4.3). Substituting equations (4.5) and (4.6) into equation (4.4) yields

$$\begin{aligned} \mu(E_N) &= (3 - 2^{-N+2})\mu(L_0) \\ &\approx 3\mu(L_0), \quad \text{for } N \text{ large.} \end{aligned} \tag{4.7}$$

Hence the amount of phase space transport $\mu(E_N)$ is nearly independent of N. In other words, it is independent of the exposure time to the wave excitation. An interesting implication for this is that most initial conditions in the safe region will either stay in the safe region forever or lead to capsize during the first few excitation periods.

The amount of phase space transport can be regarded as an estimate of the eroded area of the safe basin. Therefore, equation (4.7) is useful in this respect. By combining it with equation (4.2), one can thus obtain a simple expression for the ratio of the eroded area, denoted by ρ_e, as

$$\rho_e = 3\frac{\mu(L_0)}{A_s} \stackrel{\text{def}}{=} 3\Phi = \frac{3\epsilon}{A_s}\int_0^T M^+(\theta, 0)d\theta + O(\epsilon^2), \tag{4.8}$$

where Φ is the normalized phase space flux and we have set $\phi_0 = 0$ since the integral is independent of this phase angle. It is easy to see that ρ_e is closely related to the capsizing probability, which will be discussed in Chapter 6 for an example vessel. Similar results have been generalized to the case of random excitation ([23], [27]). In this study, they will be generalized to a multi-DOF beam sea model via the approach presented below.

4.2 Phase Space Transport in Slowly Varying Oscillators

The slow dynamics derived from the current 3-DOF ship model, i.e. equations (3.56)-(3.58), are in the form of a class of systems called slowly varying oscillators, which are defined by the standard form

$$\dot{x} = f_x(x,y,z) + \epsilon g_x(x,y,z,t), \tag{4.9}$$

$$\dot{y} = f_y(x,y,z) + \epsilon g_y(x,y,z,t), \tag{4.10}$$

$$\dot{z} = \epsilon g_z(x,y,z,t), \tag{4.11}$$

where $0 < \epsilon \ll 1$. In the present case, the g_i's are periodic in t with period T, and $f_x(x,y,z) = \frac{\partial H}{\partial y}(x,y,z)$ and $f_y(x,y,z) = -\frac{\partial H}{\partial x}(x,y,z)$ for some Hamiltonian function $H(x,y,z)$. Slowly varying oscillators usually arise from systems involving two time scales. There have been many investigations of such systems (e.g., [68], [69], [70]). For more examples and applications of such systems, please refer to [65].

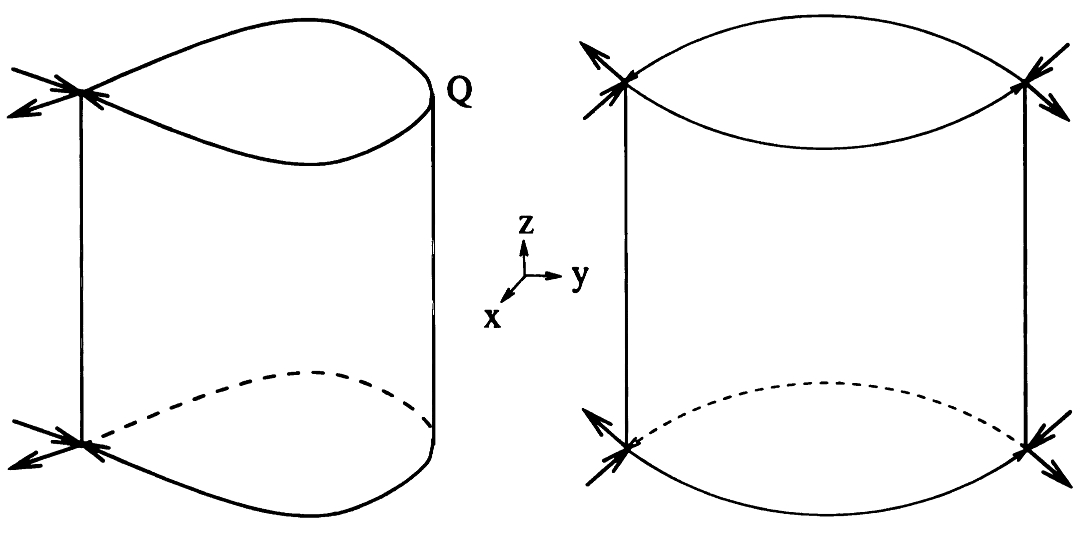

(a) The biased case. (b) The unbiased case.

Figure 4.8: The unperturbed structures of slowly varying oscillators.

The current system is a special case in that its Hamiltonian function does not depend on the slowly varying coordinate, z (here, the sway velocity). Hence, the unperturbed structures are identical at each z level of the slowly varying variable, as depicted in Figure 4.8. This unperturbed structure mimics the behavior of the unperturbed one DOF roll model. When the perturbations are added, i.e. when the wave excitation is introduced, the behavior of the present system will be significantly different from that of the corresponding single DOF one due to the coupling effects from sway and heave. In other words, the hydrodynamic coupling through added masses and dampings, a_{ij}'s and b_{ij}'s, will play an important role in determining the dynamics.

Note that systems eligible for analysis of chaotic transport by Melnikov theory are those in nearly integrable form, i.e. integrable systems with small perturbations. Slowly varying oscillators are in such a form and their Melnikov function is available in ([9], [68] , [69]), and is given by

$$M(\theta,\phi_0)=\int_{-\infty}^{\infty}(\nabla H\cdot g)(q_0(t),t+\theta+\frac{\phi_0}{\Omega})dt-\frac{\partial H}{\partial z}(\gamma_s)\int_{-\infty}^{\infty}g_z(q_0(t),t+\theta+\frac{\phi_0}{\Omega})dt, \tag{4.12}$$

where $g=[g_x\ g_y\ g_z]^T$, $q_0(t)$ is the reference homoclinic orbit, θ is the time parameter on $q_0(t)$, ϕ_0 is the phase difference with respect to the excitation, and γ_s is the saddle point, here the angle of vanishing stability.

In extending the concept of phase space transport for a single DOF model to the present system, one must be cautious. As can be seen, a slowly varying oscillator will result in a three-dimensional Poincare map. While the theory of phase space transport is relatively complete for two-dimensional maps and some special higher dimensional maps [67], it is not well developed for cases in which "lobes" are not well defined, as is the case for slowly varying oscillators; see Figure 4.9. The problem here is that the saddle point of the perturbed system in the three-dimensional phase space has a two-dimensional stable and a one-dimensional unstable manifold, and these sets do not form boundaries for pieces of the phase space (both manifolds need to be two-dimensional in this case in order to form well-defined lobes). A difficulty

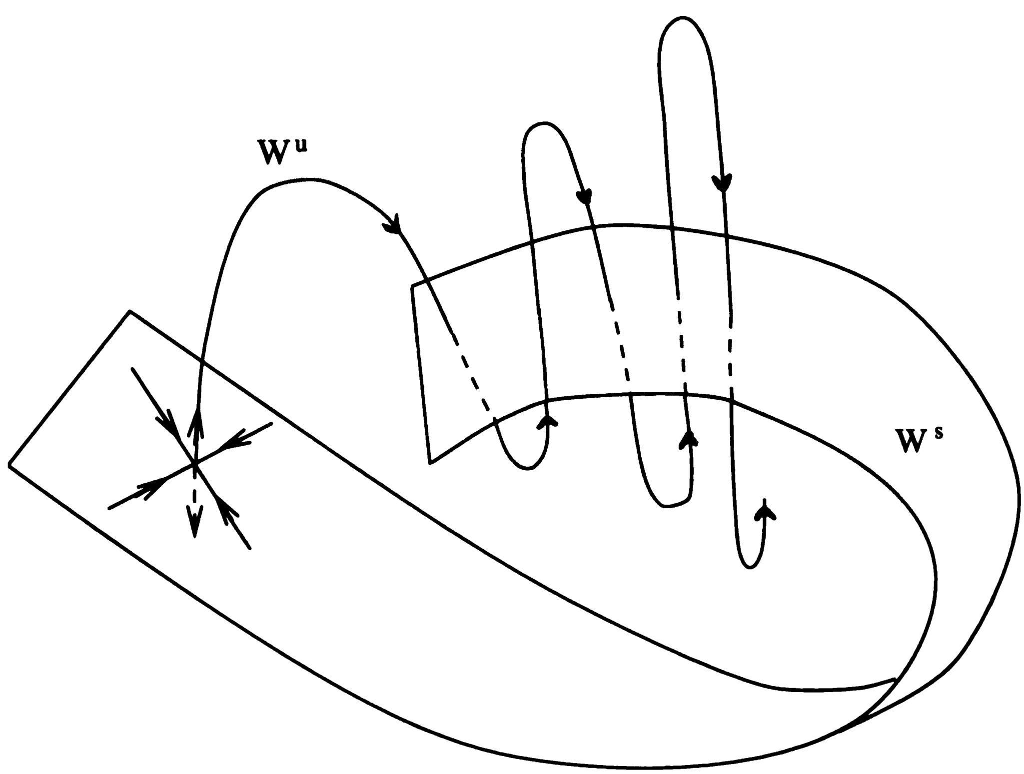

Figure 4.9: The structure of stable and unstable manifolds in a slowly varying oscillator.

thus arises about how to quantify phase space transport measures for such systems.

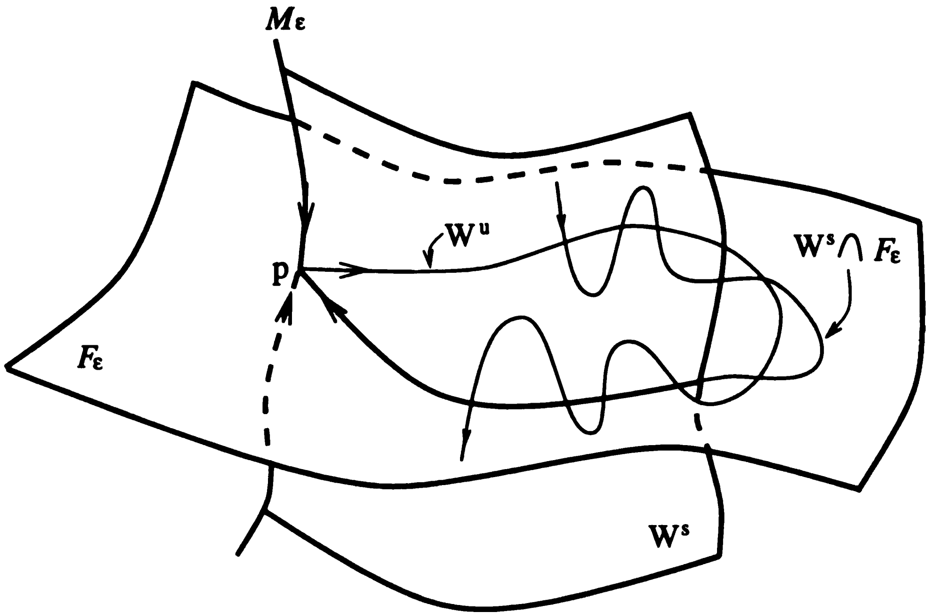

Figure 4.10: The fast manifold in a slowly varying oscillator.

It is shown in Appendix A that the fast dynamics of a slowly varying oscillator on a two dimensional fast invariant manifold has the same Melnikov function as the whole system, i.e. that given by equation (4.12). This can be easily visualized in Figure 4.10, which depicts the fast manifold F_ϵ in a slowly varying oscillator. It is interesting to note that the dynamics on the fast manifold are similar to that of a single DOF roll model, only the quasi-static effects of sway coupling are incorporated. This result suggests one approach to the above-mentioned difficulty, as the transport theory can at least be applied to the two-dimensional fast dynamics, wherein the integral of the positive part of the Melnikov function over one period can now be interpreted as the area of the two-dimensional turnstile lobes in the fast manifold. Since the fast manifold is (at least weakly) attractive, this integral of Melnikov function will serve as a measure of the transport for the overall system.

We close this section by some remarks. Recall that we started with a 3-DOF beam sea model and then restricted ourselves to a three dimensional slow manifold composed of roll and sway dynamics. In the slow manifold, we once again confined ourselves to a two dimensional fast manifold which is basically the roll dynamics with coupling from sway. The justification these steps is that the final two dimensional manifold, although slow in one sense and fast in another, is *attractive* in the entire state space and it contains the important dynamics for capsize in roll, with coupling from heave and sway accounted for in a systematic manner. One may also have noticed that the entire system has three time scales. The heave motion is the fastest, the roll motion is next, and the sway motion is the slowest. Among them, the heave and sway motions are stable, and the roll motion is essentially the one left for the analysis, as it contains the unstable dynamics that lead to capsize.

4.3 Capsizing Criterion

Let $q_0(\tau) = (x_{10}(\tau), x_{20}(\tau), \bar{y})$ be the reference (homoclinic or heteroclinic) orbit for the present slowly varying oscillator described by equations (3.56)-(3.58). This orbit is based at a sway velocity of $\bar{y}$, which can be determined by applying the theory of averaging to the slowly varying equation (3.58). This yields

$$\bar{y} = \frac{\sigma_{21}}{\delta_{22}} \cos \bar{x}_1, \tag{4.13}$$

where $\bar{x}_1$ is the x_1-coordinate of the saddle fixed point with homoclinic orbit. This velocity is the mean sway velocity of the vessel in the presence of damping and wave excitation, as the vessel is oscillated about the angle of vanishing stability, $\bar{x}_1$. Thus, the Melnikov function for the system is given by

$$M(\theta, \phi_0) = \int_{-\infty}^{\infty} x_{20}(\tau)\hat{g}_1(x_{10}(\tau), x_{20}(\tau), \bar{y}, \tau + \theta + \frac{\phi_0}{\Omega})d\tau.$$

It is more convenient to rewrite it as

$$M(\theta, \phi_0) = I_0 - \delta_{44} I_1 - \delta_{44q} I_2 + \lambda I_3(\Omega, \theta, \phi_0) + \gamma_{41} I_4(\Omega, \theta, \phi_0), \tag{4.14}$$

where

$$I_0 = \int_{-\infty}^{\infty} x_{20}(\tau)[\sigma_{41} \cos x_{10}(\tau) + \sigma_{42} \cos^2 x_{10}(\tau) - \delta_{42}\bar{y}]d\tau,$$

$$\begin{aligned}
I_1 &= \int_{-\infty}^{\infty} x_{20}^2(\tau)d\tau, \\
I_2 &= \int_{-\infty}^{\infty} x_{20}^2(\tau)|x_{20}(\tau)|d\tau, \\
I_3(\Omega,\theta,\phi_0) &= -\int_{-\infty}^{\infty} x_{20}(\tau)f_1(x_{10}(\tau))\cos(\Omega(\tau+\theta)+\phi_0)d\tau, \\
I_4(\Omega,\theta,\phi_0) &= \int_{-\infty}^{\infty} x_{20}(\tau)\sin(\Omega(\tau+\theta)+\phi_0)d\tau.
\end{aligned}$$

The advantage of representing $M(\theta,\phi_0)$ by these five integrals is that it shows the different contributions which constitute the Melnikov function. I_0 is the contribution from the wind forces. I_1 and I_2 are those from the linear and quadratic parts of the hydrodynamic damping, respectively. Finally, I_3 and I_4 are, respectively, related to parametric and external components of the wave excitation.

We now turn to some simplifications of these integrals. By taking $q_0(0)$ to be the point Q in Figure 4.8(a), namely the "midpoint" of the reference orbit, $x_{10}(\tau)$ and $x_{20}(\tau)$ will be even and odd functions in τ, respectively. Therefore, the integrand of I_0 is an odd function, implying $I_0 = 0$. Since $x_{20}(\tau)$ approaches zero exponentially as $\tau \to \pm\infty$, the integrals I_1 and I_2 are well defined and are, obviously, positive. Finally, by noting again that $x_{10}(\tau)$ is even and $x_{20}(\tau)$ is odd, I_3 and I_4 can be further simplified to

$$\begin{aligned}
I_3(\Omega,\theta,\phi_0) &= \bar{I}_3(\Omega)\sin(\Omega\theta+\phi_0), \\
I_4(\Omega,\theta,\phi_0) &= \bar{I}_4(\Omega)\cos(\Omega\theta+\phi_0),
\end{aligned}$$

where

$$\begin{aligned}
\bar{I}_3(\Omega) &= -\int_{-\infty}^{\infty} x_{20}(\tau)f_1(x_{10}(\tau))\sin\Omega\tau d\tau, \\
\bar{I}_4(\Omega) &= \int_{-\infty}^{\infty} x_{20}(\tau)\sin\Omega\tau d\tau.
\end{aligned}$$

It is interesting to point out the implications of $I_0 = 0$. It follows immediately that the wind force has no effect on the Melnikov function and hence will not affect the amount of phase space transport (to the first order). This can be understood from the energy viewpoint of the Melnikov function and by recognizing that the model adapted here for wind forces is conservative ([30], [59]). Physically, if one considers the calm water situation, a steady mild wind can hardly cause capsizing without the aid of wave excitation. No phase space transport may happen in the calm water condition. However, it should be intuitively clear that wind forces have an important influence on the possibility of capsize. This comes about through the change of the size of the (unperturbed) safe region, even in the absence of damping and forcing; for example, as shown in Figure 4.1. In other words, it will cause a bias in the upright equilibrium angle. As it is assumed to be small in this study, it is of higher order and of little importance. In the present study, the offset in the CG is used to account for bias in the equilibrium angle of the vessel.

An alternative treatment to wind is to separate it from the perturbation and to incorporate it into the unperturbed part while keeping in mind that it is small. Then, the "unperturbed" reference orbit will be altered accordingly. This will not change the results except possibly for the case when the mass center has no bias, i.e. $y_G = 0$. In this case the reference orbit will be disturbed dramatically from heteroclinic to homoclinic type, despite the smallness of the wind force. However, we will not pursue this issue further since it involves the subtle issue of the interaction of heteroclinic and homoclinic orbits and requires more careful considerations.

Based on the above discussions, the Melnikov function can be put in the concise form:

$$M(\theta, 0) = \bar{M} + \tilde{M}(\theta), \tag{4.15}$$

$$\bar{M} = -\delta_{44} I_1 - \delta_{44q} I_2, \tag{4.16}$$

$$\tilde{M}(\theta) = \tilde{I} \sin(\Omega\theta + \tilde{\phi}), \tag{4.17}$$

where

$$\tilde{I} = \sqrt{\lambda^2 \bar{I}_3^2(\Omega) + \gamma_{41}^2 \bar{I}_4^2(\Omega)},$$

$$\tilde{\phi} = \tan^{-1}\frac{\gamma_{41}\bar{I}_4(\Omega)}{\lambda\bar{I}_3(\Omega)},$$

and without loss of generality, ϕ_0 is taken to be zero for simplicity. From this simple expression, one can clearly see that the Melnikov function is harmonic in θ with same frequency as the excitation Ω, mean value $\bar{M}$, and oscillatory amplitude $\tilde{I}$, as depicted in Figure 4.6.

It is important to note from equation (4.16) that the mean value of the Melnikov function $\bar{M}$ depends linearly on the hydrodynamic damping coefficients and is independent of the wave excitation. Also, note that $\bar{M}$ is negative since both I_1 and I_2 are positive, and the combined damping coefficients δ_{44} and δ_{44_q} are in general positive as well. This negative constant indicates that without wave excitation, the unstable manifold of the saddle point lies "inside" of the corresponding stable manifold, as sketched in Figure 4.2. The physical meaning is that a ship originally located in the safe region will eventually go to the upright equilibrium position — i.e., no capsize may occur from safe initial conditions.

In contrast, the amplitude of the Melnikov function $\tilde{I}$ is independent of damping parameters and is determined by the wave height and frequency. It depends linearly on the wave height, but nonlinearly on the wave frequency. Increasing wave amplitude is equivalent to increasing $\tilde{I}$. If the wave excitation is so strong that

$$\tilde{I} \geq |\bar{M}|, \tag{4.18}$$

then the homoclinic tangles exist and the ship has the possibility of capsize from the safe region.

Following the ideas developed in Sections 4.1 and 4.2, we can now develop a quantitative measure of the likelihood for escape over N periods of excitation using the ratio of the erosion area given by equation (4.8). For a given vessel exposed over a prescribed time, the ratio ρ_e depends only on the sea state, which is characterized by the wave frequency and amplitude. (In fact, it is almost independent of the exposure time, as indicated previously.) If the sea is well behaved such that equation (4.18) is not satisfied, ρ_e is simply zero. When the sea is strong enough such that $\tilde{I}$ exceeds the critical value set by equation (4.18), ρ_e will be positive. Hence, we have the following simple relation between the ratio of erosion area and the sea state:

$$\rho_e \begin{cases} = 0, & \text{if } \tilde{I} < |\bar{M}| \\ \geq 0, & \text{if } \tilde{I} \geq |\bar{M}| \end{cases}.$$

This ratio is generally computed by numerically evaluating some well-behaved indefinite integrals.

For the special case that $y_G = 0$ and no wind force is present (the unbiased case), an analytical expression for $M(\theta, \phi_0)$ is possible. Note that $f_1(x_1)$ is an odd function in x_1 in this situation. Hence, one can use the polynomial

$$f_1(x_1) = -x_1 + \alpha x_1^3,$$

as a best-fit approximation to the actual function, as was done in many previous works ([23], [27], [61], [64]). Then, following the procedure similar to the general case, one can get the following closed-form expression for the Melnikov function

$$M(\theta, \phi_0) = -\frac{2\sqrt{2}}{3\alpha}\delta_{44} - \frac{8\delta_{44q}}{15\alpha\sqrt{\alpha}} - [\sqrt{\frac{2}{\alpha}}\gamma_{41}\pi + \frac{\lambda\pi(2\Omega + \Omega^3)}{6\alpha}]\frac{\Omega}{\sinh\frac{\pi\Omega}{\sqrt{2}}}\sin(\Omega\theta + \phi_0), \tag{4.19}$$

where some of the integrals involved are evaluated by the method of residues. The safe region for this case is bounded by a pair of heteroclinic orbits and its area can also be obtained explicitly:

$$A_s = \frac{4\sqrt{2}}{3\alpha}.$$

Once the parameters in (4.19) are specified, i.e. a given ship and sea state, we can determine the ratio of erosion area by an equation similar to (4.8), developed for the heteroclinic case. It is

$$\rho_e = \frac{6\epsilon}{A_s}\int_0^T M^+(\theta, 0)d\theta + O(\epsilon^2). \tag{4.20}$$

One should note that since there are two turnstile lobes in heteroclinic tangles (one each for positive and negative velocities), there a factor of 6 instead of 3 in equation (4.20).

4.4 Comparison With Results From 1-DOF Roll Model

The effects of coupling from sway and heave will be examined in this section by comparing the present results with those obtained from an analysis of a single DOF roll model, that is, the model considered in virtually all previous analytical studies.

The structure of the Melnikov function for our 3-DOF model, given by equations (4.15)-(4.17), is exactly the same as that for the 1-DOF roll model, but with different coefficients. The differences have two sources. One is the linear damping δ_{44}, which will affect the mean value of the Melnikov function. The other is the external excitation γ_{41}, which influences the amplitude of the Melnikov function. During the following discussion, one should recall that m_{43} is a small quantity.

In the case of the 1-DOF roll model, the linear roll damping either contains only hydrodynamic roll damping b_{44} [23], or incorporates other sources of damping in b_{44} through an assumed roll center, which is heuristic and difficult to verify ([25], [26]). In this study, all damping coefficients from roll, sway, and heave are taken into account in a systematic way to form a combined damping coefficient δ_{44}. Explicitly,

$$\begin{aligned}\epsilon\delta_{44} &= \frac{1}{m_2^2 m_0 \omega_r}[m_3(m_2^2 b_{44} - m_2 a_{24} b_{42} - m_2 a_{42} b_{24} + a_{42} a_{24} b_{22}) \\ &\quad + m_{43}(m_2 a_{32} b_{24} - a_{32} a_{24} b_{22} - m_2^2 b_{34} + m_2 a_{24} b_{32})].\end{aligned} \tag{4.21}$$

It is obvious from equation (4.21) that the effect of heave coupling is small since m_{43} is small. Compared to the simple roll model, the additional dominant term for the current 3-DOF model is

$$\frac{m_3}{m_2^2 m_0 \omega_r}(-m_2 a_{24} b_{42} - m_2 a_{42} b_{24} + a_{42} a_{24} b_{22}). \tag{4.22}$$

Note that m_0, m_2, m_3, ω_r, and b_{22} are always positive, but a_{24}, a_{42}, b_{24}, and b_{42} could be positive or negative, depending on the wave frequency and the position of the CG. Since the three terms in equation (4.22) have the same order of magnitude, it is hard to conclude the overall effect on δ_{44} and hence on the mean value of the Melnikov function. It will be shown in Chapter 6 that for the *Patti-B*, the coupling effect on the mean value of the Melnikov function is negligible.

On the other hand, the amplitude of the external excitation is

$$\epsilon\gamma_{41} = \frac{\omega_w^4 a}{\alpha_1 m_2 g}(m_2 m_3 I_{44} - m_3 m a_{42} z_G + m_{43} m a_{32} z_G). \tag{4.23}$$

If the hydrodynamic couplings are neglected, only the first term in equation (4.23) will be retained ([61] and cf. equation (4.1)). It is clear from equation (4.23) that the contribution from heave coupling (the third term) is small since m_{43} is small, whereas that from sway coupling (the second term) can be significant. Recall that

$$a_{42} z_G = \hat{a}_{42} z_G - \hat{a}_{22} z_G^2,$$

is usually negative; see Tables 3.2 and 6.1. Thus, γ_{41} will be larger if the coupling effects are taken into account, resulting in the increase of the amplitude of the Melnikov function. This will lead to an increase in the amount of phase space transport. Also from equation (4.23), we can deduce that the coupling effects will increase with the wave amplitude since the additional term is proportional to a.

In summary, there are two major points to be made. First, the coupling from heave has little effect on the Melnikov function, and thus on the capsizing probability. Second, the overall sway coupling effects turn out to increase the amount of phase space transport. So, for a particular ship under a given sea state, the 3-DOF model will propose a higher capsizing probability than does the 1-DOF model. The implication for this is that there are situations which are predicted to be relatively safe by the single DOF criterion, that are actually vulnerable to capsize. This, and other features of the ship dynamics, will be illustrated by numerical simulations in Chapter 6.

CHAPTER 5

ROBUST SHIP STABILIZATION

After understanding the dynamics of the nonlinear 3-DOF ship model from the analysis in previous chapters, we can now proceed to consider roll stabilization by feedback control. The objective is to design a stabilizing feedback controller against capsizing that takes into account model uncertainties. In other words, in addition to stabilization, robustness is a major consideration. As is clear in Chapter 3, it is virtually impossible to develop accurate models for large amplitude ship motions, due to the difficulties involved in solving the associated free-surface hydrodynamic problem. Therefore, model uncertainties always exist and can be substantial in magnitude.

Because of the uncertainties, the best one can achieve is ultimate boundedness of the motion. That is, the vessel is not guaranteed to settle to a single equilibrium position in steady state, but its motion is restricted to a small bounded region. This is sufficient for our purposes, as there will be a significant reduction of the rolling motions, and the control will prevent the ship from capsizing even under severe sea conditions. It is obvious from Chapter 4 that without any controller, the vessel system is subject to the possibility of capsize in unfavorable sea states ([10], [13], [23], [27]).

To this aim, anti-roll tanks are employed as actuators, since other methods are either impractical, such as the gyroscopic method and moving weight scheme, or not effective at low vessel speeds, such as the fin stabilizer and rudder-roll systems. The main goal of the anti-roll tank is to dynamically change the horizontal position of a ship's center of gravity in such a way that the roll motions are reduced. However, the position of the CG cannot be shifted instantaneously, and therefore the control scheme will involve a dynamic state feedback controller.

Our approach for the robust controller design is based on a smooth version of sliding mode control, which handles the uncertainties, together with the backstepping method and the idea of composite control for singularly perturbed systems [31].

5.1 Uncertainties in the Ship Model

The nondimensional state equations (3.49)-(3.53) for the current 3-DOF ship model can be rewritten to include the uncertainties existing in the model and to explicitly show the dependence on y_G as follows:

$$\begin{aligned}
\dot{x}_1 &= x_2, &(5.1)\\
\dot{x}_2 &= f_{11}(x_1) + f_{12}(x_1)x_3 + \Delta f(x_1, x_3)\\
&\quad + \epsilon(g_1 + \Delta g_1)(x_1, x_2, x_3, y, z_1, z_2, \tau), &(5.2)\\
\dot{y} &= \epsilon(g_2 + \Delta g_2)(x_1, x_2, y, z_2, \tau), &(5.3)\\
\epsilon \dot{z}_1 &= z_2, &(5.4)\\
\epsilon \dot{z}_2 &= -b_1 z_1 - b_2 z_2 + \epsilon(g_3 + \Delta g_3)(x_1, x_2, x_3, y, z_1, z_2, \tau), &(5.5)
\end{aligned}$$

where $x_3 = y_G/k_4$[1] is the (normalized) horizontal position of the CG, and the f_{ij}'s are hydrostatic functions induced by the f_i's. Note that the arguments of the perturbation functions now include x_3, but we shall still use the g_i's to denote these functions for brevity. Note also that here the time variable has been rescaled using the unbiased roll natural frequency.

There are two sources of model uncertainties, one from hydrostatics and the other from hydrodynamics. The functions f_{ij}'s in the state equation represent the contributions from hydrostatic forces. For a given hull shape, these functions can

---

[1] k_4 is a constant in the unbiased GZ function, defined in Section 6.1 below.

be obtained in an integral form, but quite often they cannot be expressed in a closed form in terms of the roll angle. However, in most cases, polynomials can well approximate them in an appropriate best-fit sense. It should be noted that if better functional fits for f_{ij}'s are available, they can be easily used in place of the polynomials. The discrepancy between the actual and approximate righting moment (i.e., $f_{11}(x_1) + f_{12}(x_1)x_3$) is represented by the uncertainty function $\Delta f(x_1, x_3)$. For the other hydrostatic functions, the differences are contained in the functions Δg_i's.

On the other hand, the significant model uncertainties arising from the hydrodynamics are represented in part by the uncertainty functions Δg_i's and in part by the unknown positive constants b_1 and b_2 in equation (5.5)[2]. All these uncertainty functions are assumed to be continuously differentiable in their arguments.

5.2 Design of a Robust Stabilizing Controller

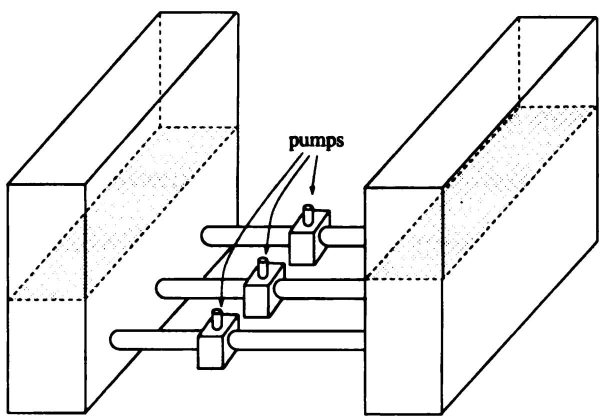

Figure 5.1: The active anti-roll tanks.

In this section, a robust state feedback controller will be designed using the method of anti-roll tanks. The anti-roll tanks, as shown in Figure 5.1, consist of two tanks connected at the bottom with one on the port side of the vessel and the other

---

[2] In comparison with equation (3.53), it should be clear that b_1 is $\bar{\omega}^2$ plus uncertainty, and b_2 is δ_{33} plus uncertainty.

on the starboard side. The fluid in the tanks can be moved from one side to the other through the connection tubes, and in this way, the CG of the vessel can be controlled.

When equipped with such anti-roll tanks, a dynamic equation for these tanks needs to be included in addition to the state equations given by (5.1)-(5.5). Assume that the flow rate of the fluid can be directly controlled by actuators, such as pumps, added to the connection tubes. Then the additional equation takes the form:

$$\dot{x}_3 = u, \tag{5.6}$$

where u is proportional to the flow rate and serves as the control input.

Due to space limitations, the fluid weight in the tanks is usually less than 5% of the vessel displacement [53]. This implies that in order to shift the CG by 1 inch, we need to move the CG of the fluid by at least 20 inches. Hence, x_3 is limited by available space. On the other hand, the flow rate (the control effort) also has practical limitations. These limitations must be monitored when designing the controller. The overall system can thus be illustrated by the block diagram shown in Figure 5.2. The two limiters in the diagram stand for the practical limitations on x_3 and u.

Before starting the controller design, a specific statement of the problem is given. Let S_0 be the unperturbed, unbiased safe region in the (x_1, x_2) invariant manifold, i.e. the one enclosed by the heteroclinic cycle in the roll manifold. Let S_1 be some compact set containing S_0 in the same manifold. Then the domain of interest is defined by

$$D = \{(x_1, x_2, x_3, y, z_1, z_2) | (x_1, x_2) \in S_1, |x_3| \leq L_x, |y| \leq L_y, ||(z_1, z_2)|| \leq L_z\}, \tag{5.7}$$

where $||\cdot||$ denotes the Euclidean 2-norm, and L_x, L_y, and L_z are positive constants.

Our goal is to design a feedback law

$$u = \psi(x_1, x_2, x_3, y, z_1, z_2) \tag{5.8}$$

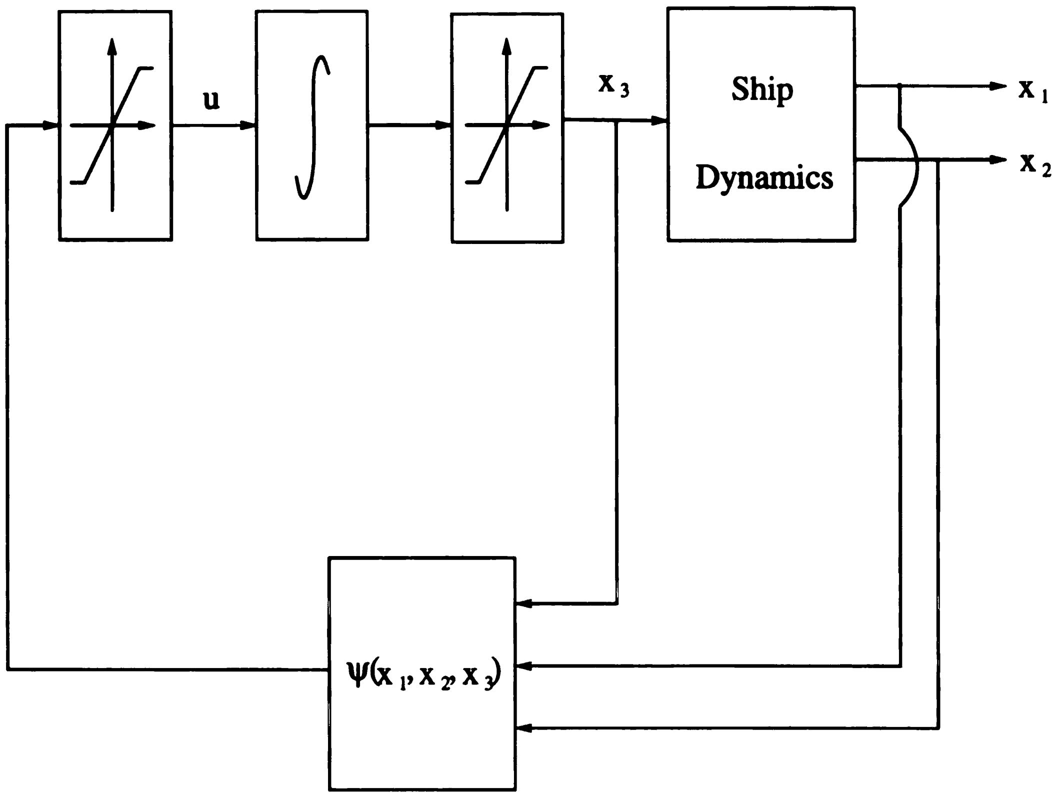

Figure 5.2: The ship control system.

such that for any initial condition in D,

(i) All state variables are bounded for $\tau \geq 0$;

(ii) $(x_1(\tau), x_2(\tau))$ asymptotically approaches a small neighborhood of the origin as $\tau \to \infty$.

In other words, for the ship initially in the safe region, we want to reduce the roll motions as much as possible and, at the same time, maintain bounded motions of the other degrees of freedom. It will be shown below that the desired feedback function can be chosen to depend only on x_1, x_2, and x_3. That is, partial state feedback is sufficient to achieve the goal. This is due to the large damping in heave and the essentially inconsequential nature of sway.

The full control system given by equations (5.1)-(5.6) is a singularly perturbed system. Therefore, it is natural to design the controller via the approach of composite control ([31], [32]). The composite control is a sum of two components, the *slow control* and the *fast control*. The former is designed on the slow manifold to satisfy the desired requirement. The fast control, on the other hand, is designed to guarantee that the slow manifold is attractive. In the following analysis, we will first assume that the slowly varying variable y is bounded for all $\tau \geq 0$ and then investigate this assumption at the final stage of the design.

5.2.1 The Controller on the Slow Manifold

We start with the design of the slow control by restricting ourselves to the slow manifold which, to leading order, is given by

$$z_1 = 0, \tag{5.9}$$

$$z_2 = 0. \tag{5.10}$$

The slow system is thus given by

$$\dot{x}_1 = x_2, \tag{5.11}$$

$$\dot{x}_2 = f_{11}(x_1) + f_{12}(x_1)x_3 + \Delta f(x_1, x_3) + \epsilon(g_1 + \Delta g_1)(x_1, x_2, x_3, y, 0, 0, \tau), \tag{5.12}$$

$$\dot{x}_3 = u, \tag{5.13}$$

where y is taken to be a bounded constant. The controller for this system will constitute the slow control for the full system.

It is clear that the uncertainties in the slow dynamical system do not satisfy the *matching condition* [31]. In other words, the uncertainties and the control input enter the state equations at different points. As a consequence, most robust control methods can not be applied without incorporating the backstepping technique ([31], [33]). In what follows, we shall design the slow control by a smooth version of sliding mode control with the help of the backstepping technique.

As the first step in the backstepping procedure, let us pretend for the moment that x_3 is our control input, i.e., that the CG can be altered instantaneously. Thus, we arrive at the following 2-D dynamical system on the slow manifold:

$$\dot{x}_1 = x_2, \tag{5.14}$$

$$\dot{x}_2 = f_{11}(x_1) + f_{12}(x_1)x_3 + \Delta_1(x_1, x_2, x_3, y, \tau), \tag{5.15}$$

where

$$\Delta_1 = \Delta f(x_1, x_3) + \epsilon(g_1 + \Delta g_1)(x_1, x_2, x_3, y, 0, 0, \tau) \tag{5.16}$$

is viewed as the uncertainty.

Since $f_{12}(x_1)$ is basically a normalized inertia term, it is always positive within the angles of vanishing stability. Hence, the uncertain term Δ_1 will now satisfy the matching condition by treating x_3 as the control input. The problem now is to design a smooth feedback law $x_3 = \psi_x(x_1, x_2)$ such that the 2-D system in (5.14)-(5.15) is ultimately bounded. Note that the smoothness requirement is due to the use of backstepping.

This 2-D control problem appears to be well suited for the method of sliding mode control. Other methods like Lyapunov redesign and adaptive control are also possible choices. However, it is easier to obtain a simple smooth feedback law by employing a smooth version of sliding mode control.

The idea of sliding mode control is to design a *sliding manifold*,

$$x_2 = s(x_1),$$

such that the dynamics on this manifold, given by

$$\dot{x}_1 = s(x_1), \tag{5.17}$$

will be asymptotically stable. The sliding mode control thus consists of two parts. One part is used to bring the system onto the sliding manifold in finite time; this is called the *switching control* and is denoted by ψ_s. The other part is used is to maintain the situation afterwards, which is called the *equivalent control* and denoted by ψ_{eq}.

Let us design the equivalent control first. The sliding manifold will be taken as the linear form

$$s(x_1) = -\beta x_1, \quad \beta > 0,$$

resulting in an asymptotically stable reduced system

$$\dot{x}_1 = -\beta x_1,$$

on the sliding manifold. Let

$$\sigma_1(x_1, x_2) = x_2 - s(x_1) = \beta x_1 + x_2,$$

so that the sliding manifold is represented by $\sigma_1(x_1, x_2) = 0$. Then, maintaining the system on $\sigma_1 = 0$, once it is there, is equivalent to maintaining

$$\dot{\sigma}_1 = 0, \tag{5.18}$$

which is to be done by ψ_{eq} in the absence of the uncertainty. Without the uncertainty, condition (5.18) leads to

$$\beta x_2 + f_{11}(x_1) + f_{12}(x_1)\psi_{eq}(x_1, x_2) = 0,$$

yielding

$$\psi_{eq}(x_1, x_2) = -\frac{f_{11}(x_1) + \beta x_2}{f_{12}(x_1)}. \tag{5.19}$$

Upon applying

$$x_3 = \psi_x(x_1, x_2) = \psi_{eq}(x_1, x_2) + \psi_s(x_1, x_2)$$

with $\psi_{eq}(x_1, x_2)$ given by equation (5.19), the $\dot{\sigma}_1$-equation becomes

$$\begin{aligned} \dot{\sigma}_1 &= f_{12}(x_1)\psi_s(x_1, x_2) + \Delta_1(x_1, x_2, \psi_{eq} + \psi_s, y, \tau) \\ &= v + \Delta_1(x_1, x_2, \psi_{eq} + \frac{v}{f_{12}(x_1)}, y, \tau), \end{aligned} \tag{5.20}$$

where we have set $\psi_s = v/f_{12}(x_1)$. Our task now is to choose v to force σ_1 toward the manifold $\sigma_1 = 0$ in the presence of the uncertainty. To this end, we assume that there are constants $\rho_1 \geq 0$ and $0 \leq k < 1$ such that

$$|\Delta_1(x_1, x_2, \psi_{eq} + \frac{v}{f_{12}(x_1)}, y, \tau)| \leq \rho_1 + k|v|, \tag{5.21}$$

within the domain of interest. The positive constant ρ_1 represents an upper bound on the uncertainty and is not necessarily small.

With inequality (5.21), a Lyapunov analysis using the candidate function $V_\sigma = \frac{1}{2}\sigma_1^2$ suggests that

$$v = -\frac{\lambda_1 + \rho_1}{1 - k}\operatorname{sgn}(\sigma_1), \quad \lambda_1 > 0, \tag{5.22}$$

will satisfy the requirement. However, the feedback function needs to be smooth in order to apply the backstepping method. Hence, we will replace (5.22) with its smooth counterpart,

$$v = -\frac{\lambda_1 + \rho_1}{(1 - k)\tanh(1)}\tanh(\frac{\sigma_1}{\epsilon_1}), \quad \epsilon_1 > 0, \tag{5.23}$$

where ϵ_1 is the thickness of the boundary layer near the sliding manifold. While asymptotic stability is guaranteed by the discontinuous feedback law (5.22), only ultimate boundedness can be achieved by its smooth version (5.23). This can be shown by a Lyapunov analysis, which is discussed in Section 5.2.4 below.

Next, consider the 3-D system given by equations (5.11)-(5.13). With the above preliminary analysis, the backstepping method proceeds by applying the sliding mode control again, with the sliding manifold now given by

$$\sigma_2(x_1, x_2, x_3) = x_3 - \psi_x(x_1, x_2) = 0,$$

where ψ_x is the "controller" for the 2-D system and is summarized here

$$\begin{aligned} \psi_x(x_1, x_2) &= \psi_{eq}(x_1, x_2) + \psi_s(x_1, x_2) \\ &= -\frac{1}{f_{12}(x_1)}[f_{11}(x_1) + \beta x_2 + \frac{\lambda_1 + \rho_1}{(1-k)\tanh(1)}\tanh(\frac{\sigma_1}{\epsilon_1})]. \end{aligned} \tag{5.24}$$

In other words, on the sliding manifold, we have the foregoing desired results. The time derivative of σ_2 with respect to the 3-D system is

$$\dot{\sigma}_2 = f_{13}(x_1, x_2, x_3) + u + \Delta_2(x_1, x_2, x_3, y, \tau), \tag{5.25}$$

where

$$\begin{aligned} f_{13} &= -\frac{\partial \psi_x}{\partial x_1}x_2 - \frac{\partial \psi_x}{\partial x_2}(f_{11}(x_1) + f_{12}(x_1)x_3), \\ \Delta_2 &= -\frac{\partial \psi_x}{\partial x_2}\Delta_1. \end{aligned}$$

Hence, the equivalent control for present is simply

$$u_{eq} = -f_{13}(x_1, x_2, x_3).$$

Similar to the previous 2-D system, we have an upper bound on the uncertainty Δ_2 within the domain of interest

$$|\Delta_2(x_1, x_2, x_3, y, \tau)| \leq \rho_2, \quad \rho_2 \geq 0, \tag{5.26}$$

by the continuity of the uncertain functions and the smoothness of ψ_x. Thus the switching control is taken as

$$u_s = -\frac{\lambda_2 + \rho_2}{\tanh(1)} \tanh(\frac{\sigma_2}{\epsilon_2}), \quad \lambda_2 \geq 0, \quad \epsilon_2 \geq 0.$$

This completes the design on the slow manifold and we finally have the slow control

$$\begin{aligned} u &= u_{eq} + u_s \\ &= \frac{\partial \psi_x}{\partial x_1} x_2 + \frac{\partial \psi_x}{\partial x_2}(f_{11}(x_1) + f_{12}(x_1)x_3) - \frac{\lambda_2 + \rho_2}{\tanh(1)} \tanh(\frac{\sigma_2}{\epsilon_2}), \end{aligned} \tag{5.27}$$

where $\psi_x(x_1, x_2)$ is given in equation (5.24).

5.2.2 The Fast Dynamics

Given the slow control established in Section 5.2.1, the next step in the design of a composite controller is to obtain a fast control to ensure the attractiveness of the slow manifold. However, in the light of the asymptotically stable linear part in the fast dynamics (equations (5.4)-(5.5)), feedback control of the fast dynamics is not necessary. Physically, this simply means that the large heave damping will do the job. On the other hand, one can see from the previous analysis that the attractiveness of the slow manifold is not crucial as long as z_1 and z_2 remain bounded. This is because that the fast variables only show up in the perturbation terms. Therefore, we expect that the heave damping will naturally bound the motions. Indeed, the following Lyapunov analysis will confirm this point.

Let

$$W(z) = z^T P z,$$

where $z = [z_1 \; z_2]^T$ and P satisfies

$$PA + A^T P = -I, \quad \text{with} \quad A = \begin{bmatrix} 0 & 1 \\ -b_1 & -b_2 \end{bmatrix},$$

where recall that b_1 and b_2 are positive constants. The continuity of Δg_3 suggests that within the domain of interest,

$$|(g_3 + \Delta g_3)(x_1, x_2, x_3, y, z_1, z_2, \tau)| \leq l_1, \quad l_1 \geq 0. \tag{5.28}$$

Then an easy calculation gives

$$\begin{aligned} \dot{W} &\leq -\frac{1}{\epsilon}||z||^2 + 2||z||||P|||g_3 + \Delta g_3| \\ &\leq -\frac{1}{\epsilon}||z||(||z|| - 2\epsilon l_1||P||) \\ &< 0 \quad \text{for} \quad ||z|| \geq 2\epsilon l_1||P||, \end{aligned}$$

which demonstrates the ultimate boundedness of z_1 and z_2 with a bound of $O(\epsilon)$ for ϵ small enough.

5.2.3 The Slowly Varying Sway Motion

The analysis to this point has been predicated on the boundedness of the sway velocity, y. The validity of this assumption is investigated in this subsection. It should be physically correct since the little energy fed into the sway direction through coupling from heave and roll is easily absorbed by the sway damping. As one can see below, like the heave damping, the sway damping plays an important role in limiting the sway velocity.

Again, we use the Lyapunov analysis to verify the boundedness of y. In view of the expression for g_2, it is assumed that the only y-dependent term in the uncertainty Δg_2 is $\Delta\delta_{22}y$ and that the actual sway damping is

$$\delta_{22} - \Delta\delta_{22} \geq \hat{\delta}_{22} > 0.$$

This is reasonable since in practice, the sway damping always exists and is positive. Now, we rewrite the sway equation as

$$\dot{y} = \epsilon[-(\delta_{22} - \Delta\delta_{22})y + (\hat{g}_2 + \Delta\hat{g}_2)(x_1, x_2, z_2, \tau)],$$

where

$$\hat{g}_2(x_1, x_2, z_2, \tau) = g_2(x_1, x_2, y, z_2, \tau) + \delta_{22} y,$$
$$\Delta\hat{g}_2(x_1, x_2, z_2, \tau) = \Delta g_2(x_1, x_2, y, z_2, \tau) - \Delta\delta_{22} y.$$

By the continuity of $\Delta\hat{g}_2$, there exists $\hat{L} > 0$, independent of y, such that

$$|(\hat{g}_2 + \Delta\hat{g}_2)(x_1, x_2, z_2, \tau)| \leq \hat{L}, \tag{5.29}$$

within the domain of interest.

Let $V_y = \frac{1}{2}y^2$. Then

$$\begin{aligned}
\dot{V}_y &\leq \epsilon(-\hat{\delta}_{22} y^2 + |y||\hat{g}_2 + \Delta\hat{g}_2|) \\
&\leq -\epsilon\hat{\delta}_{22}|y|(|y| - \frac{\hat{L}}{\hat{\delta}_{22}}) \\
&\leq 0 \quad \text{for } |y| \geq \hat{L}/\hat{\delta}_{22}.
\end{aligned}$$

Let us take

$$L_y \geq \hat{L}/\hat{\delta}_{22}. \tag{5.30}$$

Then $\forall |y(0)| \leq L_y$, we must have

$$|y(\tau)| \leq L_y, \quad \forall \tau \geq 0,$$

provided that all other states are also within the domain of interest D.

5.2.4 Summary of the Controller Design

The design of a robust stabilizing controller for the full vessel system has been decomposed into several simple control problems. In each subsystem, it is easy to verify that the design indeed works. A question thus arises: Will it work in the full system? Specifically, there are usually some interconnection (coupling) terms between subsystems. For the design to be valid for the full system, these interconnection terms must be well behaved in the sense that they will not destroy the established analysis. Generally, they are required to satisfy some smallness conditions.

For the current system, as one can see from the state equations, the coupling terms are not dominant, indicating that the design should work for the full system, as will be shown below. Indeed, in addition to the inequalities satisfied by the uncertainties and perturbations, an inequality is satisfied by the interconnection term between the slow and fast systems. That is, within the domain of interest,

$$|\tilde{g}_1(x_1, x_2, x_3, y, z_1, z_2, \tau)| \leq l_2, \quad l_2 \geq 0, \tag{5.31}$$

since $\tilde{g}_1$, which is defined by

$$\tilde{g}_1 = (g_1 + \Delta g_1)(x_1, x_2, x_3, y, z_1, z_2, \tau) - (g_1 + \Delta g_1)(x_1, x_2, x_3, y, 0, 0, \tau),$$

is a continuous function in its arguments.

The foregoing analysis is now summarized as the main theorem, followed by a proof based on Lyapunov analysis. Recall that the compact set $D \subset \Re^6$ given by equation (5.7) is our domain of interest. Also, let

$$D_0 = \{(x_1, x_2, x_3, y, z_1, z_2) | (x_1, x_2) \in S_0, |x_3| \leq L_x, |y| \leq L_y, ||(z_1, z_2)|| \leq L_z\}$$

be our stabilization region.

Theorem. Consider the vessel control system given by equations (5.1)-(5.6). Suppose that within the domain of interest D, the perturbations and uncertainties satisfy the inequalities (5.21), (5.26), (5.28), and (5.29), and the interconnection term satisfies the inequality (5.31). Then for λ_1, λ_2, and β large enough and ϵ_1, ϵ_2, and ϵ sufficiently small, the partial state feedback controller given by equation (5.27) will stabilize the vessel system in the sense that for any initial condition in D_0, we have

(i) x_1, x_2, and x_3 are ultimately bounded with bounds depending on ϵ_1 and ϵ_2.

(ii) z_1 and z_2 are ultimately bounded with bounds depending on ϵ.

(iii) $|y(\tau)| \le L_y, \ \ \forall \tau \ge 0.$

Proof: Since (ii) and (iii) have been established in Sections 5.2.2 and 5.2.3 respectively, it remains to show (i).

As is standard in the analysis of sliding mode control, we begin by examining the attractive property of the sliding manifold $\sigma_2 = 0$ by defining a Lyapunov function candidate

$$V_1 = \frac{1}{2}\sigma_2^2.$$

Recalling that $\sigma_2 = x_3 - \psi_x(x_1, x_2)$, we have

$$\begin{aligned} \dot{V}_1 &= \sigma_2\dot{\sigma}_2 \\ &= \sigma_2[f_{13}(x_1,x_2,x_3) + u + \Delta_2(x_1,x_2,x_3,y,\tau) \\ &\quad - \epsilon\frac{\partial\psi_x}{\partial x_2}\tilde{g}_1(x_1,x_2,x_3,y,z_1,z_2,\tau)]. \end{aligned} \tag{5.32}$$

Note that the interconnection term $\tilde{g}_1$ appears in $\dot{\sigma}_2$ in addition to those given by equation (5.25). By the smoothness of ψ_x, we have

$$\left|\frac{\partial\psi_x(x_1,x_2)}{\partial x_2}\right| \le l_3, \ \ l_3 \ge 0, \tag{5.33}$$

within the domain of interest. Using the inequalities (5.26), (5.31), and (5.33), equation (5.32) becomes

$$\dot{V}_1 \le -\frac{(\lambda_2+\rho_2)\sigma_2}{\tanh(1)}\tanh(\frac{\sigma_2}{\epsilon_2}) + \rho_2|\sigma_2| + \epsilon l_2 l_3|\sigma_2|,$$

upon applying the feedback control law (5.27).

Note that $\forall\xi \in \Re$,

$$\frac{\xi\tanh(\xi)}{\tanh(1)} \ge \begin{cases} |\xi|, & \text{for } |\xi| \ge 1 \\ \xi^2, & \text{for } |\xi| < 1 \end{cases}. \tag{5.34}$$

Hence, for $|\sigma_2| \ge \epsilon_2$, we can get

$$\begin{aligned} \dot{V}_1 &\le (-\lambda_2 - \rho_2 + \rho_2 + \epsilon l_2 l_3)|\sigma_2| \\ &= -(\lambda_2 - \epsilon l_2 l_3)|\sigma_2| \\ &< 0 \text{ if } \lambda_2 > \epsilon l_2 l_3. \end{aligned}$$

In other words, for λ_2 large enough, the set $\{|\sigma_2| \leq \epsilon_2\}$ is positively invariant.

Next, inside this positively invariant set, the roll dynamics are investigated by rewriting equations (5.1)-(5.2) in terms of σ_1 and σ_2 as

$$\dot{x}_1 = -\beta x_1 + \sigma_1, \tag{5.35}$$

$$\begin{aligned} \dot{\sigma}_1 &= \beta x_2 + f_{11}(x_1) + f_{12}(x_1)(\psi_x + \sigma_2) + \Delta_1(x_1, x_2, \psi_x, y, \tau) \\ &\quad + \Delta_3(x_1, x_2, \sigma_2, y, \tau) + \epsilon \tilde{g}_1(x_1, x_2, x_3, y, z_1, z_2, \tau) \\ &= -\frac{\lambda_1 + \rho_1}{(1-k)\tanh(1)} \tanh(\frac{\sigma_1}{\epsilon_1}) + \Delta_1 + f_{12}\sigma_2 + \Delta_3 + \epsilon \tilde{g}_1, \end{aligned} \tag{5.36}$$

where

$$\Delta_3 = \Delta_1(x_1, x_2, \psi_x + \sigma_2, y, \tau) - \Delta_1(x_1, x_2, \psi_x, y, \tau).$$

Now, let

$$V_2 = \frac{\theta_1}{2} x_1^2 + \frac{\theta_2}{2} \sigma_1^2, \;\; 0 < \theta_1, \; \theta_2 < 1, \;\; \theta_1 + \theta_2 = 1.$$

Then with respect to equations (5.35)-(5.36), we have

$$\begin{aligned} \dot{V}_2 &= \theta_1(-\beta x_1^2 + x_1\sigma_1) + \theta_2[-\frac{(\lambda_1 + \rho_1)\sigma_1}{(1-k)\tanh(1)} \tanh(\frac{\sigma_1}{\epsilon_1}) \\ &\quad + \sigma_1\Delta_1 + f_{12}\sigma_1\sigma_2 + \sigma_1\Delta_3 + \epsilon\sigma_1\tilde{g}_1]. \end{aligned}$$

In view of the smoothness of the uncertain functions, we have the following bound within the domain of interest,

$$|f_{12}\sigma_1\sigma_2 + \sigma_1\Delta_3| \leq l_4|\sigma_2|, \;\; l_4 \geq 0,$$

where one should note that $\Delta_3|_{\sigma_2=0} = 0$. Thus we can get

$$\begin{aligned} \dot{V}_2 &\leq -\theta_1\beta x_1^2 + \theta_1|x_1\sigma_1| + \theta_2[-\frac{(\lambda_1 + \rho_1)\sigma_1}{(1-k)\tanh(1)} \tanh(\frac{\sigma_1}{\epsilon_1}) \\ &\quad + (\rho_1 + \epsilon l_2)|\sigma_1|] + \theta_2 l_4|\sigma_2|. \end{aligned} \tag{5.37}$$

For $|\sigma_1| \geq \epsilon_1$, by (5.34), the inequality (5.37) reads

$$\begin{aligned} \dot{V}_2 &\leq -[\theta_1\beta x_1^2 + (\theta_2\lambda_1 - \epsilon\theta_2 l_2 - \theta_1|x_1|)|\sigma_1|] + \theta_2 l_4|\sigma_2| \\ &\leq -\gamma_1(||(x_1, x_2)||) + \epsilon_2\theta_2 l_4, \end{aligned} \tag{5.38}$$

for λ_1 large enough such that $\theta_2\lambda_1 - \epsilon\theta_2 l_2 - \theta_1|x_1| > 0$ within D, where $\gamma_1(\cdot)$ is a class $\mathcal{K}$ function[3].

On the other hand, for $|\sigma_1| \le \epsilon_1$, and by (5.34) again, (5.37) will become

$$\begin{aligned} \dot{V}_2 &\le -[\theta_1\beta x_1^2 - \theta_1|x_1\sigma_1| + \frac{\theta_2(\lambda_1+\rho_1)}{\epsilon_1}\sigma_1^2] + \theta_2[\epsilon_1(\rho_1+\epsilon l_2) + \epsilon_2 l_4] \\ &\le -\gamma_2(||(x_1,x_2)||) + \theta_2[\epsilon_1(\rho_1+\epsilon l_2)+\epsilon_2 l_4], \end{aligned} \tag{5.39}$$

for λ_1 large enough and ϵ_1 sufficiently small, where $\gamma_2(\cdot)$ is also a class $\mathcal{K}$ function. By (5.38) and (5.39), we conclude that x_1 and x_2 will be ultimately bounded with bounds depending on ϵ_1 and ϵ_2. Together with the positive invariance of $\{|\sigma_2| \le \epsilon_2\}$, we obtain conclusion (i) and hence complete the proof.

Remarks. (i) All the bounds on the perturbations, uncertainties, and interconnection terms in the inequalities (5.21), (5.26), (5.28), (5.29) and (5.31) can be obtained from the fact that these functions are continuous on the compact domain of interest. (ii) The perturbations and uncertainties depend on the wave amplitude. Hence, the upper bounds should be chosen to include the worst sea condition expected to be encountered. (iii) For given values of θ_1 and θ_2, there exists a positive constant c_0 such that $S_0 \subset \{V_2 \le c_0\}$, which can be used to serve as S_1. This is demonstrated by Figure 5.3.

---

[3] A continuous function $\gamma_1 : \Re \to \Re$ is said to be class $\mathcal{K}$ if (i) $\gamma(\cdot)$ is nondecreasing, (ii) $\gamma_1(0) = 0$, and (iii) $\gamma_1(q) > 0$ whenever $q > 0$.

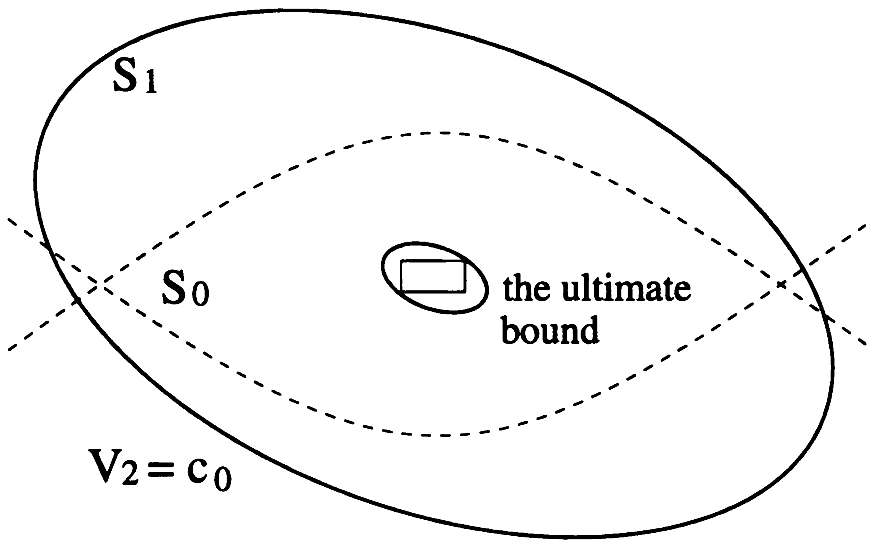

Figure 5.3: The domain of interest and the ultimate bound.

CHAPTER 6

NUMERICAL RESULTS AND DISCUSSIONS

In order to illustrate and confirm the analysis given in previous chapters, a typical fishing vessel, the twice-capsized clam dredge *Patti-B* [42], is numerically investigated in this chapter. While the 1-DOF model of this vessel has been analyzed in many previous studies ([13], [23], [27]), the multi-DOF model is emphasized here.

Table 6.1: Hydrodynamic coefficients for the *Patti-B* w.r.t. S at $\omega_w = 0.6$ rad/s.

symbol	value	symbol	value
$\hat{a}_{22}$	2.648×10^5 kg	$\hat{a}_{23}(=\hat{a}_{32})$	0
$\hat{a}_{24}(=\hat{a}_{42})$	-5.671×10^4 kg $\cdot$ m	$\hat{a}_{33}$	4.396×10^5 kg
$\hat{a}_{34}(=\hat{a}_{43})$	0	$\hat{a}_{44}$	1.780×10^5 kg $\cdot$ m^2
$\hat{b}_{22}$	9.290×10^3 kg/sec	$\hat{b}_{23}(=\hat{b}_{32})$	0
$\hat{b}_{24}(=\hat{b}_{42})$	-3.190×10^3 kg $\cdot$ m/sec	$\hat{b}_{33}$	3.048×10^5 kg/sec
$\hat{b}_{34}(=\hat{b}_{43})$	0	$\hat{b}_{44}$	2.140×10^3 kg $\cdot$ m^2/sec
$\hat{b}_{44q}$	9.88×10^4 kg $\cdot$ m^2		

The numerical simulation performed in this chapter is based on the state equations (3.49)-(3.53) and on equations (5.1)-(5.6) when implemented with the controller. The nondimensional coefficients therein can be obtained from *Patti-B*'s system parameters provided in Table 6.2 together with the hydrodynamic coefficients given in Tables 3.2 and 6.1. (These coefficients have been computed by the standard

Table 6.2: System parameters for the *Patti-B*.

parameter	value	parameter	value
I_{44}	1.255×10^6 kg $\cdot$ m^2	m	2.413×10^5 kg
h	3.0 m	z_G	-0.329 m
k_1	-1.273×10^5 kg/m	k_2	-2.097×10^3 kg
k_3	6.365×10^3 kg/m	k_4	0.214 m
k_5	0.05	k_6	-0.671 m
k_7	-0.1		

linear seakeeping program SHIPMO using the given hull form data [3].) In addition to nondimensional system parameters, the state equations also include some nondimensional functions $f_i(x_1)$ and $f_{ij}(x_1)$, which depend on the ship hull shape and need to be made specific for the *Patti-B*.

6.1 The Nondimensional Hydrostatic Functions

The hydrostatic functions $R_0(z_0, \varphi)$ and $GZ_0(z_0, \varphi)$ can be approximated in an appropriate best-fit sense as

$$\begin{aligned} R_0(z_0, \varphi) &= k_1 z_0 + (k_2 + k_3 z_0)\varphi^2, \\ GZ_0(z_0, \varphi) &= (k_4 + k_5 z_0)\varphi + (k_6 + k_7 z_0)\varphi^3, \end{aligned}$$

where the key properties of $R(z_0, \varphi)$ and $GZ_0(z_0, \varphi)$ are retained, namely, the former is even and the latter is odd in φ. Note also that z_0 appears linearly because in the range of interest, it is relatively small and the functions are approximately linear in z_0. Unfortunately, only coefficients k_1, k_4, and k_6 are available for the *Patti-B*, which are given in Table 6.2. By the arguments given at the end of Section 3.1.2, it should be clear that the others (i.e., k_2, k_3, k_5 and k_7) are relatively small. Hence we arbitrarily set (relatively) small values to them; see Table 6.2, where we set $k_2 = -k_3 z_G$ and $k_3 = -0.05k_1$.

From this set of coefficients, one immediately has the angles of vanishing stability for the unbiased *Patti-B*, i.e. $\pm 32.3^o$ ($\pm\sqrt{-k_4/k_6}$ rad.). For the biased case, these angles will be even smaller. Hence, within the angles of vanishing stability, $\sin\varphi$ and $\cos\varphi$ can be well approximated by the first two terms in their Taylor series about the origin. Then, the biased hydrostatic functions

$$
\begin{aligned}
R(z_0,\varphi) &= R_0(z_0 + y_G\sin\varphi, \varphi), \\
GZ(z_0,\varphi) &= y_G\cos\varphi + GZ_0(z_0 + y_G\sin\varphi, \varphi),
\end{aligned}
$$

can also be approximated by polynomials of z_0 and φ. In doing so, however, the static roll moment $K_{sc}(z_0,\varphi)$ will become a polynomial in φ up to 7-th degree. It is easy to see that the lower order terms are dominant, and we keep up through cubic order terms. The static roll moment $K_{sc}(z_0,\varphi)$ and heave force $Z_{sc}(z_0,\varphi)$ will then take the following form

$$
\begin{aligned}
K_{sc}(z_0,\varphi) &= \hat{k}_{11} + \hat{k}_{12}z_0 + (\hat{k}_{13} + \hat{k}_{14}z_0)\varphi + (\hat{k}_{15} + \hat{k}_{16}z_0)\varphi^2 \\
&\quad + (\hat{k}_{17} + \hat{k}_{18}z_0)\varphi^3, \qquad (6.1)\\
Z_{sc}(z_0,\varphi) &= \hat{k}_{21} + \hat{k}_{22}z_0 + (\hat{k}_{23} + \hat{k}_{24}z_0)\varphi + (\hat{k}_{25} + \hat{k}_{26}z_0)\varphi^2 \\
&\quad + (\hat{k}_{27} + \hat{k}_{28}z_0)\varphi^3, \qquad (6.2)
\end{aligned}
$$

where the $\hat{k}_{ij}$'s are related to the k_i's, and these relationships are given in Table 6.3. Note that these coefficients are functions of the bias y_G. If experimental or numerical data for $R_0(z_0, \varphi)$ and $GZ_0(z_0, \varphi)$ are available, then one can perform a best-fit approximation directly on $K_{sc}(z_0, \varphi)$ and $Z_{sc}(z_0, \varphi)$ to obtain the form and/or coefficients of equations (6.1) and (6.2).

Table 6.3: Hydrostatic constants.

symbol	definition	symbol	definition
$\hat{k}_{11}$	$-mgy_G$	$\hat{k}_{12}$	$-k_1 g y_G$
$\hat{k}_{13}$	$-g(k_1 y_G^2 + mk_4)$	$\hat{k}_{14}$	$-g(mk_5 + k_1 k_4)$
$\hat{k}_{15}$	$-gy_G(m(k_5 - 0.5) + k_2 + k_1 k_4)$	$\hat{k}_{16}$	$-gy_G(k_1(2k_5 - 0.5) + k_3)$
$\hat{k}_{17}$	$-g((-\frac{2}{3}k_1 + k_3 + k_1 k_5)y_G^2 + k_2 k_4 + mk_6)$	$\hat{k}_{18}$	$-g(k_2 k_5 + k_3 k_4 + mk_7 + k_1 k_6)$
$\hat{k}_{21}$	0	$\hat{k}_{22}$	$k_1 g$
$\hat{k}_{23}$	$k_1 g y_G$	$\hat{k}_{24}$	0
$\hat{k}_{25}$	$k_2 g$	$\hat{k}_{26}$	$k_3 g$
$\hat{k}_{27}$	$gy_G(k_3 - \frac{1}{6}k_1)$	$\hat{k}_{28}$	0
k_{11}	$-\hat{k}_{41}/\hat{k}_{43}$	k_{12}	$-\hat{k}_{45}/\hat{k}_{43}$
k_{13}	$-\hat{k}_{47}/\hat{k}_{43}$		
k_{21}	$-\hat{k}_{42}h/\hat{k}_{43}$	k_{22}	$-\hat{k}_{44}h/\hat{k}_{43}$
k_{23}	$-\hat{k}_{46}h/\hat{k}_{43}$	k_{24}	$-\hat{k}_{48}h/\hat{k}_{43}$
k_{31}	$-\hat{k}_{31}/(\hat{k}_{43}h)$	k_{32}	$-\hat{k}_{33}/(\hat{k}_{43}h)$
k_{33}	$-\hat{k}_{35}/(\hat{k}_{43}h)$	k_{34}	$-\hat{k}_{37}/(\hat{k}_{43}h)$

Thus, we immediately have

$$\begin{aligned} F_3(z_0, \varphi) &= \hat{k}_{31} + \hat{k}_{32}z_0 + (\hat{k}_{33} + \hat{k}_{34}z_0)\varphi + (\hat{k}_{35} + \hat{k}_{36}z_0)\varphi^2 \\ &\quad + (\hat{k}_{37} + \hat{k}_{38}z_0)\varphi^3, \qquad (6.3) \\ F_4(z_0, \varphi) &= \hat{k}_{41} + \hat{k}_{42}z_0 + (\hat{k}_{43} + \hat{k}_{44}z_0)\varphi + (\hat{k}_{45} + \hat{k}_{46}z_0)\varphi^2 \end{aligned}$$

where $\hat{\lambda}$

$a_1 = -$

nondim

are obta

where c

Patti-B

finds th

$y_C^{\dagger}$	
α	
k_1	
k_1	
k_2	
k_2	
k_3	
k_4	

To

$$+ (\hat{k}_{47} + \hat{k}_{48} z_0)\varphi^3, \tag{6.4}$$

where $\hat{k}_{3i} = -m_{34}\hat{k}_{1i} + m_4\hat{k}_{2i}$ and $\hat{k}_{4i} = m_3\hat{k}_{1i} - m_{43}\hat{k}_{2i}$, $i = 1, \ldots, 8$. Note that $\alpha_1 = -\hat{k}_{43}$ and $\alpha_4 = -\hat{k}_{32}$. Finally, after dividing (6.3) by $\alpha_1 h$ and (6.4) by α_1, the nondimensional restoring force functions $f_i(\varphi)$ in the state equations (3.49)-(3.53) are obtained as

$$\begin{aligned} f_1(\varphi) &= k_{11} - \varphi + k_{12}\varphi^2 + k_{13}\varphi^3, \\ f_2(\varphi) &= k_{21} + k_{22}\varphi + k_{23}\varphi^2 + k_{24}\varphi^3, \\ f_3(\varphi) &= k_{31} + k_{32}\varphi + k_{33}\varphi^2 + k_{34}\varphi^3, \end{aligned}$$

where α_1, α_4, and the k_{ij}'s are collected in Table 6.4 with 3 sets of values for the *Patti-B*, depending on y_G, the bias of the center of gravity G. From Table 6.4, one finds that $\omega_r/\omega_h \approx 0.4$. Hence, we will take $\epsilon = 0.1$ as the perturbation parameter.

Table 6.4: Hydrostatic coefficients for the *Patti-B* with different levels of biases.

$y_G^\dagger$	0	0.01	0.025	y_G	0	0.01	0.025
$\alpha_1^\ddagger$	3.450	3.449	3.448 ($\times 10^{11}$)	$\alpha_4^\ddagger$	1.776	1.776	1.776 ($\times 10^{12}$)
k_{11}	0	−0.047	−0.117	k_{12}	0	0.026	0.065
k_{13}	3.127	3.127	3.128				
k_{21}	0	0.026	0.065	k_{22}	0.882	0.882	0.882
k_{23}	0	−0.031	−0.077	k_{24}	−3.645	−3.646	−3.647
k_{31}	0	0	0	k_{32}	0	−0.017	−0.048
k_{43}	0.028	0.028	0.028	k_{44}	0	0.010	0.026

†unit: m. ‡unit: $kg^2 \cdot m^2/s^2$.

To explicitly show the dependence of $f_1(x_1)$ on y_G for the use in designing the feedback controller, we can extract y_G from the k_{1j}'s and rewrite $f_1(x_1)$ as

$$f_1(x_1) = f_{11}(x_1) + f_{12}(x_1)x_3 + \Delta f(x_1, x_3),$$

where recall that $x_3 = y_G/k_4$ and $\Delta f(x_1, x_3)$ represents the discrepancy between the actual and approximate functions, and for the *Patti-B*,

$$\begin{aligned} f_{11}(x_1) &= -x_1 + 3.144x_1^3, \\ f_{12}(x_1) &= 1 - 0.572x_1^2. \end{aligned}$$

A similar procedure can also be done for f_2 and f_3, but it is not necessary since the feedback control law involves only f_1.

6.2 The Invariant Manifolds

In the figures that follow, the symbol "x" is used to denote iterates of the mapping as started from the initial condition. The number beside each such point indicates the order of the mapping sequence. The mapping is the usual time periodic Poincaré map using the period of wave excitation. The (approximate) analytical roll invariant manifold in the figures is determined from equations (3.54) and (3.55) with the sway variable y given by equation (4.13).

Figure 6.1 shows that a two dimensional invariant manifold, which contains essentially the roll motions, indeed exists and is attractive. The sea state for this figure is: wave amplitude a = 0.14 m and wave frequency ω_w = 0.6 rad/s and no wind force is present. The initial condition is $x(0) = [-0.4\ 0\ 1\ 1\ 1]^T$, where $x(t) = [x_1(t)\ x_2(t)\ y(t)\ z_1(t)\ z_2(t)]^T$.

As shown in Figures 6.1(a) and 6.1(b), it takes only one or two iterates for the

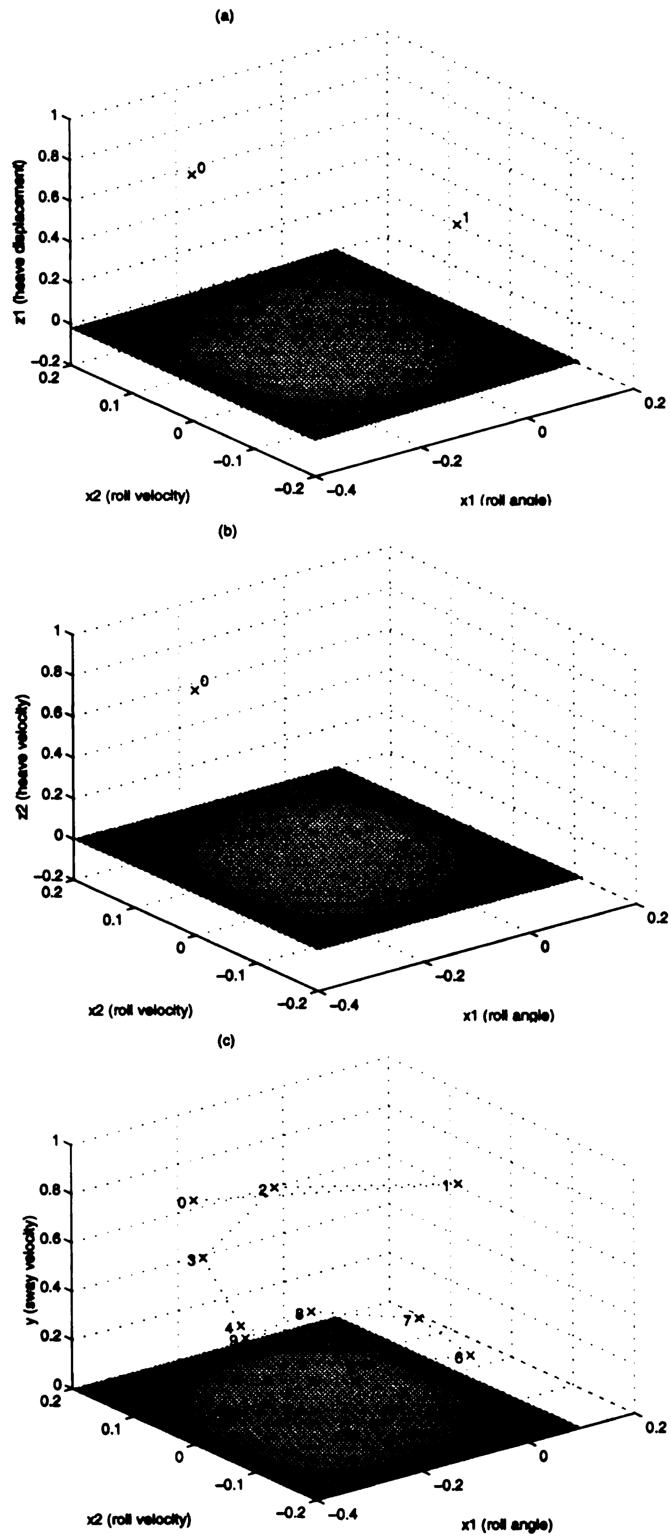

Figure 6.1: The 2-D invariant manifold.

heave motions to settle down to the invariant manifold, while in Figure 6.1(c), we see that the sway motion requires about 15 iterates. This reveals the special feature of the 2-D invariant manifold, which is slow compared to the heave dynamics, but fast with respect to the sway motions. Note that in the figures, some points have numbers but without a corresponding "x" — this simply implies that the points are beneath the approximate invariant manifold. This is because that equations (3.54) and (3.55) are only an $O(\epsilon)$ approximation to the actual manifold. The actual manifold is a bit more tilted. Note also that in Figure 6.1(c), we connect the adjacent points by a straight dotted line to clearly display the relative positions of the mapping points, although the reader should be aware that the motion follows a very different path in the phase space between iterates.

6.3 The Critical Wave Amplitude

The critical wave amplitudes predicted by the Melnikov analysis for different wave frequencies are depicted in Figure 6.2. It is clear from the figure that 1-DOF models give higher critical amplitudes than do 3-DOF models, as claimed in Chapter 4. However, they are very close, especially for wave excitations in the mid-frequency range. One should recall that the difference between the two models is dictated by the hydrodynamic coefficients such as a_{24}, a_{42}, b_{24}, b_{42}, and b_{22}. For other vessels where the couplings are more significant, the difference could be large.

The significance of the critical wave amplitude is that it signals a new possibility for the dynamics of the vessel. For a fixed wave frequency, there is no homoclinic/heteroclinic intersection and hence no erosion in the safe basin if the wave

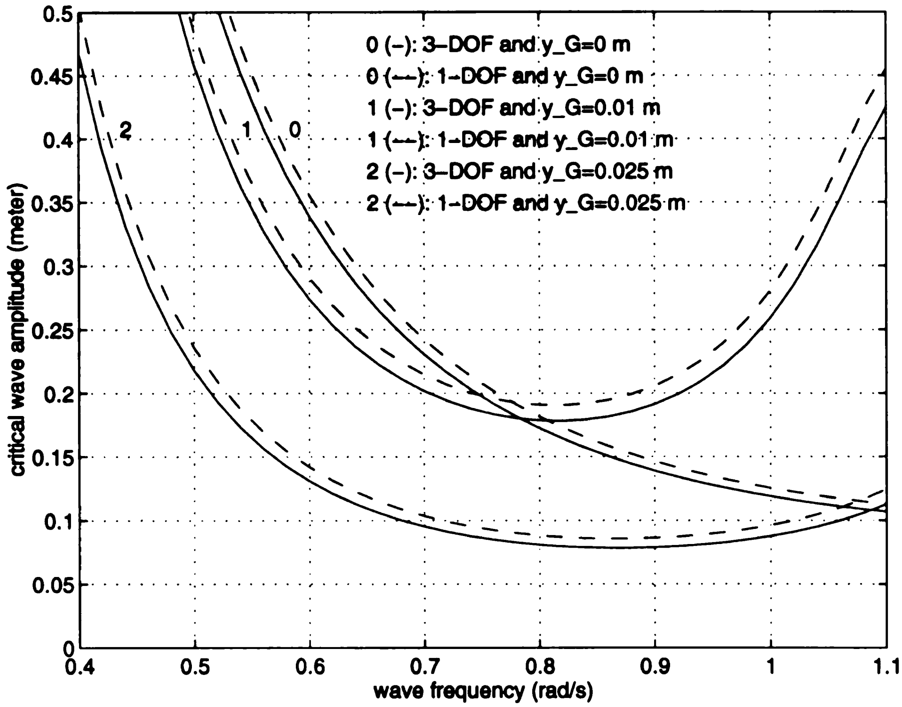

Figure 6.2: The critical wave amplitudes predicted by Melnikov analysis.

amplitude is below the critical value. For higher amplitudes, however, we will have some erosion of the safe area, implying that there is a chance of capsize from the safe area. This is illustrated in Figure 6.3, where $\omega_w = 0.6$ rad/s and $y_G = 0.025$ m. The unperturbed homoclinic orbit in the roll manifold is represented by the dashed curve. The initial condition $x(0) = [-0.3719 \ 0.10256 \ 0 \ 0 \ 0]^T$, which is inside the unperturbed safe region, is taken in Figure 6.3 for two different wave amplitudes with one above (0.14 m) and one below (0.13 m) the critical value (0.1309 m).

One can see that the fate of this initial point is dramatically different for the two wave amplitudes, even though they differ only by 0.01 m. With a below-critical wave amplitude, the initial point will lead to a bounded motion. On the other hand, for the above-critical case, capsizing is inevitable after 4 periods of wave excitation.

For a small wave excitation, but one exceeding the critical amplitude, capsizing

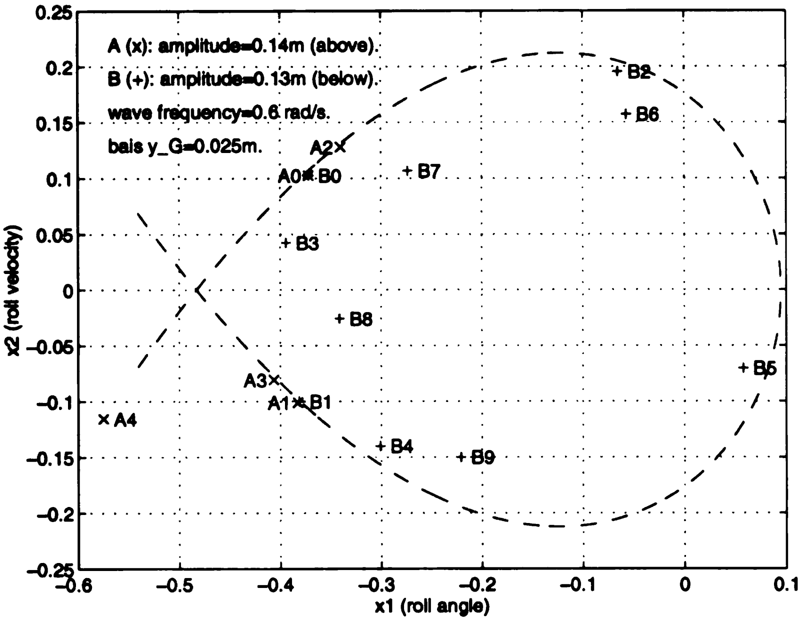

Figure 6.3: The significance of critical wave amplitude: 0.1309 m.

is possible only for initial conditions near the boundary area of the unperturbed safe region, such as point A in Figure 6.3. As the wave amplitudes get larger, some inner regions will also be eroded such as points C and D in Figure 6.4, where $a = 1.0$ m. A more detailed account of this erosion for a simple roll model is given by McRobie and Thompson [37].

It is important to point out that in practice, unless the wave amplitude is large enough, a vessel will rarely capsize in an above-critical sea state. One may have noticed that the wave amplitude of 0.1309 m is quite small. In a real situation, a vessel in such a sea state will not find itself near the capsize boundary, and hence capsize will only occur if some large disturbance causes a large motion that would be nearly critical even in calm seas. Consequently, the sea state should not be considered dangerous until its wave amplitude is considerably larger than the critical one. This is also the reason why the ratio of erosion area ρ_e can not be directly interpreted as

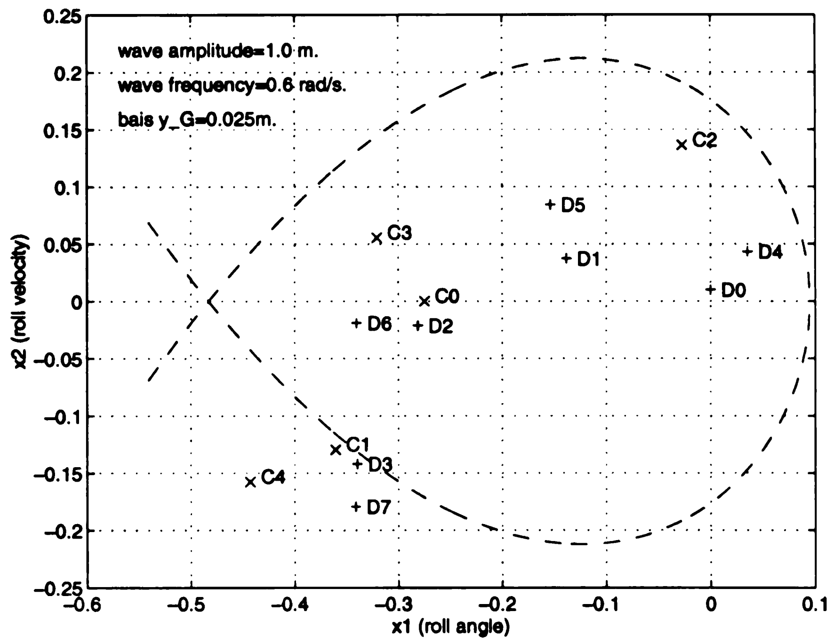

Figure 6.4: The escape from inner regions of the safe basin.

the capsizing probability, although they are closely related.

However, it is true that the capsizing probability from the safe region is zero below the critical case, and that the critical case signals the beginning of an important change in the system dynamics. And, as demonstrated by Thompson *et al.* ([60], [61]), erosion of safe basin begins in earnest as the wave height is raised beyond the critical value. Also, since this critical case is not difficult to obtain and is related directly to system parameters, it can be used for improving hull design and for detecting unsafe conditions. The higher critical wave amplitude a vessel has, the more severe environment it can resist.

6.4 The Erosion Area Ratio

Next, the ratio of the erosion area to that of the entire safe basin will be calculated for both 1-DOF and 3-DOF models. To this end, a uniform grid of points in the unperturbed safe region is taken as initial conditions and the percentage of those points which will lead to capsizing after N wave periods is computed. For 1-DOF models, the safe region simply means the two-dimensional region bounded by the homoclinic/heteroclinic orbit(s) denoted by S_a[1]. For 3-DOF models, the safe region is five-dimensional, and is defined as

$$\begin{aligned} S_b &= \{(x_1, x_2, y, z_1, z_2) | z_1 \in [-d_1 + h(x_1, x_2, y), d_1 + h(x_1, x_2, y)], \\ &\qquad z_2 \in [-d_2, d_2], y \in [-d_3 + \bar{y}, d_3 + \bar{y}], (x_1, x_2) \in S_a\}, \end{aligned}$$

where $\bar{y}$ is given by equation (4.13) which determines the steady state sway velocity and $h(x_1, x_2, y)$ is given by equation (3.54), which defines the slow manifold. Apparently, S_b can be interpreted as the two-dimensional safe region in the roll invariant manifold with some thickness in z_1, z_2, and y directions. (The full safe region in this case may have an extremely complicated shape; we are using only a part of it near the stable, two-dimensional invariant manifold.) For simplicity, we will take $d_1 = n_1 d$, $d_2 = n_2 d$, and $d_3 = n_3 d$, where d is the grid step size.

The results are presented in Figure 6.5, where $d = 9.65 \times 10^{-3}$ and $n_1 = n_2 = n_3 = 1$. With these values, there exists a total of 49761 points for the grid at each parameter value. The parameters are $\omega_w = 0.6$ rad/s and $y_G = 0.025$ m with wave amplitude varying from 0 to 1 m. From the figure, one can see that the 3-DOF model has more erosion area than the 1-DOF one for any fixed wave amplitude and the discrepancy grows as the wave amplitude increases, as pointed out in section 4.4. The ratio of phase space transport given by equation (4.8) is also plotted in Figure 6.5 for both models. It is indicated that equation (4.8) provides a very good estimate of the

---

[1] For the unbiased case, S_a is the same as S_0 defined in Chapter 5.

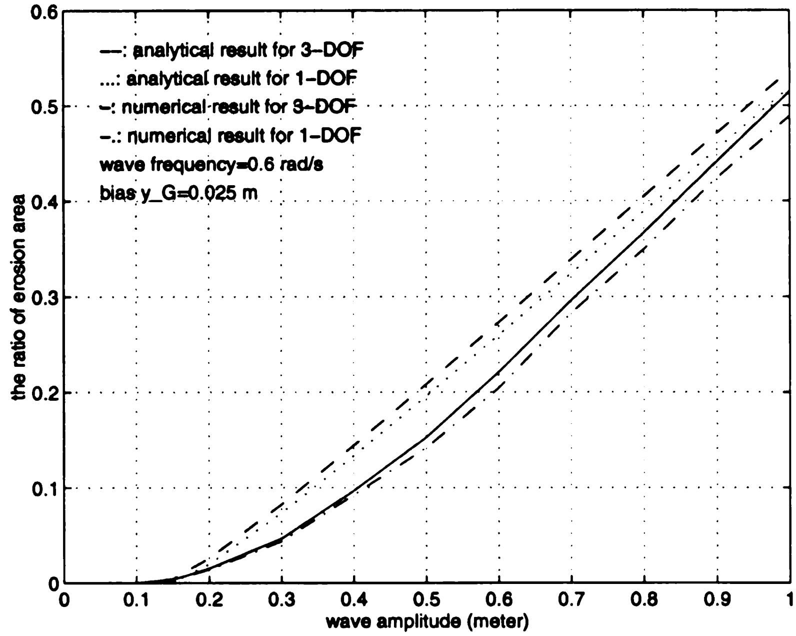

Figure 6.5: The ratio of erosion area and the phase space transport.

ratio of the eroded area (especially in light of the crudeness of the approximations and the assumptions used). This is of practical usage as the analytical estimate is much faster than the simulation results.

One of the implications of Figure 6.5 is that some capsizing situations can not be predicted solely by the 1-DOF roll model, as emphasized in section 4.4. One such example is demonstrated in Figure 6.6, where the sea state is $\omega_w = 0.6$ rad/s and $a = 0.14$ m, and the bias is $y_G = 0.025$ m. Consider the initial condition $x(0) = [-0.3719\ 0.10256\ 0\ 0\ 0]^T$. For the single-DOF model, it is predicted to be safe. For the multi-DOF model, on the contrary, it capsizes after 4 periods of wave excitation.

6.5 The Closed Loop System

In this section, numerical simulations for the closed loop system are carried out

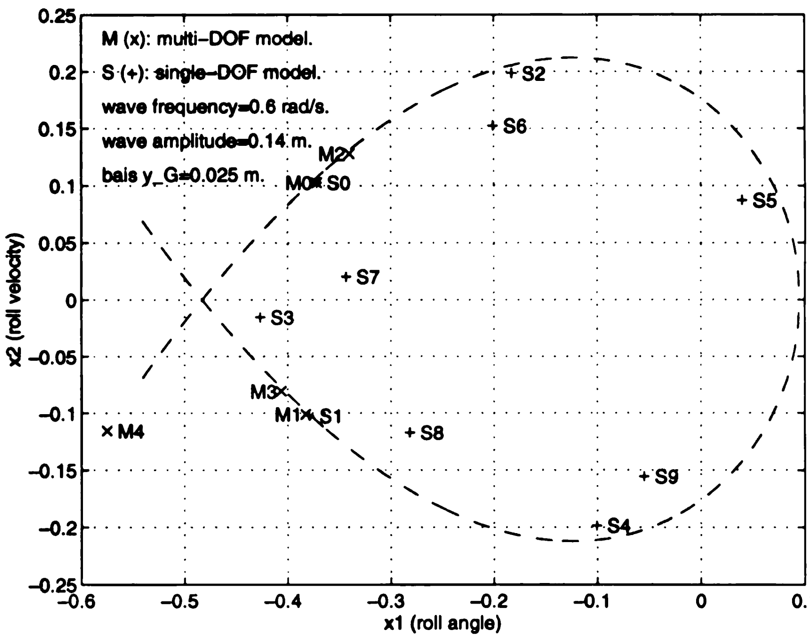

Figure 6.6: The evolution with different DOF models for the same initial condition.

to examine the performance of the robust controller designed in Chapter 5. We will focus on the comparison of open loop and closed loop systems under severe sea conditions. Practical issues regarding the control effort will also be addressed.

Given a vessel, like the *Patti-B*, a simple procedure based on our main results in Chapter 5 can be followed to obtain a robust stabilizing controller. The procedure includes the following 6 steps:

1. Determine β.

2. Choose the domain of interest D.

3. Estimate ρ_1 and k in inequality (5.21).

4. Determine λ_1 and ϵ_1 for $\psi_x(x_1, x_2)$.

5. Estimate ρ_2 in inequality (5.25).

6. Determine λ_2 and ϵ_2.

Step 1 amounts to determine the sliding plane for the 2-D roll system and the stability on the sliding plane. It will also affect the level of control effort required. This step precedes step 2 due to the fact that the choice of D involves S_1, which depends on β.

Ideally, we want the controller to meet the following requirements:

(a) It can stabilize a large set of initial conditions;

(b) It will work under severe sea states.

Requirement (a) is equivalent to enlarging D as much as possible, which will increase the estimated bounds for ρ_1, ρ_2 and k. Requirement (b) also leads to large values for ρ_1, ρ_2 and k. Then a choice of large values for the parameters λ_1, λ_2 and β is needed, as indicated in the previous analysis. In other words, both requirements need sufficiently large control effort. However, in reality the control effort cannot be arbitrarily large, as mentioned in the beginning. Therefore, there is a tradeoff between the ideal requirements and practical limitations in choosing the domain of interest D and the design parameters λ_1, λ_2 and β. A feasible approach is to choose D as small as possible such that it still includes most of the safe region. Moreover, the design parameters can be tuned according to the sea conditions, where larger values are used in bad conditions.

It is also important to point out that the analysis in Chapter 5 is conservative, typical for a Lyapunov-based design. The main purpose of the analysis is to ensure that such a controller design will work. Although it can also provide some estimates on the ultimate bounds of states and lower bounds for design parameters, quite often the controller works better than predicted. This is why these bounds were not explicitly calculated in Chapter 5. Hence, one can be a a bit generous when choosing design parameters, as we will see below.

For a chosen β, we can take θ_1, θ_2 and c_0 to minimize the range of $S_1 = \{V_2 \leq c_0\}$ that contains S_0 in its interior. It can be shown that

$$\theta_1 = \frac{\beta^2}{1+\beta^2}, \quad \theta_2 = \frac{1}{1+\beta^2}, \quad \text{and} \quad c_0 = \frac{\beta^2}{\eta_1(1+\beta^2)}, \tag{6.5}$$

is the set of parameters needed. In the following numerical results, the domain of interest D is chosen with S_1 determined from (6.5), $L_x = 2.0$, L_y given by equation (5.30), and $L_z = 2.0$.

Three different control systems for the *Patti-B* are considered for purposes of comparison. The first is the open loop system, i.e. an unbiased ship. The second is a closed loop system with linear partial state feedback law, i.e.,

$$u = k_1 x_1 + k_2 x_2 + k_3 x_3. \tag{6.6}$$

The third is the closed loop system with the nonlinear partial state feedback controller designed in Chapter 5.

The linear feedback gains in equation (6.6) are chosen as:

$$k_1 = 0, \quad k_2 = -10, \quad \text{and} \quad k_3 = -6,$$

which assign the closed loop poles of the linearized slow system to -1, -2, and -3. The design parameters for the nonlinear feedback system are taken to be

$$\beta = 0.1, \quad \lambda_1 = 0.005, \quad \lambda_2 = 0.01, \quad \epsilon_1 = 0.3, \quad \text{and} \quad \epsilon_2 = 0.01.$$

The above linear feedback gains and parameters for nonlinear controller are chosen to yield the same order of control effort. The sea condition for each run is set at a wave amplitude of 5 m and a wave frequency of 0.6 rad/s.

Figure 6.7 shows the state-space trajectories for each of the three systems with the following three sets of initial conditions:

IC1: $x_1 = 0.1$, $x_2 = 0$, $x_3 = 0$, $y = 0$, $z_1 = 0$, $z_2 = 0$.

IC2: $x_1 = 0.5$, $x_2 = 0$, $x_3 = 0.1$, $y = 1$, $z_1 = 1$, $z_2 = 1$.

IC3: $x_1 = 0$, $x_2 = 0.4$, $x_3 = 0.1$, $y = 1$, $z_1 = 1$, $z_2 = 1$.

The first initial condition is near the calm-water stable operating point, whereas the latter two are near the boundary of the calm-water safe region. From Figure 6.7(a), one can see that for the open loop system, the vessel readily capsizes, even when the initial condition is close to the origin. With linear feedback control, the situation is much improved. However, as seen from Figure 6.7(b), the linear controller is inadequate for some states near the boundary of the safe region. On the other hand, the nonlinear controller demonstrates good stabilization for any initial conditions inside the safe region.

The position of the CG, y_G (obtained from x_3), is shown in Figure 6.8(a) for the two controlled systems, whereas the corresponding control effort is plotted in Figure 6.8(b). It can be seen from Figure 6.8(a) that with an initial bias of 0.021 m, the transient y_G can reach as large as 0.14m, although it settles down soon after. For anti-roll tanks using 5% of the ship weight (which is about 12 tons for the *Patti-B*), this accounts for 2.8 m movement of the CG of the water required.

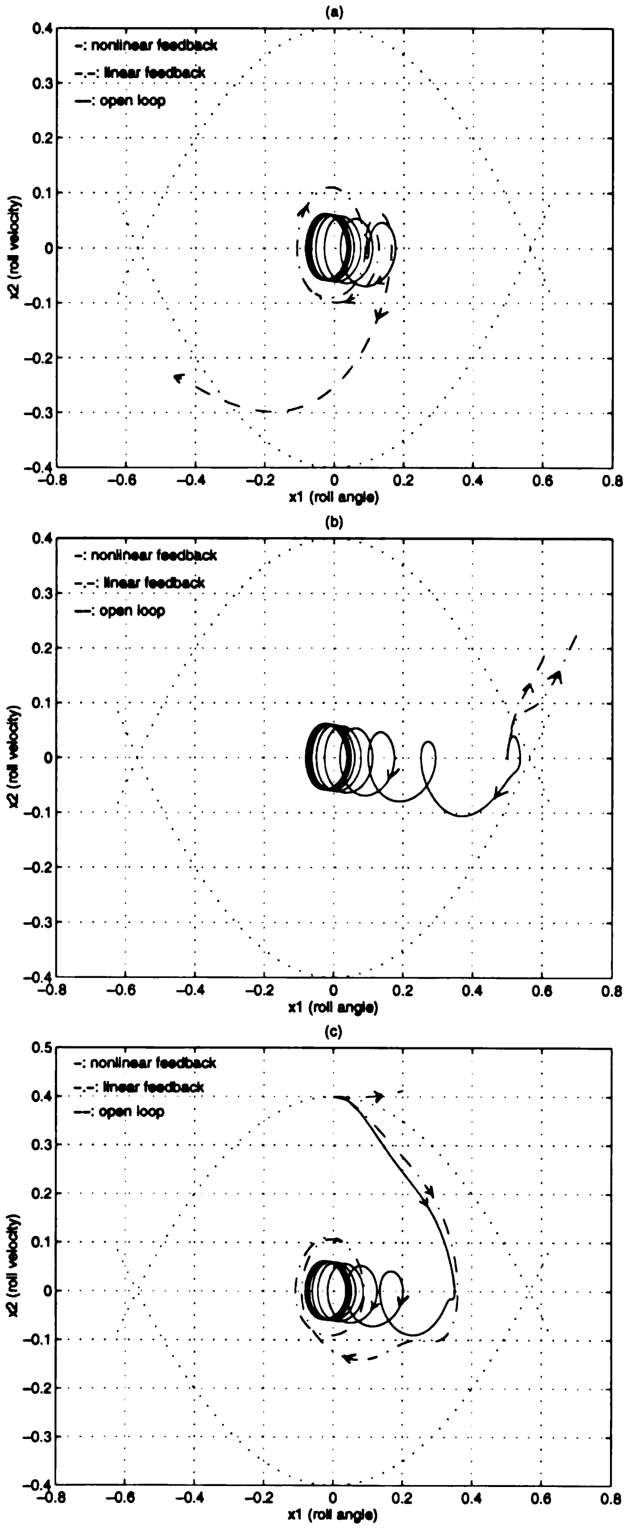

Figure 6.7: System behaviors with different controllers for (a) IC1, (b) IC2, and (c) IC3.

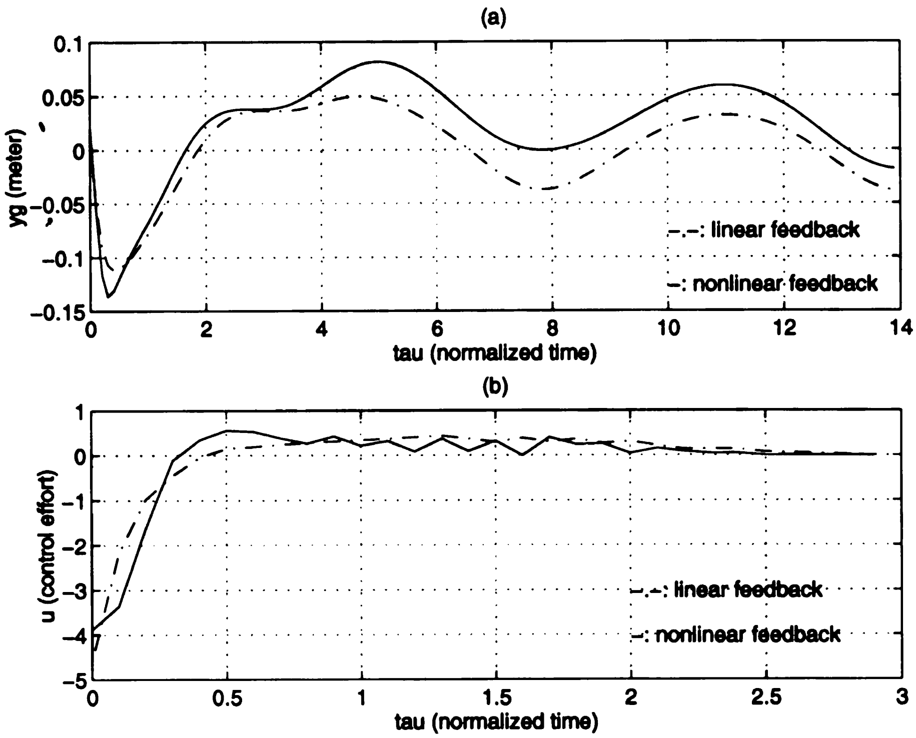

Figure 6.8: Comparison of linear and nonlinear feedback controllers with IC3 for (a) y_G, and (b) control effort u.

From Figure 6.8(b), it is clear that like y_G, most peak control efforts occur during the initial transient period (here the peak value is about -4). The control effort will determine the specifications of the actuators needed. Suppose that the two tanks are separated by 6 m. Then, in order to reach $u = -4$, it is required that the total flow rate be 103 liters/sec or 27 gallons/sec. If the control effort goes beyond practical limitations, one should tune down the design parameters. The nonlinear controller provided in this study has a large flexibility in tuning the parameters. For the linear feedback controller, the tuning is restricted in that high feedback gains in general must be used in order to stabilize the initial conditions far away from the origin. For example, the feedback gains $k_1 = -3$, $k_2 = -10$, and $k_3 = -6$ can stabilize IC2. However, the peak control effort for this case is more than two times that of the nonlinear case, and this may lead to practical difficulties in implementation.

CHAPTER 7

CONCLUSIONS AND FUTURE WORK

In this study, the modeling, dynamics and control of large amplitude motions of vessels in regular beam seas have been considered. First, based on the wave-fixed coordinate system, a 3-DOF model, including roll, sway, and heave motions, is obtained which balances model accuracy against the desire to obtain analytical estimates of certain features of large amplitude motions. After nondimensionalization and rescaling, a 5-th order state model is obtained which is amenable to analysis using invariant manifold and singular perturbation techniques.

The emphasis of the dynamic analysis is on the coupling effects from sway and heave to the roll capsizing problem. A fast invariant manifold approach to the Melnikov analysis is incorporated with the phase space transport theory to propose a capsizing criterion for both biased and unbiased ships. It is found that for typical fishing vessels, the coupling effect from heave is negligible, whereas that from sway tends to increase the tendency to capsize. Moreover, the coupling effects, which are generally quite small, do increase with wave amplitudes.

While the results obtained herein are not dramatic in terms of corrections to capsize criteria, they do put the results obtained from simple roll models on a firmer foundation. In addition, they point the way to more systematic analyses of large amplitude vessel motions.

Next, we designed a nonlinear state feedback controller using a Lyapunov-based approach to stabilize the nonlinear 3-DOF vessel system. The vessel is fitted with anti-roll tanks whose flow rate can be controlled by actuators like pumps. The nonlinear controller is robust in the sense that it takes into account the model uncertainties, resulting primarily from unknown hydrodynamic contributions.

The design procedure follows the idea of composite control for singularly perturbed systems. The slow control for the dynamics on the slow manifold is considered first. It consists of two parts, linked by the backstepping technique. Both parts in the slow control use a smooth version of sliding mode control which can handle large uncertainties. It is shown by a Lyapunov analysis that the slow control alone can restrict the roll motions to a small region in the state space, and at the same time, keeps the motions in other degrees of freedom bounded.

Numerical simulations for a fishing vessel, the clam dredge *Patti-B*, were carried out for the open loop system, the closed loop system with linear feedback, and the closed loop system with the designed nonlinear feedback. The simulation results for the open loop system verify the proposed capsizing criterion as well as other analytical results. It is also shown that only the nonlinear controller can effectively stabilize the system against capsizing using a reasonable amount of control effort.

Many improvements and extensions of the current work are worthy of future consideration, both in the areas of fundamental dynamical systems and in their application to vessel dynamics. Some of these are listed below.

- Although only the 3-DOF beam sea model is analyzed in this study, one should note that the current approach can be applied to the fully 6-DOF ship model. The resultant state equation will again be of singularly perturbed form where the fast manifold will contain heave and pitch motions, whereas the slow manifold includes roll, sway, yaw, and surge. The slow dynamics will be again in the form of slowly varying oscillators with sway, yaw, and surge as stable, slowly varying variables. Of course, the derivations and calculations involved will be much more complicated than the present work.

- The present results can be generalized to the case of random excitation following the line of analysis in [23] for the 1-DOF models. Here one will need results on invariant manifolds for stochastic systems.

- One can use these ideas to calculate a capsizing probability. To achieve this, some distribution must be assigned for the initial conditions, rather than using a uniform distribution. The capsizing probability will be a combined probability of initial states and escape. Such a measure may provide a more useful capsize criterion.

- A more accurate analytical estimation of $\mu(E_N)$, the amount of chaotic transport, can be achieved by utilizing the analytical unperturbed homoclinic solution and the distance function between stable and unstable manifolds in Melnikov's theorem.

- The phase space transport on the 2-D fast invariant manifold in the 3-D slowly varying oscillator is used in this paper as a measure for the transport of the overall 3-D system. Although it provides a satisfactory result, the chaotic transport for general higher dimensional maps and their relationship with the current measure remain open.

- When the bias is relatively small, the homoclinic and heteroclinic tangles may coexist and interact with each other. So far there are no satisfactory analytical results on this subject.

- The use of linear hydrodynamics remains the weak link in this line of work. It would be of use to consider general forms of nonlinear coefficients and determine their effect on the results. This type of analysis could be used as a guide for determining which coefficients need to be measured most accurately for predicting large amplitude motions of vessels.

- This study suggests a very promising approach to the question of the existence and solution of the roll center. Namely, an invariant manifold approach offers a systematic way to study this question for a large range of vessel motions.

- The controller design procedure provided here can be applied to other stabilizers, such as fin and rudder-roll stabilizers, for different purposes.

- The effects of the limitations of x_3 and u on the performance of the closed loop system can be investigated analytically using Lyapunov analysis.

APPENDICES

APPENDIX A

A FAST-MANIFOLD APPROACH TO MELNIKOV FUNCTIONS FOR SLOWLY VARYING OSCILLATORS

Consider the slowly varying oscillator given by equations (4.9)-(4.11). Suppose that for each value of z in some open interval $J \subset \Re$, the planar Hamiltonian system

$$\begin{aligned}\dot{x} &= f_1(x, y, z),\\ \dot{y} &= f_2(x, y, z),\end{aligned}$$

possesses a homoclinic orbit to a hyperbolic saddle point, denoted by $\gamma(z) = (x(z), y(z), z)$ which satisfies $f_i(x(z), y(z), z) = 0$. Of interest here is the fate of these orbits under the action of the perturbations.

To better visualize the structure of the system, we shall take the usual time-T Poincare section Σ^{t_0} defined by

$$\Sigma^{t_0} = \{(x, y, z, \phi) | \phi = t_0 \in [0, T]\},$$

where $\phi = t \bmod T$. The associated Poincare map is then given by $P : \Sigma^{t_0} \to \Sigma^{t_0}$. Following the notation of Wiggins and Holmes [68], we denote the unperturbed normally hyperbolic one-manifold of saddle points by

$$\mathcal{M} = \{(\gamma(z), \phi) | \phi \in S^1,\ z \in J\}$$

and its perturbed version by

$$\mathcal{M}_\epsilon = \{(\gamma(z, \phi; \epsilon), \phi) = (\gamma(z) + O(\epsilon), \phi) | \phi \in S^1,\ z \in J\}.$$

It is assumed that on $\mathcal{M}_\epsilon$ near $z = z_0$, there exists a fixed point of the Poincare map, denoted by p, that is preserved under the perturbation. The value of z_0 can be approximated by application of the averaging theorem restricted to $\mathcal{M}_\epsilon$. It is found that p can be approximated by $\gamma(z_0)$ up to $O(\epsilon)$ [68]. The structure of the perturbed system is shown in Figure A.1. (In Figure A.1 and throughout this appendix, we assume that the stable manifold of p, $W^s(p)$, is two-dimensional and the unstable manifold, $W^u(p)$, is one-dimensional. The argument for the other case, i.e., $W^s(p)$ is one-dimensional and $W^u(p)$ is two dimensional, is the same.)

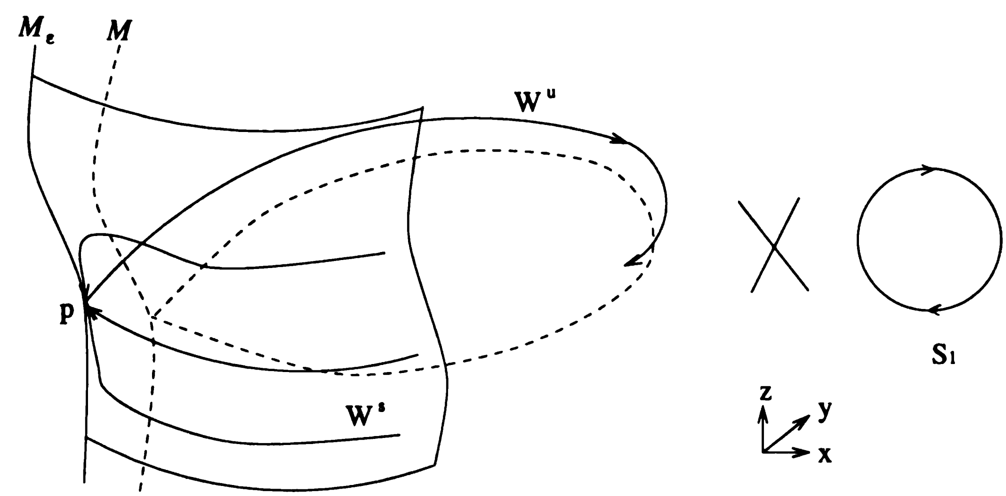

Figure A.1: Perturbed (solid) and unperturbed (dashed) manifolds for slowly varying oscillators with homoclinic orbits.

A Melnikov function for equations (4.9)-(4.11) was developed in Wiggins and Holmes [68] for detecting the persistence of homoclinic orbits when $\epsilon \neq 0$. The approach utilizes a distance function between the stable and unstable manifolds of the preserved fixed point p in the three-dimensional Poincare section. The purpose of this appendix is to show that without dealing with the three-dimensional distance problem, the same Melnikov function can be derived by examining the dynamics of the system on a two-dimensional fast manifold and applying the usual two-dimensional

Melnikov analysis. The motivation for presenting this alternative derivation is that it offers some potentially useful insight into the system dynamics.

A.1 The Fast Manifold

For $\epsilon = 0$ the fast manifold is nothing more than the plane at $z = z_0$. The existence of this fast invariant manifold when $\epsilon \neq 0$ can be examined from center manifold-like arguments [7] and Fenichel's theory on the persistence of invariant manifolds under perturbation [14]. Although a fast invariant manifold is not always guaranteed for a dynamical system, the special structure of the slowly varying oscillator along with its assumptions make this possible for the present system. In this section, the existence of such a fast manifold will be established by construction.

Let the fast invariant manifold be denoted by

$$\mathcal{F}_\epsilon = \{(x, y, z) \mid z = F_0(x, y, t) + \epsilon F_1(x, y, t) + O(\epsilon^2)\}. \tag{A.1}$$

Note that by the nature of the system, this manifold is also periodic in t with period T. By setting $\epsilon = 0$, we immediately have

$$F_0(x, y, t) \equiv z_0.$$

For invariance, $\mathcal{F}_\epsilon$ has to satisfy the dynamical equations (4.9)-(4.11). Substituting equation (A.1) into equation (4.11) yields

$$\epsilon \frac{d}{dt} F_1(x, y, t) + O(\epsilon^2) = \epsilon g_3(x, y, z_0 + \epsilon F_1(x, y, t) + O(\epsilon^2), t),$$

and equating both sides for $O(\epsilon)$ terms gives the following differential equation that F_1 must satisfy:

$$\frac{d}{dt} F_1(x, y, t) = g_3(x, y, z_0, t), \tag{A.2}$$

which, to the first order, is equivalent to

$$\frac{\partial F_1}{\partial t} + \frac{\partial F_1}{\partial x} f_1(x, y, z_0) + \frac{\partial F_1}{\partial y} f_2(x, y, z_0) = g_3(x, y, z_0, t). \tag{A.3}$$

Equation (A.3) is a linear partial differential equation in F_1 whose solutions can be obtained by the method of characteristics [28]. Note that the right-hand-side of equation (A.3) is independent of F_1, making it easier to solve. Indeed, one can show that F_1 can be expressed as an integral of $g_3(x(t), y(t), z_0, t)$, where $x(t)$ and $y(t)$ are the solution to the unperturbed planar Hamiltonian system. However, to get an explicit form for F_1 by this method, one needs *a priori* knowledge about the fast manifold (to prescribe initial Cauchy data for equation (A.3)). Therefore, the function F_1, which would yield the first-order geometry of the fast manifold via equation (A.1) and the dynamics on it via equations (A.4)-(A.5) below, is not easily obtained. Alternatively, one could obtain a polynomial approximation to F_1, local to the fixed point p, by using a procedure similar to that used in finding center manifolds [7]. We will not pursue this here, as we need nonlocal information. In fact, and as is typical in derivations of Melnikov functions, we will circumvent the need for computing F_1 explicitly.

One should note that since $\mathcal{F}_\epsilon$ is an invariant manifold for the dynamical system in equations (4.9)-(4.11), it must consist of a collection of solution trajectories of equations (4.9)-(4.11). Furthermore, it passes through the fixed point p. Hence, we can conclude that the one-dimensional unstable manifold $W^u(p)$ and an invariant one-dimensional piece of the two-dimensional stable manifold $W^s(p)$ lie on the fast manifold $\mathcal{F}_\epsilon$; see Figure 4.10.

Using equation (A.1), the dynamics on $\mathcal{F}_\epsilon$ can thus be expressed up to $O(\epsilon^2)$ by

$$\begin{aligned}
\dot{x} &= f_1(x,y,z_0) + \epsilon[(\frac{\partial f_1}{\partial z}(x,y,z_0))F_1(x,y,t) + g_1(x,y,z_0,t)] + O(\epsilon^2), \quad (A.4) \\
\dot{y} &= f_2(x,y,z_0) + \epsilon[(\frac{\partial f_2}{\partial z}(x,y,z_0))F_1(x,y,t) + g_2(x,y,z_0,t)] + O(\epsilon^2). \quad (A.5)
\end{aligned}$$

One can directly apply the two-dimensional Melnikov analysis to this system.

A.2 Melnikov Analysis

Let $q_0(t)$ be the homoclinic orbit of the unperturbed system on the $z = z_0$ plane. Then applying the usual two-dimensional Melnikov analysis [22] to equations (A.4)-(A.5), we obtain the following Melnikov function

$$\begin{aligned}
M(\theta, t_0) &= \int_{-\infty}^{\infty} [f_1(\frac{\partial f_2}{\partial z}F_1 + g_2) - f_2(\frac{\partial f_1}{\partial z}F_1 + g_1)](q_0(t), t+\theta+t_0)dt \\
&= \int_{-\infty}^{\infty} (f_1 g_2 - f_2 g_1)dt + \int_{-\infty}^{\infty} (f_1\frac{\partial f_2}{\partial z} - f_2\frac{\partial f_1}{\partial z})F_1 dt. \quad (A.6)
\end{aligned}$$

Now, note the following identity

$$f_1\frac{\partial f_2}{\partial z} - f_2\frac{\partial f_1}{\partial z} = -\frac{\partial H}{\partial y}\frac{\partial^2 H}{\partial x \partial z} + \frac{\partial H}{\partial x}\frac{\partial^2 H}{\partial y \partial z} = -\frac{d}{dt}(\frac{\partial H}{\partial z}) + \frac{\partial^2 H}{\partial z^2}\dot{z}. \quad (A.7)$$

Evaluating this on $q_0(t)$, equation (A.7) becomes

$$(f_1\frac{\partial f_2}{\partial z} - f_2\frac{\partial f_1}{\partial z})(q_0(t)) = -\frac{d}{dt}(\frac{\partial H}{\partial z}(q_0(t))) \quad (A.8)$$

since $z = z_0$, a constant, on $q_0(t)$. Then, by integration by parts, we have

$$\begin{aligned}
&\int_{-\infty}^{\infty} [(f_1\frac{\partial f_2}{\partial z} - f_2\frac{\partial f_1}{\partial z})F_1](q_0(t), t+\theta+t_0)dt = \\
&\quad \frac{\partial H}{\partial z}(q_0(-\infty))F_1(q_0(-\infty), -\infty) - \frac{\partial H}{\partial z}(q_0(\infty))F_1(q_0(\infty), \infty) + \\
&\quad \int_{-\infty}^{\infty} \frac{\partial H}{\partial z}(q_0(t))g_3(q_0(t), t+\theta+t_0)dt, \quad (A.9)
\end{aligned}$$

where we have used equations (A.2) and (A.8). Recalling that $q_0(t)$ is the unperturbed homoclinic orbit on $z = z_0$, its limits are at the saddle point, as follows:

$$q_0(-\infty) = q_0(\infty) = \gamma(z_0).$$

Also, from integration of equation (A.2),

$$F_1(q_0(\infty), \infty) - F_1(q_0(-\infty), -\infty) = \int_{-\infty}^{\infty} g_3(q_0(t), t + \theta + t_0)dt.$$

Hence equation (A.9) now reads

$$\begin{aligned}
&\int_{-\infty}^{\infty} [(f_1 \frac{\partial f_2}{\partial z} - f_2 \frac{\partial f_1}{\partial z}) F_1](q_0(t), t + \theta + t_0)dt = \\
&\quad \int_{-\infty}^{\infty} \frac{\partial H}{\partial z}(q_0(t)) g_3(q_0(t), t + \theta + t_0)dt - \\
&\quad \frac{\partial H}{\partial z}(\gamma(z_0)) \int_{-\infty}^{\infty} g_3(q_0(t), t + \theta + t_0)dt. \qquad \text{(A.10)}
\end{aligned}$$

Inserting equation (A.10) into equation (A.6), we finally arrive at an expression for the Melnikov function

$$\begin{aligned}
M(\theta, t_0) &= \int_{-\infty}^{\infty} (f_1 g_2 - f_2 g_1 + \frac{\partial H}{\partial z} g_3)(q_0(t), t + \theta + t_0)dt - \\
&\quad \frac{\partial H}{\partial z}(\gamma(z_0)) \int_{-\infty}^{\infty} g_3(q_0(t), t + \theta + t_0)dt \\
&= \int_{-\infty}^{\infty} (\nabla H \cdot g)(q_0(t), t + \theta + t_0)dt - \frac{\partial H}{\partial z}(\gamma(z_0)) \int_{-\infty}^{\infty} g_3(q_0(t), t + \theta + t_0)dt,
\end{aligned}$$

where $g = [g_1\ g_2\ g_3]^T$. This Melnikov function is exactly the same as that given in Wiggins and Holmes [68] and errata [69]. However, the derivation presented here is quite different.

APPENDIX B

THE RELATIONSHIP BETWEEN BIASED AND UNBIASED HYDROSTATIC FUNCTIONS

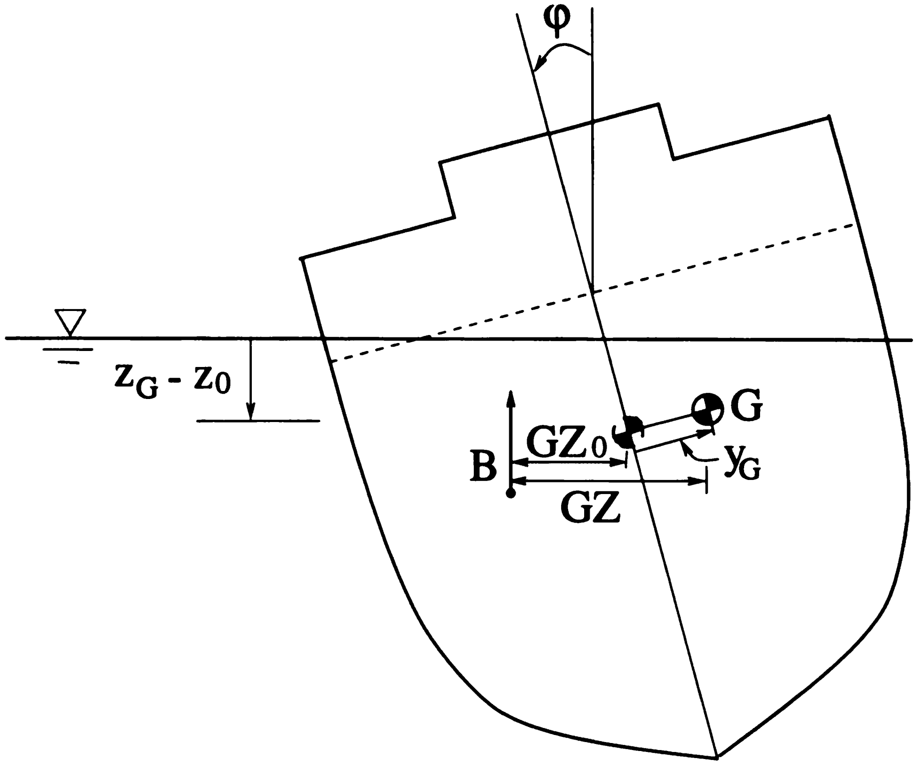

Figure B.1: GZ for biased and unbiased ships.

This appendix is devoted to relating the biased hydrostatic functions $R(z_0, \varphi)$ and $GZ(z_0, \varphi)$ to its unbiased counterparts $R_0((z_0)_0, \varphi)$ and $GZ_0((z_0)_0, \varphi)$ for a given hull shape. The additional subscript 0 to z_0 in the latter cases denotes zero bias. Suppose that the bias for the biased ship is measured by y_G and that both ships have the same z_G. Then, given z_0 and φ (the position of the biased vessel), we want to determine

R and GZ in terms of R_0 and GZ_0.

As shown in Figure B.1, it is seen that in order for the biased and unbiased ships to have the same buoyancy force and buoyancy center (in the inertial frame), i.e. for the submerged portions of the two ships to be coincident, it is required that

$$(z_0)_0 = z_0 + y_G \sin\varphi.$$

Hence it follows that

$$R(z_0, \varphi) = R_0(z_0 + y_G \sin\varphi, \varphi).$$

Moreover, it is also clear from Figure B.1 that

$$GZ(z_0, \varphi) = y_G \cos\varphi + GZ_0(z_0 + y_G \sin\varphi, \varphi).$$

BIBLIOGRAPHY

BIBLIOGRAPHY

[1] Abkowitz, M. 1969. *Stability and Motion Control of Ocean Vehicles.* Cambridge, Massachusetts : The M.I.T. Press.

[2] Allen, J. 1945. The stabilization of ships by activated fins. *Transactions of the Institution of Naval Architecture* 87:123–159.

[3] Beck, F. and A. Troesch 1990. Documentation and User's Manual for the Computer Program SHIPMO. Department of Naval Architecture and Marine Engineering, The University of Michigan.

[4] Bennett, S. 1991. Ship stabilization: history. In *Concise Encyclopedia of traffic and transportation systems*, ed. Papageorgiou, M., 454–459. Pergamon Press.

[5] Cardo, A., A. Francescutto, and R. Nabergoj 1981. Ultraharmonics and subharmonics in the rolling motion of a ship: steady-state solution. *International Shipbuilding Progress* 28:234–251.

[6] Cardo, A., A. Francescutto, and R. Nabergoj 1984. Subharmonic oscillation in nonlinear rolling. *Ocean Engineering* 11:663.

[7] Carr, J. 1982. *Applications of Center Manifold Theory.* New York : Springer-Verlag.

[8] Chadwick, J. 1955. On the stabilization of roll. *SNAME Transactions* 63:234–280.

[9] Chen, S.-L. and S. Shaw 1996. A fast manifold approach to melnikov functions for slowly varying oscillators. *International Journal of Bifurcation and Chaos.*

[10] Chen, S.-L., S. Shaw, and A. Troesch. 1996. An analysis of roll/sway/heave dynamics in relation to vessel capsizing in regular beam seas.

[11] Dalzell, J. 1973. A note on the distribution of maxima of ship rolling. *Journal of Ship Research* 17:217–226.

[12] Ding, M., E. Ott, and C. Grebogi 1994. Controlling chaos in a temporally irregular environment. *Physica D* 74:386–394.

[13] Falzarano, J., S. Shaw, and A. Troesch 1992. Application of global methods for analyzing dynamical systems to ship rolling motion and capsizing. *International Journal of Bifurcation and Chaos* 2:101–116.

[14] Fenichel, N. 1971. Persistence and smoothness of invariant manifolds for flows. *Indiana University Mathematics Journal* 21:193–226.

[15] Fortuna, L. and G. Muscato 1996. A roll stabilization system for a monohull ship: modeling, identification, and adaptive control. *IEEE Transactions on Control Systems Technology* 4:18–28.

[16] Fossen, T. 1995. *Guidance and Control of Ocean Vehicles.* New York : John Wiley & Sons.

[17] Frahm, H. 1911. Results of trials of the anti-rolling tanks at sea. *Transactions of the Institution of Naval Architecture* 53:183–216.

[18] Francescuntto, A. 1990. On the nonlinear motions of ships and structures in narrow band sea. In *Proc. IUTAM Symposium on Dynamics of Marine Vehicles and Structures in Waves* 291–304. London.

[19] Francescuntto, A. 1992. Stochastic modeling of nonlinear motions in the presence of narrow band excitation. In *Proc. International Society of Offshore and Polar Engineers* 91–96. San Francisco.

[20] Frey, M. and E. Simiu 1993. Noise-induced chaos and phase space flux. *Physica D* 63:312–340.

[21] Georgiou, I., M. Corless, and A. Bajaj 1994. Invariant manifolds and normal modes in a singularly perturbed nonlinear oscillator with applications to structural dynamics. *ZAMP: Journal of Applied Mathematics and Physics.*

[22] Guckenheimer, J. and P. Holmes 1983. *Nonlinear Oscillations, Dynamical Systems, and Bifurcations of Vector Fields.* : Springer-Verlag.

[23] Hsieh, S., S. Shaw, and A. Troesch 1994. A nonlinear probabilistic method for predicting vessel capsizing in random beam seas. *Proc. Royal Society of London, Series A* 446:195–211.

[24] Hutchison, B. 1990. Seakeeping studies: A status report. *SNAME Transactions* 98:263–317.

[25] Hutchison, B. 1991. The transverse plane motions of ships. *Marine Technology* 28(2).

[26] Jiang, C. Highly Nonlinear Rolling Motion Leading to Capsize. PhD thesis Department of Naval Architecture and Marine Engineering, The University of Michigan Ann Arbor 1995.

[27] Jiang, C., A. Troesch, and S. Shaw 1996. Highly nonlinear roll motion leading to capsize. *Journal of Ship Research.*

[28] John, F. 1982. *Partial Differential Equations.* New York : Springer-Verlag 4th edition.

[29] Jons, O., G. Fuller, and R. Letorneau 1987. Fishing vessel stability: a case study for operator guidance and investment. *SNAME Transactions.*

[30] Ketema, Y. 1992. A physical interpretation of melnikov's method. *International Journal of Bifurcation and Chaos* 2:1–9.

[31] Khalil, H. 1996. *Nonlinear Systems.* Upper Saddle River, NJ : Prentice-Hall second edition.

[32] Kokotovic, P., H. Khalil, and J. O'Reilly 1986. *Singular Perturbations Mehtods in Control: Analysis and Design.* New York : Academic Press.

[33] Kristic, M., I. Kanellakopoulos, and P. Kokotovic 1995. *Nonlinear and Adaptive Control Design.* New York : Wiley-Interscience.

[34] Lewis, E. 1989. *Principles of Naval Architecture.* New Jersey : SNAME second edition.

[35] Liaw, C., S. Bishop, and J. Thompson 1993. Heave-excited rolling motion of a rectangular vessel in head seas. *International Journal of Offshore and Polar Engineering* 3:26–31.

[36] Liaw, C. and S. Bishop 1995. Nonlinear heave-roll coupling and ship rolling. *Nonlinear Dynamics* 8:197–211.

[37] McRobie, F. and J. Thompson 1991. Lobe dynamics and the escape from a potential well. *Proc. Royal Society of London, Series A* 435:659–672.

[38] Minorsky, N. 1941. Note on the angular motions of ships. *Transactions of the ASME* 63:A111–A120.

[39] Minorsky, N. 1947. Experiments with activated tanks. *Transactions of the ASME* 69:735–747.

[40] Mook, D., L. Marshall, and A. Nayfeh 1974. Subharmonics and superharmonics resonance in the pitch and roll modes of ship motions. *Journal of Hydronautics* 8:32–40.

[41] Moshchuk, N., R. Ibrahim, R. Khasminskii, and P. Chow 1995. Asymptotic expansion of ship capsizing in random sea waves: Parts i and ii. *International Journal of Non-Linear Mechanics* 30:727–757.

[42] National Transportation Safety Board (NTSB) 1979. Grounding and Capsizing of the Clam Dredge Patti-B: NTSB Marine Accident Report.

[43] Nayfeh, A. and A. Khdeir 1986. Nonlinear rolling of biased ships in regular beam seas. *International Shipbuilding Progress* 33:84–93.

[44] Nayfeh, A. and A. Khdeir 1986. Nonlinear rolling of ships in regular beam seas. *International Shipbuilding Progress* 33:40–49.

[45] Nayfeh, A., D. Mook, and L. Marshall 1973. Nonlinear coupling of pitch and roll modes in ship motions. *Journal of Hydronautics* 7:145–152.

[46] Nayfeh, A. and N. Sanchez 1988. Chaos and dynamic instability in the rolling motion of ships. In *17th Symposium on Naval Hydrodynamics* 617–632. The Hague.

[47] Newhouse, S. 1974. Diffeomorphisms with infinitely many sinks. *Topology* 13:9–18.

[48] Norden, C. 1929. Ship Stabilizer: U.S. Patent No. 1708679.

[49] Odabassi, A. 1977. Ultimate stability of ships. *RINA Transactions* 199:237–264.

[50] Roberts, J. 1982. A stochastic theory for nonlinear ship rolling in irregular seas. *Journal of Ship Research* 26:299–245.

[51] Roberts, J. and N. Dacunha 1985. Roll motion of a ship in random beam waves: Comparison between theory and experiment. *Journal of Ship Research* 29:112–126.

[52] Schlick, O. 1904. The gyroscopic effect of fly-wheels on board ship. *Transactions of the Institution of Naval Architecture* 46:117–144.

[53] Sellars, F. and J. Martin 1992. Selection and evaluation of ship roll stabilization systems. *Marine Technology* 29:84–101.

[54] Senjanovic, I. 1994. Harmonic analysis of nonlinear oscillation of cubic dynamical systems. *Journal of ship research* 129:112–126.

[55] Shaw, S. and S. Wiggins 1988. Chaotic dynamics of a whirling pendulum. *Physica D* 31:190–211.

[56] Simiu, E. and M. Frey 1996. Melnikov process and noise-induced exits from a well. *Journal of Engineering Mechanics* 122:263–270.

[57] Soliman, M. and J. Thompson 1989. Integrity measures quantifying the erosion of smooth and fractal basins of attraction. *Journal of Sound and Vibration* 135:453–475.

[58] Sperry, E. 1915. Ship's gyroscope: U.S. Patent No. 1150311.

[59] Tan, N. and P. Radmore 1995. Alternative approaches to melnikov analysis for forced oscillators. *Journal of Sound and Vibration* 187:815–824.

[60] Thompson, J. 1990. Transient basins: A new tool for designing ships against capsize. In *IUTAM Symposium on the Dynamics of Marine Vehicles* 325–332. London.

[61] Thompson, J., R. Rainey, and M. Soliman 1993. Mechanics of ship capsize under direct and parametric wave excitation. *Phil. Trans. R. Soc. London Ser. A*.

[62] Troesch, A. 1986. Naval Architecture 440, Marine Dynamics II: Course Notes. Department of Naval Architecture and Marine Engineering, The University of Michigan Ann Arbor, Michigan.

[63] vanAmerongen, J. 1991. Ship rudder roll stabilization. In *Concise Encyclopedia of traffic and transportation systems*, ed. Papageorgiou, M., 448–454. Pergamon Press.

[64] Virgin, L. 1989. Approximate criterion for capsize based on deterministic dynamics. *Dynamics and Stability of Systems* 4:55–70.

[65] Wiggins, S. 1988. *Global Bifurcations and Chaos.* New York : Springer-Verlag.

[66] Wiggins, S. 1990. *Introduction to Applied Nonlinear Dynamical Systems and Chaos.* New York : Springer-Verlag.

[67] Wiggins, S. 1992. *Chaotic Transport in Dynamical Systems.* New York : Springer-Verlag.

[68] Wiggins, S. and P. Holmes 1987. Homoclinic orbits in slowly varying oscillators. *SIAM Journal of Mathematical Analysis* 18:612–629.

[69] Wiggins, S. and P. Holmes 1988. Errata: Homoclinic orbits in slowly varying oscillators. *SIAM Journal of Mathematical Analysis* 19:1254–1255.

[70] Wiggins, S. and S. Shaw 1988. Chaos and three dimensional horseshoes in slowly varying oscillators. *Journal of Applied Mechanics* 55:959–968.

[71] Wright, J. and W. Marshfield 1980. Ship roll response and capsize behavior in beam seas. *RINA Transactions* 122:129–144.